

# 1 Real-time UV-Index retrieval in Europe using Earth Observation 2 based techniques and validation against ground-based measurements

3 Panagiotis G. Kosmopoulos<sup>1</sup>, Stelios Kazadzis<sup>2</sup>, Alois W. Schmalwieser<sup>3</sup>, Panagiotis I. Raptis<sup>1</sup>,  
4 Kyriakoula Papachristopoulou<sup>1</sup>, Ilias Fountoulakis<sup>1,4</sup>, Akriti Masoom<sup>5</sup>, Alkiviadis F. Bais<sup>6</sup>, Julia Bilbao<sup>7</sup>,  
5 Mario Blumthaler<sup>8</sup>, Axel Kreuter<sup>8,9</sup>, Anna Maria Siani<sup>10</sup>, Kostas Eleftheratos<sup>11</sup>, Chrysanthi Topaloglou<sup>6</sup>,  
6 Julian Gröbner<sup>2</sup>, Bjørn Johnsen<sup>12</sup>, Tove Svendby<sup>13</sup>, Jose Manuel Vilaplana<sup>14</sup>, Lionel Doppler<sup>15</sup>, Ann R.  
7 Webb<sup>16</sup>, Marina Khazova<sup>17</sup>, Hugo De Backer<sup>18</sup>, Anu Heikkilä<sup>19</sup>, Kaisa Lakkala<sup>20</sup>, Janusz Jaroslawski<sup>21</sup>,  
8 Charikleia Meleti<sup>5</sup>, Henri Diémoz<sup>4</sup>, Gregor Hülsen<sup>2</sup>, Barbara Klotz<sup>8</sup>, John Rimmer<sup>16</sup>, Charalampos  
9 Kontoes<sup>1</sup>

10

11 <sup>1</sup>National Observatory of Athens, Athens, Greece

12 <sup>2</sup>Physikalisch-Meteorologisches Observatorium Davos, World Radiation Center, Davos Dorf, Switzerland

13 <sup>3</sup>University of Veterinary Medicine, Vienna, Austria

14 <sup>4</sup>Environmental Protection Agency of Aosta Valley, Aosta, Italy

15 <sup>5</sup>Indian Institute of Technology Roorkee, India

16 <sup>6</sup>Aristotle University of Thessaloniki, Greece

17 <sup>7</sup>Valladolid University, Valladolid, Spain

18 <sup>8</sup>Innsbruck Medical University, Innsbruck, Austria

19 <sup>9</sup>Luftblick OG, Innsbruck, Austria

20 <sup>10</sup>Sapienza University of Rome, Rome, Italy

21 <sup>11</sup>National and Kapodistrian University of Athens, Athens, Greece

22 <sup>12</sup>Norwegian Radiation and Nuclear Safety Authority, Bærum, Norway

23 <sup>13</sup>Norwegian Institute for Air Research, Bærum, Norway

24 <sup>14</sup>National Institute for Aerospace Technology, Torrejón de Ardoz, Spain

25 <sup>15</sup>German Weather Service, Offenbach, Germany

26 <sup>16</sup>University of Manchester, Manchester, UK

27 <sup>17</sup>Public Health England, London, UK

28 <sup>18</sup>Royal Meteorological Institute of Belgium, Bruxelles, Belgium

29 <sup>19</sup>Finnish Meteorological Institute, Helsinki, Finland

30 <sup>20</sup>Finnish Meteorological Institute, Sodankylä, Finland

31 <sup>21</sup>Institute of Geophysics, Polish Academy of Sciences, Warsaw, Poland

32

33 *Correspondence to:* P.G. Kosmopoulos (pkosmo@noa.gr)

34 **Abstract.** This study introduces an Earth observation (EO)-based system which is capable of operationally estimating and  
35 continuously monitoring the ultraviolet index (UVI) in Europe. The UVIOS (i.e. UV-Index Operating System) exploits a  
36 synergy of radiative transfer models with high performance computing and EO data from satellites (Meteosat Second  
37 Generation and Meteorological Operational Satellite-B), and retrieval processes (Tropospheric Emission Monitoring Internet  
38 Service, Copernicus Atmosphere Monitoring Service and the Global Land Service). It provides a near-real-time now-casting

39 and short-term forecasting service for UV radiation over Europe. The main atmospheric inputs for the UVI simulations include  
40 ozone, clouds and aerosols while the impacts of ground elevation and surface albedo are also taken into account. The UVIOS  
41 output is the UVI at high spatial and temporal resolution (5 km and 15 minutes, respectively) for Europe (i.e. 1.5 million pixels)  
42 in real-time. The UVI is empirically related to biologically important UV dose rates and the reliability of this EO-based solution  
43 was verified against ground-based measurements from 17 stations across Europe. Stations are equipped with spectral,  
44 broadband or multi-filter instruments and cover a range of topographic and atmospheric conditions. A period of over one year  
45 of forecasted 15-min retrievals under all sky conditions were compared with the ground-based measurements. UVIOS  
46 forecasts were within  $\pm 0.5$  of measured UVI for at least 70% of the data compared at all stations. For clear sky conditions the  
47 agreement was better than 0.5 UVI for 80% of the data. A sensitivity analysis of EO inputs and UVIOS outputs was performed  
48 in order to quantify the level of uncertainty in the derived products, and to identify the covariance between the accuracy of the  
49 output and the spatial and temporal resolution, and the quality of the inputs. Overall, UVIOS slightly overestimated UVI due  
50 to observational uncertainties in inputs of cloud and aerosol. This service will hopefully contribute to EO capabilities and will  
51 assist the provision of operational early warning systems that will help raise awareness among European Union citizens of the  
52 health implications of high UVI doses.

53 **Keywords.** Ultraviolet Index; Earth Observation; Radiative Transfer; High Performance Computing; Clouds; Aerosols;  
54 Ozone; Solar Zenith Angle; Ground Elevation; Surface Albedo

## 55 **1 Introduction**

56 Human exposure to ultraviolet (UV) radiation has both beneficial and harmful effects (Andrady et al., 2015; Juzeniene et al.,  
57 2011; Lucas et al., 2006). Overexposure to UV radiation (UVR) has a number of implications, such as the acute response of  
58 erythema, the risk of skin cancer and a number of eye diseases (snow blindness, cataract). Nevertheless, exposure to solar  
59 UVB radiation is the main mechanism for the synthesis of Vitamin D in the human skin (Holick, 2002; Webb and Engelsen,  
60 2008; Webb et al., 2011). Low levels of the Vitamin D are associated with depression of the immune system and there is  
61 evidence that is linked to a number of medical implications (Lucas et al., 2015).

62 The UV index was introduced by WHO/WMO in 1994 (WMO, 1995), as a simple method of informing the general public  
63 about the erythema effective (sun-burning) UV. It is a unitless, scaled version of erythemally-weighted UV determined by  
64 multiplying the erythema weighted irradiance (in  $\text{W/m}^2$ ) by  $40 \text{ m}^2/\text{W}$  (Fioletov et al., 2010 ; Vanicek et al., 2000; WHO, 2002).  
65 The response of UV radiation to climatic changes is of great concern (Bais et al., 2019; Bais et al., 2018; McKenzie et al.,  
66 2011). According to the latest work of Bais et al. (2019) greater values of UV are expected by the end of 21st century, relative  
67 to the present decade, at low latitudes, while at higher latitudes UV will decrease but these projections are associated with  
68 high uncertainty (up to 30%).

69 There are many factors affecting UV irradiance reaching Earth's surface (Kerr and Fioletov, 2008). The dependence of UV  
70 irradiance on astronomical and geometrical parameters is generally well understood, and in many cases the changes are  
71 periodical (e.g., (Blumthaler et al., 1997; Gröbner et al., 2017; Larkin et al., 2000; Seckmeyer et al., 2008)). Atmospheric gases  
72 play a crucial role in attenuating UV irradiance, specifically NO<sub>2</sub> is a major absorber in this spectral region (e.g., Cede et al.  
73 (2006)), while O<sub>3</sub> is the main absorber at lower (UVB) wavelengths. Other gases that have significant absorption in the UV  
74 include SO<sub>2</sub> (Fioletov et al., 1998) and HCHO (Gratien et al., 2007), but their –usually- smaller atmospheric abundances,  
75 result in minor effects to incoming UV (with major exceptions such as volcanic incidents). Aerosols are another important  
76 parameter controlling UV irradiance levels at the surface (e.g., Kazadzis et al. (2009b)). Aerosol optical depth (AOD) that  
77 quantifies the attenuation of the direct solar beam by aerosols is a parameter varying with wavelength, as well as single  
78 scattering albedo (SSA), which determines the scattering ratio to total extinction. Several recent studies based on incoming  
79 UV irradiance measurements or calculations reveal the enhanced absorption by aerosols in the UV relative to the visible  
80 spectral range. They show the importance of using SSA in the UV spectral region, instead of interpolating SSA at visible  
81 wavelengths to the UV, or directly using SSA at visible wavelengths, options that systematically overestimate UV irradiance  
82 (Corr et al., 2009; Fountoulakis et al., 2019; Kazadzis et al., 2016; Mok et al., 2018; Raptis et al., 2018).

83 All the aforementioned parameters are particularly important under cloud free conditions. The cloudy sky complicates the  
84 propagation of solar radiation, predominantly in the troposphere, through multiple cloud - radiation interactions. Nonetheless,  
85 UVR is less affected than the total solar radiation by clouds (e.g., Badosa et al. (2014)). Bais et al. (1993) quantified that for  
86 the city of Thessaloniki the change from 0 to 8 oktas for cloud coverage corresponds to 80% reduction in the UVR and pointed  
87 out that there is very low wavelength dependence of UVR attenuation by cloud cover. Although, the transmittance of clouds  
88 does not vary significantly with wavelength, some studies (Mayer et al., 1998; Seckmeyer et al., 1996) have found that the  
89 diffuse component of the surface UVR is affected by clouds in a spectrally dependent way, due to more efficient scattering  
90 and absorption of shorter UV wavelengths, in case of large air masses. In cases of partially cloudy sky but unobscured sun,  
91 UVR tends to be higher than in clear sky conditions (e.g., Badosa et al. (2014)), as is the case for total solar radiation. For short  
92 timescale analysis the variability of UVR introduced by clouds should be considered.

93 Solar UV irradiance at the surface increases with increasing surface albedo. This increment affects the UV radiant exposure,  
94 which becomes crucial for outdoor human activities (Schmalwieser and Siani, 2018; Schmalwieser, 2020; Siani et al., 2008).  
95 Measurements and computations of effective surface albedo for heterogeneous surfaces reveal its strong spectral dependence,  
96 with snow-covered surfaces having significantly higher values of albedo for short wavelengths compared to total solar radiation  
97 (Blumthaler and Ambach, 1988; Kreuter et al., 2014). Stronger enhancement of the UV relative to visible radiation over highly  
98 reflective surfaces is also due to the more effective multiple scattering of shorter wavelengths in the atmosphere.

99 Any systematic changes in any of the parameters described in previous paragraphs have the potential to lead to changes for  
100 UVR. These changes vary significantly throughout the globe and are attributed to different possible drivers (Bernhard and  
101 Stierle, 2020; Fountoulakis et al., 2018; McKenzie et al., 2019). Fountoulakis et al. (2020a) gives a review of recent  
102 publications concerning UV trends since 1990s, and associated factors, summarizing these as positive trends for South and

Central Europe and negative trends at higher latitudes, and recognizing the important role of aerosols and cloud coverage for these trends. Findings from the same study demonstrated that the long – term changes of UV irradiance recorded at four stations around Europe during the last two decades are mainly attributed to aerosols, cloud coverage and surface albedo variations, with total ozone changes being of minor importance.

Chubarova et al. (2020) found a long term increase of 3% per decade in UV at Northern Eurasia for the 1979-2015 period. For the northern mid-latitudes Zerefos et al. (2012) showed that the long-term (1995-2006) positive trend in total ozone wasn't enough to compensate for, let alone reverse, the UVB increase attributed to tropospheric aerosol decline (brightening effect). Since 2007, a slowdown or even a possible turning point in the positive UVB trend was detected, which was attributed to the continued upward trend in total ozone overwhelming the aerosol effect (Zerefos et al., 2012). By contrast, the long-term variability of UVB irradiance over northern high latitudes was determined by ozone and not by aerosol trends, as shown by Eleftheratos et al. (2015) who found a statistically significant negative trend of -3.9% per decade for the UVB irradiance during the time period 1999-2011, from ground-based measurements at 7 stations. This was in agreement with statistically significant increase of spaceborne measured total ozone by about 1.5% per decade (ozone recovery) for the same area. For Arctic regions changes in snow cover have a great impact on UV trends according to Bernhard (2011), who concluded that the future Arctic UV climate may be affected more by a warming climate changing the snow cover than changes in stratospheric ozone concentrations.

The continuous monitoring of the UV index is currently performed by about 160 stations from 25 countries around Europe (Schmalwieser et al., 2017), with all monitoring instruments having the potential to provide other effective doses such as the effective dose for the production of vitamin D in human skin (e.g., Fioletov et al. (2009)).

There are three types of instruments for UV irradiance measurements; those measuring the integral of UV irradiance (broadband sensors) tailored to a specific response, narrow band instruments such as filter radiometers with coarse spectral resolution, and instruments performing high resolution spectral measurements – the most versatile but most challenging and least robust instruments. Concerning the current UV monitoring measurement accuracy; The European reference UV spectroradiometer (QASUME) is a traveling instrument which provides a common standard through inter-comparison on-site (Gröbner et al., 2005; Hülsen et al., 2016). During the period 2000-2005 the QASUME visited 27 spectroradiometers sites. Out of the 27 instruments, 13 showed deviations of less than 4% relative to the QASUME reference spectroradiometer in the UVB (for 15 instruments in the UVA) for solar zenith angles below 75°. The expanded relative uncertainty (coverage factor  $k=2$ ) of solar UV irradiance measurements by QASUME, for SZA smaller than 75° and wavelengths longer than 310 nm, was 4.6% in 2002 – 2014 (Gröbner and Sperfeld, 2005), and has been 2 % since 2014 (Hülsen et al., 2016). For broadband instruments, the current instrument uncertainties are summarized in (Hülsen et al., 2020; Hülsen et al., 2008). In 2017, 75 broad-band instruments measuring the UV index, the UVB or/and the UVA irradiance participated in the solar UV broadband radiometer comparison in Davos Switzerland. Using the instrument/user calibration factors, the differences between the datasets by the broad-band instruments and the reference (QASUME) dataset were within  $\pm 5$  % for 32 (43 %) of the instrument datasets,  $\pm 10$  % for 48 (64 %), and exceeded  $\pm 10$  for % 27 (35 %).

Although ground-based monitoring of solar UVR is more accurate than satellite retrievals, ground based stations are sparse, and the only way for continuous monitoring of the UVR on a global scale is through satellites. In recent decades instruments on-board satellites have provided the necessary data for estimates of UV irradiance reaching the Earth surface on a global scale (Herman, 2010) and hence satellite-derived UVR climatological studies have been conducted (Vitt et al., 2020; Verdebout, 2004). The satellite UV irradiance record started with the Total Ozone Mapping Spectrometer (TOMS) on-board Nimbus-7 in 1978 and continued with Ozone Monitoring Instrument (OMI) on-board NASA's satellite EOS-Aura. The OMI retrieval algorithm for surface UVR estimates was based on the experience gained from TOMS (Levelt et al., 2018; Levelt et al., 2006). The early surface UVR retrieval algorithms from satellite data didn't account for the enhanced aerosol absorption in the UV spectral range, resulting in overestimated values (Krotkov et al., 1998). A lot of scientific effort has been put into correcting the products (Arola et al., 2009). TROPospheric Monitoring Instrument (TROPOMI) onboard Sentinel – 5 Precursor (Lindfors et al., 2018) is the current satellite instrument that provides the surface UVR product on a daily basis with global coverage, including 36 UVR parameters. As the aforementioned instruments were installed onboard polar orbiting satellites, providing global spatial coverage, the temporal resolution of the data is daily since there are only one or two overpasses per day for every point. Geostationary satellites provide continuous (in time) measurements over wide areas. The geostationary meteorological satellites Meteosat monitor the full Earth Disk including Europe and their frequent data acquisition of rapidly changing parameters e.g., cloud is essential for estimating daily UV doses (Verdebout, 2000). Comparison of OMI surface UV irradiance estimates with ground-based measurements for Thessaloniki, Greece showed that OMI irradiances overestimate surface observations for UVB wavelengths by between ~1.5% to 13.5% in contrast to underestimated satellite values for UVA wavelengths (Zempila et al., 2016). Results from the validation of TROPOMI surface UV radiation product showed that most of the satellite data agreed within  $\pm 10\%$  with ground-based measurements for snow-free surfaces (Lakkala et al., 2020). Larger differences between satellite data and ground-based measurements were observed for sites with non-homogeneous topography and non-homogeneous surface albedo conditions. The differences between ground-based and satellite UVR data are mostly due to uncertainties in the input parameters to the satellite algorithm used to retrieve the UV irradiance at the surface. Based on a recent study of Garane et al. (2019) a mean bias of 0-1.5% and a mean standard deviation of 2.5 – 4.5 % was found for the relative difference between TROPOMI total ozone column (TOC) product and ground based quality assured Brewer and Dobson TOC measurements.

In this study we introduce a novel UV-Index Operating System, called UVIOS, which is able to efficiently combine information on geophysical input parameters from different modelled and satellite-based data sources in order to provide for the European region the best possible UV-Index (UVI) estimates operationally and in real-time. UVIOS is based on pre-calculated radiative transfer model simulations in the form of analytical look-up tables (LUT) in conjunction with geophysical input parameters and high performance computing for instantaneous outputs. The reliability of the UVIOS input and output parameters was tested for the year 2017 against ground-based measurements and an analytical sensitivity analysis was performed in order to quantify the uncertainties and to provide information about the limitations and about the optimum operating conditions of the proposed system. Since UVIOS can produce massive UVI outputs of the order of 1.5 million

simulations in less than 5 minutes following the proposed simulation and computing architecture (see section 2.1.2), this means that it can be used for both operational applications and real-time estimations. The exact use of UVIOS depends only on the available input data sources. For this study both nowcasts (clouds) and forecasts (ozone, aerosol) were used as inputs to the system. The nowcasts represent the continuous monitoring dimension (i.e. what is happening now) in terms of cloud microphysics data every 15 minutes retrieved in real-time by the geostationary satellite Meteosat Second Generation (MSG). The forecasts represent the future estimations (day ahead in our study) of aerosol optical properties and total ozone column based on deterministic approaches (ECMWF) and assimilated satellite data for better accuracy. As a result, UVIOS under cloudless conditions operates as a forecast system since it uses forecasted inputs and provides the clear-sky UVI forecasts operationally. By adding the nowcast cloud information as input to UVIOS (i.e. all sky conditions), the whole procedure will follow the time steps of MSG cloud microphysics data collocated and synchronized with the forecast data. So, following the proposed operation method of this study, the UVIOS can be used as a UVI forecast system for cloudless conditions or as a UVI nowcast system for all sky conditions.

In Section 2 we describe the UVIOS, the input data sources and the ground-based measurements used for the validation. Section 3 presents the results in terms of model performance and factors that affect the UVIOS retrievals and the overall accuracy. Finally, Section 4 summarizes the findings and the main conclusions of this study.

## **2 Data and Methodology**

### **2.1 The UV Index operating system (UVIOS)**

#### **2.1.1 UVIOS modelling**

The UVIOS system is a novel model that uses real-time and forecasted atmospheric inputs based on satellite retrievals and modelling techniques and databases in order to nowcast and forecast the UVI with a spatial resolution of 5 km and a temporal resolution of 15 minutes. The UVIOS calculation scheme is based on the libRadtran library of radiative transfer models (RTM) (Mayer and Kylling, 2005) within which all the available inputs (i.e. solar elevation, cloud and aerosol optical properties, ozone) can be integrated in real-time into the radiative transfer code and calculate the UVI for each pixel. Afterwards, post processing correction for the elevation of each location and the surface albedo is also performed. In order to be able to simulate the UVI for 1.5 million pixels in real-time we use pre-determined spectral solar irradiance LUTs based on the Libradtran RTM, in combination with high performance computing (HPC) architectures that speed up the process of choosing and interpolating/extrapolating the right combinations from the LUTs (Kosmopoulos et al., 2018; Taylor et al., 2016). The result is the retrieval of UVI for 1.5 million pixels covering the European domain in less than 5 minutes after receiving all necessary input parameters.

As mentioned the UVIOS architecture does not include a clear sky model and the subsequent calculation of individual sources of UV attenuation, but instead it directly uses the following parameters: solar zenith angle (SZA), the aerosol optical depth (AOD) and other aerosol optical properties (e.g., single scattering albedo (SSA), asymmetry parameter, and Ångström exponent (AE)), the total ozone column (TOC), the cloud optical thickness (COT), as well as the surface elevation (ELE) and the surface albedo (ALB) as RTM inputs. Table 1 presents the EO data used as inputs for the UVI real time simulations, their description and sources. The Meteosat Second Generation (MSG4) cloud microphysics includes the nowcasted cloud optical thickness (COT) at 550 nm, and cloud phase (CPH) obtained at a spatial and temporal resolutions of 5 km (average, depending on latitude) and 15 minutes, respectively. Typical values of other cloud properties (e.g., cloud height, cloud thickness) have been assumed based on the cloud type (information which is also available from MSG) (for more detailed information see Taylor et al. (2016)). The 1-day forecast CAMS aerosol optical depth (AOD) at 550 nm is obtained at a spatial and temporal resolutions of 40 km and 3 h, respectively and the monthly aerosol optical properties obtained from AeroCom (Kinne, 2019) includes asymmetry parameter, single scattering albedo (SSA) and Ångström exponent (AE) at  $1^\circ \times 1^\circ$  (latitude x longitude) spatial resolution. Solar elevation is taken from the Astronomical model (NREL) (5 km – 15 minutes) (Reda and Andreas, 2008) and climatological surface albedo (ALB) is retrieved from Copernicus Global Land Service (CGLS) (1 km – 12 days) (Carrer et al., 2010). Surface elevation (ELE) is obtained from the Digital Elevation Model (DEM) of NOAA (NOAA, 1988). The Tropospheric Emission Monitoring Internet Service (TEMIS) 1-day forecast of total ozone column (TOC) is at a spatial resolution of  $1^\circ \times 1^\circ$  – 1 day with assimilated ozone fields from GOME-2 (METOP-B) (Eskes et al., 2003). We have to mention also here that the selection of the RTM inputs has been decided based on their real-time availability.

### 2.1.2 UVIOS real-time processing concept

The LUT approach, despite its large size (almost 2.5 million spectral RTM simulations for clear and all sky conditions) (Kosmopoulos et al., 2018), still provides estimates at discrete input parameters values. To overcome this mathematical issue, we performed a multi-parametric interpolation technique to correct the input-output parameter intervals. This solution is computationally more costly than a continuous function-approximation model, i.e. a Neural Network (NN) model (Kosmopoulos et al., 2018), but the accuracy improvement is significant. Indicatively, using a test set of 1 million RTM simulations for UVI from the developed LUT, we applied the NN developed in Kosmopoulos et al. (2018) and found a mean execution time of around 144 seconds followed by a mean absolute error (MAE) of 0.0321, while by using the proposed UVIOS multi-parametric interpolation exploiting the HPC and distributed computing benefits we found for the same test set an execution time of 295 seconds with a MAE of 0.0001. The inclusion of many parameters (in this study we incorporated eight, i.e. AOD, SZA, TOC, COT, ELE, ALB, AE, SSA) with small step sizes dramatically increase the LUT size, followed by high computing requirements for the multi-parametric interpolation/extrapolation procedures.

For the UVIOS simulations performed in this study, a 32-core UNIX server was used equipped with 256 Gb of RAM and 12 Tb of storage system working in a RAID10 architecture. The combination of the HPC with the analytical LUTs, which were

developed by using the libRadtran RTM, allow a high speed multi-parametric interpolation and polynomial reconstruction (Gal, 1986) to increase accuracy between the LUT records following a mathematical equation relating the UVIOS outputs to the EO inputs.

An example of the UVIOS input output data is presented in Figure 1 through a flowchart illustration of the modelling technique scheme. The inputs, including the solar and surface elevation, albedo, aerosol, ozone forecasts and the cloud observations as described in Table 1, are fed to the real-time solver that results in spectrally weighted output of UVI for the European region. Figure 2 shows the memory usage and error statistics for a range of different LUT sizes. The LUT error decreases as the LUT size increases, regardless of the function being approximated. The LUT sizes in Figure 2 fit into cache on our HPC environment, thus performance in terms of processing speed and overall output accuracy vary only slightly between the table sizes shown. In our case, UVIOS shows that LUT transformation can provide a significant performance increase without incurring an unreasonable amount of error, provided there is sufficient memory available. We note that the cache size is a critical factor for LUT performance, while under a HPC environment practically there is no limit. Such techniques can be implemented in hardware with distributed computing that operates in parallel to provide optimum performance.

## **2.2 The description of the geophysical parameters**

The Cloud Optical Thickness (COT) data from Meteosat was used, whose retrieval algorithm is based on 0.6 and 1.6 micron channel radiances of Meteosat's Spinning Enhanced Visible and InfraRed Imager (SEVIRI). MSG products have been described in Derrien and Le Gléau (2005) and the MétéoFrance (2013) technical report. The COT impact uncertainty on UVI deals with the MSG COT reliability and accuracy and hence introduces errors into the UVIOS simulations (Derrien and Le Gléau, 2005; Pfeifroth et al., 2016). In addition, comparison principles of (point) station UVI measurements with a 5 km MSG COT matrix are possibly responsible for at least part of the observed deviations (e.g., Kazadzis et al. (2009a)). For instance, when a MSG pixel is partly cloudy, the ground measurements of UVI could fluctuate more than 100%, depending on whether the sun is visible or whether clouds attenuate the direct component of the solar irradiance. The result is that in cases of partly covered MSG pixels and in the absence of clouds between the ground measurement and the sun, the ground truth UVI would be much higher than the UVIOS one. Of course, the presence of small clouds which have not been identified by MSG and cover (part of) the sun disk, is plausible as well, consequently causing an overestimation of the modelled UVI (Koren et al., 2007). Furthermore, sensors onboard geostationary satellites suffer from the parallax error, which contributes to the spatial errors of the images and the overall uncertainty of the products (Bieliński, 2020; Henken et al., 2011). The error depends on the altitude of the cloud and the viewing angle (parallax errors are more significant for high viewing angles).

UVIOS calculations at high solar zenith angles ( $>70$  deg) are retrieved assuming cloudless skies since the MSG COT product is not available in these conditions, facing reliability issues (Kato and Marshak, 2009). This has an effect on the quality of the UVIOS overall performance at high solar zenith angles, where there is no cloud information as input to the model in order to quantify the consequent impact on UVI. However, such measurements under high solar zenith angles are accompanied with



264 very low UVI levels ( $<1$ ) both in the performed RTM simulations and in the ground-based measurements. This inconsistency,  
265 even if does not affect UVIOS UVI results associated with dangerous effects on human health, nevertheless it is still affected  
266 by the rest of input parameters (i.e. ozone, aerosol etc) mitigating the UVIOS uncertainty in the absence of cloud information  
267 under such high solar zenith angles. There is more discussion in the next section on how we use these data for the UVIOS  
268 validation.

269 For the total aerosol optical depth, we used 1-day forecast data from the Copernicus Atmospheric Monitoring Service (CAMS)  
270 as the basic input parameter. These forecasts are based on the Monitoring Atmospheric Composition and Climate (MACC)  
271 analysis and provide accurate data of aerosol optical depth (AOD) at 550 nm with a time step of 1 h and spatial resolution of  
272  $0.4^\circ$ . For aerosol single scattering albedo properties climatological values from MACv2 aerosol climatology (Kinne, 2019)  
273 was utilized. Monthly means of single scattering albedo at 310nm were acquired from global gridded data at a  $1^\circ \times 1^\circ$  spatial  
274 resolution. Also, in order to derive the Angstrom exponent, monthly means of AOD at 340nm and 550nm were used. The  
275 calculated Ångström exponent was then applied to the 550 nm AOD (from CAMS) in order to get AOD in the UV.

276 The surface albedo data were obtained from the Copernicus global land service (CGLS: Geiger et al., 2008; Carrer et al., 2010).  
277 As a global surface ALB product is not available in the UV region, for this study we have used the climatological product of  
278 CGLS (in the visible range) (Lacaze et al., 2013) as follows: based on the findings of Feister and Grewe (1995), we used a UV  
279 albedo of 0.05 for non-snow cases and a UV ALB equal with CGLS when CGLS exceeded 0.5 (snow cover). The total ozone  
280 column forecasts were obtained from Tropospheric Emission Monitoring Internet Service (TEMIS) which is a near- real time  
281 service which uses the satellite observations of total ozone column by the Global Ozone Monitoring Experiment (GOME) and  
282 SCIAMACHY assimilated in a transport model, driven by the European Centre for Medium-Range Weather Forecasts  
283 (ECMWF) forecast meteorological fields (Eskes et al., 2003). The elevation data was obtained from the 5-minute Gridded  
284 Global Relief Data (ETOPO5) database, which provides land and seafloor elevation information at a 5-minute  
285 latitude/longitude grid, with a 1-meter precision in the region of Europe and is freely available from NOAA (NOAA, 1988).  
286 An analytical description of the above geophysical parameters including their specifications and resolution can be found in  
287 Table 1, followed by the corresponding references for more technical details. Figure 3 shows an example of the input-output  
288 UVIOS parameters. An extensive validation of the MACC analysis and forecasting system products were performed by Eskes  
289 et al. (2015). The aerosol optical properties were validated against 3-year (Apr. 2011 – Aug. 2014) near real time level 1.5  
290 AERONET measurements and for AOD at 550 nm an overall overestimation was exhibited. Due to dedicated validation  
291 activity of the MACC service a validation report that covers the time period of this study (Eskes et al., 2018) is also available,  
292 presenting an overall positive modified normalized mean bias during 2017, ranging from 0 to 0.4, with the same range of  
293 values over the study region (Europe). This overestimation of AOD at 550 nm may explain some of the UVI underestimation  
294 under clear sky conditions (see section 3.2.2).

## 295 **2.3 Ground-based measurements**

296 In order to validate the UVIOS results 17 ground based stations were selected, for which measurements of the UVI were  
 297 available during 2017. The stations are shown in Fig. 4. Comparisons were performed with a 15-minute step. The ground based  
 298 measurements were obtained from spectrophotometers (Brewer), spectroradiometers (Bentham), filter radiometers (GUV) and  
 299 broadband instruments (SL501 and YES) as Table 2 shows. Note that UV data in table 2 has been calibrated, processed and  
 300 provided directly by the responsible scientists for each station. References wherein more information for the data quality of  
 301 particular instruments can be found are also provided. Brewer spectrophotometers measure the global spectral UV irradiance  
 302 with a step of 0.5 nm, and a resolution which is approximately 0.5 nm (usually between 0.4 and 0.6 nm). Depending on their  
 303 type the spectral range is usually 290-325 nm (MKII, MKIV) or 290-363 nm (MKIII.). Since Brewer spectrophotometers  
 304 measure the spectrum up to a wavelength which is shorter than 400 nm, extension of the spectrum up to 400 nm in order to  
 305 calculate the UV index is usually achieved using empirical methods (e.g., (Fioletov et al., 2003; Slaper et al., 1995)). The  
 306 additional uncertainty in the UVI due to the latter approximation is well below the overall uncertainty in the measurements.  
 307 Bentham spectroradiometers measure the whole UV spectrum (290 – 400 nm) with step and resolution which can be  
 308 determined by the operator. The spectra from AOS and LIN (measured by Bentham spectroradiometers) used in this study  
 309 have been recorded with a step of either 0.25 or 0.5 nm and a resolution of ~ 0.5 nm. The Brewer Spectrophotometer measures  
 310 the total column of ozone using the differential absorption method, i.e. measuring the direct solar irradiance at four wavelengths  
 311 and then comparing the intensity at wavelengths that are weakly and strongly absorbed by ozone (Kerr et al., 1985). Brewer  
 312 TOC measurements are used in the present document to validate the TEMIS forecasts. The Ground-based Ultraviolet (GUV)  
 313 instrument is a multichannel radiometer that measures UV radiation in five spectral bands having central wavelengths as 305,  
 314 313, 320, 340 and 380 nm. However, in addition to UV irradiances, other data that can be obtained from GUV instruments are  
 315 total ozone and the cloud optical depth (Dahlback, 1996; Lakkala et al., 2018). GUV measurements are used for LAN station  
 316 of Norway. At stations AKR, INN and VIE, the surface UV was measured using Solar Light (SL) 501 radiometers. It provides  
 317 direct observation of UV index with a frequency of one minute. The Yankee Environmental System (YES) has been used for  
 318 VAL station.

319 The low latitude stations include AKR, ARE, ATH, ROM, THE, and VAL. AKR has minimum altitude of 23 m and VAL has  
 320 maximum altitude of 705 m above sea level. The middle latitude locations are AOS, DAV, INN, BEL, LIN, MAN, UCC, and  
 321 VIE among which the minimum altitude is 10 m in LAN and maximum altitude is in DAV at 1610 m above mean sea level.  
 322 HEL, LAN, and SOD represent the high latitude zone, with HEL having an altitude of 48 m and SOD an altitude of 185 m  
 323 above mean sea level (Table 2). A summary of basic climatic information for the validation locations was obtained from the  
 324 Köppen climate classification (Chen and Chen, 2013) and it is summarized here. THE, AKR, ARE, ROM, ATH and VAL  
 325 have a Mediterranean climate comprising of mild, wet winters and dry summers. MAN experiences maritime climate (cool  
 326 summer and cool, but not very cold, winter). AOS, UCC, LAN, BEL, HEL, LIN and VIE experience humid continental climate  
 327 with warm to hot summers, cold winters and precipitation distributed throughout the year. DAV and INN experience boreal  
 328 climate characterised by long, usually very cold winters, and short, cool to mild summers. SOD has subarctic climate having  
 329 very cold winters and mild summers.

## 2.4 Evaluation methodology

The time series period covers the whole year 2017 at 15-min intervals, following the MSG available time steps. A synchronization between the UVIOS simulations and the ground-based measurements was performed in order to match the 15-min intervals of UVIOS to the measured data. The UVIOS data availability is 93%, while for the ground stations it reaches almost 79% enabling a direct UVI data comparison of 77% of the 2017 time steps. For the comparison we used the closest instrument measurements to the 15-min intervals with a maximum deviation of 3 minutes in order to avoid solar elevation and cloud presence mismatches. Additionally, the UVIOS comparisons included measurements up to 70 degrees SZA. The rationale for this cutoff was that UVIOS retrievals at high SZA are retrieved as cloudless as COT is unavailable from MSG. In addition, the comparison is also impacted by limitation of the horizon of ground-based sites (e.g., Davos, Innsbruck, Aosta) where the diffuse component and in some cases the direct component of solar UV irradiance are affected by obstacles (mountains) on the horizon. The contribution of this mainly diffuse irradiance to the total budget is a function of solar elevation and azimuth (day of the year) and also cloudiness. Although UVIOS simulations were corrected for changing UVI with respect to altitude (see Section 3.2.3), the correction cannot be perfect for higher altitude stations. The reason is that it is not possible to take into account all different factors (aerosol load and properties, atmospheric pressure, surface albedo) (e.g., Blumthaler et al., 1997; Chubarova et al., 2016) which affect the change of UVI with altitude. This explains some of the deviations in the results as the UVIOS retrieves UVI assuming a flat horizon. Clear sky conditions were defined as the UVIOS retrieval where MSG COT equals to zero. Further discussion on the uncertainties introduced by this choice is mentioned in the cloud effect section.

Most of the comparisons have been performed using the absolute (mean bias or median) UVI differences (model – measurements). In addition, median values of the percentage differences ( $100 \cdot (\text{model} - \text{measurements}) / \text{measurements}$ ) have been used. UVIOS estimations were also evaluated in terms of mean bias and root mean square error (MBE and RMSE, respectively), defined as follows:

$$\text{MBE} = \bar{\varepsilon} = \frac{1}{N} \sum_{i=1}^N \varepsilon_i \quad (1) \quad \text{RMSE} = \sqrt{\frac{1}{N} \sum_{i=1}^N \varepsilon_i^2} \quad (2)$$

Where  $\varepsilon_i = x_f - x_o$  are the residuals (UVIOS errors), calculated as the difference between the simulated values ( $x_f$ ) and the ground-based values ( $x_o$ ), and where N is the total number of values. MBE quantifies the overall bias and detects whether the UVIOS overestimates (MBE>0) or underestimates (MBE<0). RMSE quantifies the spread of the error distribution. Finally, the correlation coefficient (r), as well as the coefficient of determination ( $R^2$ ) were used to represent the proportion of the variability between modeled and measured values.

## 3 Results

### 3.1 Overall performance of the UVIOS system

Fig. 5 presents a scatterplot of the UVIOS simulations for all stations as compared to the ground-based measurements, which is followed by a correlation coefficient ( $r$ ) of 0.944. For a more detailed view of the UVIOS performance, Fig. 6 depicts a Taylor diagram with the overall model accuracy for all ground stations under all sky and clear sky conditions as a function of the correlation coefficient, normalized standard deviation and RMSE. For both, clear sky and all sky conditions, the results are similar. The absolute differences between the UVIOS and the measured UVI are within  $\pm 0.5$ , and the correlation coefficients are between 0.85 and 0.99 for all stations. The RMSE is for most stations less than 0.5. Under all sky conditions the RMSE is higher relative to the RMSE for clear skies for MAN, DAV and SOD, which is probably due to misclassification of cloudy pixels (see also the Appendix A section). Relative differences can be misleading as they may correspond to very small absolute differences without physical meaning, especially for low levels of the UVI. Thus, we focused on absolute differences in order to have a more representative assessment of the actual effect (UV Index) and its results. The differences were categorized to low (less than 0.5), moderate (0.5 - 1) and high (more than 1). In the Appendix A, relative differences are also discussed. In Table 3, U1.0 and U0.5 represent the percentage of cases with absolute differences between modelled and ground based UVI measurements within 1 and 0.5, respectively, for all comparisons between the 15-minute model retrievals and the corresponding ground-based measurements. As shown in Table 3, for all stations and for both, clear- and all sky conditions, differences were within 0.5 UVI for at least 70% of the cases. Under clear sky conditions, AOS, BEL, HEL, LAN, LIN, SOD and THE had above 90% of U0.5 cases, while others have 75-90% of U0.5 cases. All stations but DAV had above 90% of U1.0 cases for clear skies, while the correlation coefficients for most of the stations were above 0.9 (exceptions are ATH and MAN). For all-skies differences were within 1 UVI for 90% of the cases for all stations with the correlation coefficients exceeding 0.9 for most of them (exceptions are DAV, MAN and SOD). Median differences for all skies for every station were well within  $\pm 0.2$  UVI, with the 25-75 percentiles being within  $\pm 0.5$  UVI and the 5-95 percentiles within  $\pm 1$  UVI. For clear skies the corresponding values are  $\pm 0.1$ ,  $\pm 0.4$  and  $\pm 0.8$  respectively. In the following sections we try to investigate the factors that contribute to the differences between UVIOS and ground-based measurements.

## 3.2 Factors affecting UVIOS retrievals

### 3.2.1 Ozone effect

All the available collocated Total Ozone Column (TOC) measurements for the stations used in UVIOS evaluation have been obtained from the WOUDC (<https://woudc.org/>) database. In this database 8 out of 17 UVIOS evaluation stations (AOS, ATH, DAV, MAN, ROM, SOD, THE and UCC) were found, providing TOC ground-based measurements. TOC comparison has been performed by calculating daily means of ground-based measurements and the TOC from TEMIS. In order to quantify the effect of the uncertainty of the forecasted TOC used as input at UVIOS we have calculated the mean differences of the forecasted and measured TOCs and used a radiative transfer model to investigate their effect on UVIOS retrieved UVI. Table 4 shows the mean differences in D.U. from TEMIS TOC (used as inputs in UVIOS) as compared to the WOUDC ground-based measurements for one year of comparison data. It is seen that for the stations AOS, DAV, MAN and UCC the values of

the TEMIS observations are higher as compared to the ground-based measurements (by 7.6, 1.9, 5, and 2.9 DU respectively) while for the other stations TEMIS observations are lower (by 0.9, 5.4, 9.9, and 2.2 DU for ATH, ROM, SOD, and THE respectively). The negative bias is seen to be highest for ROM station (-9.9) and the positive bias is highest for AOS station (7.6). Part of the large differences over the complex terrain sites can be explained by the difference between the actual altitude of the station and the average altitude of the corresponding grid points of TEMIS. For example, for AOS the average altitude of the pixel is 2000 m while the real altitude of the station is 570 m, resulting in an underestimation of the tropospheric column of ozone by TEMIS. In general, differences can be explained by the combined effects of uncertainties in TOC retrieval from satellite and ground-based platforms (Rimmer et al., 2018; Boynard et al., 2018; Garane et al., 2018). Figure 7 shows the effect of this TOC bias on the calculated UVIOS. As seen in Table 4, there is a mix of small underestimation and overestimation cases in the TOCs used within UVIOS, with average absolute differences of 4-5 DU. Worst TOC UVIOS inputs were found in AOS and ROM (7.6 and -9.9 DU) leading to maximum (at 30 degrees SZA) differences in UVI of -0.22 and 0.3 for AOS and ROM, respectively. In general, in most of the cases UVI mean differences are less than 0.1. It has to be noted that the TOC differences have a larger impact when expressed in percent at higher SZAs, while in Figure 7 higher absolute differences for low SZA's are associated with higher UVIs at these SZAs. Detailed comparisons for each station are shown in the Appendix A figures.

### 3.2.2 Aerosol effect

Aerosol optical depth measurements used for the UVIOS aerosol input evaluation have been collected from the AERONET-NASA web site (Giles et al., 2019) for 12 out of our total 17 stations (AKR, ARE, ATH, DAV, HEL, LIN, ROM, SOD, THE, UCC, VAL and VIE. AERONET (level 2, version 3) values of AOD at 500 nm were interpolated at 550nm using the AERONET derived 440-870nm Angstrom exponent for each individual measurement. In order to compare those measurements with CAMS forecasted AOD used for the UVIOS their daily means were derived. The comparison of forecasted and measured daily means was based on all available data due to gaps in the AERONET time series. The AOD MBE and RMSE statistical scores are shown in Table 5 in absolute units and correlation coefficient as well. All the stations have a mean positive bias up to 0.071 except UCC which is showing a mean negative bias of 0.007. The comparison of all individual stations with CAMS data used as inputs on UVIOS showed that under all cases CAMS AOD is higher than that from AERONET with a mean difference of 0.07 at 550nm. The correlation between the modeled and the measured values varies from 0.10 for VIE to 0.91 for ARE with most of the stations showing the correlation coefficient above 0.7. As in the case of the TOC, AOD CAMS data are forecasts from the previous day and real time WOUDC or AERONET level 2.0 data do not exist. Although real time TOC (and in due course AOD in the UV) is available from Eubrewnet (López-Solano et al., 2018; Rimmer et al., 2018), it is only for particular locations and not for the whole European domain. Thus, the only choice in providing for a real time UV Index for Europe is using the CAMS (for AOD) and the TEMIS (for TOC) data.

423 In order to evaluate the effect of AOD on UVI, UVI differences between the UVIOS using both AOD datasets (CAMS and  
 424 AERONET) as UVIOS inputs were analyzed. Figure 8 shows the mean bias error of the CAMS – AERONET AOD impact on  
 425 UVI for all stations with available ground based AOD data as a function of SZA together with the uncertainty range ( $\pm 1 \sigma$ ).  
 426 It can be seen that UVIOS with CAMS AOD input underestimates UVI compared to the UVIOS with AERONET data, except  
 427 for the UCC station. This is consistent with CAMS overestimations of AOD compared to the AERONET measurements,  
 428 except for the station UCC as shown in Table 5. Higher aerosol levels in the atmosphere tend to lower the UVI. Highest  
 429 difference in UVI is observed for the stations HEL, SOD, VIE. Since, the aerosol level at the stations HEL and SOD is very  
 430 low, the percent difference between the AOD from CAMS and AERONET is larger for these stations (although the absolute  
 431 difference is similar) relative to stations with higher AOD, leading to higher differences in the UVI. Aerosol content for VIE  
 432 is higher than HEL and SOD but still within 0.2 which might be the reason for the higher UVI difference. In terms of SZA, it  
 433 is observed that the mean bias decreases with an increase in the SZA as the values of UVI also decrease with SZA and the  
 434 most deviation is for station VIE which is consistent with the poor correlation between the CAMS forecasted input and the  
 435 measurements for this station as seen from Table 5.

436 The use of single scattering albedo in the UV region is a difficult task and many studies have shown that such measurements  
 437 need extra effort and it is not possible to perform them worldwide (Arola et al., 2009; Kazadzis et al., 2016; Raptis et al.,  
 438 2018). The monthly values of the single scattering albedo used in UVIOS for the UV region were derived from the MACv2  
 439 database at the 310 nm wavelength (Kinne, 2019). Fig 9 shows the intra annual variability of SSA for the 17 stations. For all  
 440 stations, SSA values range from 0.76 to 0.93, with most of them having SSA values between 0.83 to 0.93, and relatively small  
 441 variability. In contrast, there are stations like ARE, BEL, INN, LIN, VIE and THE which have relatively smaller SSA values  
 442 (0.76-0.9) and greater variability than the other stations.

### 443 **3.2.3 Albedo effect & surface elevation correction**

444 Surface albedo at UV wavelengths is small (2 – 5%) for most types of surfaces (Feister and Grewe, 1995; Madronich, 1993)  
 445 except for features like sand (with a typical albedo of ~0.3) and snow (up to 1 for fresh snow) (Meinander et al., 2013; Myhre  
 446 and Myhre, 2003; Vanicek et al., 2000; Henderson-Sellers and Wilson, 1983). Renaud et al. (2000), found an enhancement of  
 447 about 15 to 25% in UVI for clear-skies and snow conditions due to the multiple ground-atmosphere reflections and this relative  
 448 increment was about 80% larger for overcast conditions. The combined effect of aerosols and snow lead to an enhancement of  
 449 about 50% in UVI in cloud-free condition for moderately polluted atmospheres (Badosa and Van Weele, 2002). Fig. 10 (a)  
 450 presents the effect of surface albedo on the UVI percentage difference (i.e. for various albedo values under clear sky conditions)  
 451 as a function of SZA, while Fig. 10 (b) shows the effect of surface elevation on UVI as a function of the percentage difference  
 452 for various total ozone columns. It is observed that the UVI percentage difference increases almost linearly with albedo for a  
 453 particular SZA and the variation is found to be almost identical for all SZA. This indicates that the UVI percentage difference  
 454 is independent of the SZA and increases with surface albedo. The UVI percentage difference is found also to increase almost

linearly with the increase in elevation for a particular total ozone column. The percentage difference is similar for all ozone columns up to 1km, after which the differences with ozone column become more apparent. That is, at a particular elevation, the percentage difference is higher for less total ozone column. A 1% fluctuation (decline or increase) in column ozone can lead to about a 1.2% fluctuation (increase or decline) in the UV Index (Fioletov et al., 2003; Probst et al., 2012). Indicatively, the average maximum surface elevation correction in terms of UVI for the DAV station (due to UVIOS input deviation from to actual elevation) was of the order of 1.6 (15%), while for INN and AOS it was 0.5 and 0.6 respectively (6%) and for the VAL station close to 0.8 (8%).

Uncertainties introduced in UVIOS from the use of a constant surface albedo value of 0.05 for non-snow conditions are quite low. For the case of albedo values used for snow conditions based on the CGLS monthly mean product uncertainties can be related to: the small difference of UV and visible albedo values; the fact that the CGLS provides an albedo of a certain area around the station that does not necessarily coincide with the “effective” albedo area affecting UV measurements; and finally that the monthly albedo product represents a monthly average while a real time CGLS product represents the last 12 days (dynamically changing albedo). In order to investigate this last point, we have compared the UV effects from the use of the two albedo datasets for DAV station, where the average difference between an example ground-based dataset and UVIOS was found to be 0.14 UVI (Gröbner, 2021). In Fig. 11, the effect of surface albedo correction is shown for the Davos station, for a period with snow cover and low percentage cloudiness. The climatological and the dynamically changing albedo are presented in terms of percentage differences between modelled and ground measurements as a function of SZA. In the case of climatological albedo, most of the percentage difference between forecasted and the measured UVI value is found to vary from -30% to 10% for SZA between 20° to 70°, showing more underestimation than overestimation from the UVIOS simulations. Similarly, in the case of dynamically changing albedo, most of the percentage difference between forecasted and the measured UVI value is found to vary from -20% to 10% for SZA between 20° to 70°. The mean percentage difference between the results using the two different albedo inputs is -2.76% in terms of accuracy improvement. However, beyond 70 degree SZA, there is a huge variation in the percentage difference with mostly underestimations from the UVIOS simulations (not shown in Fig. 11).

#### 3.2.4 Cloud effect

For the evaluation we used measurements at SZA lower than 70 degrees, based on the lack of cloud input from MSG for higher SZAs. The lack of MSG data results in an overestimation of UVIOS in high SZAs and the UVI is systematically overestimated for long periods during winter at high latitude regions when SZA does not get below 70 degrees during the day. However, based on the simulations performed by UVIOS, this overestimation is low in terms of absolute UVI and does not usually exceed 0.2 UVI because maximum UVIs at such SZAs rarely exceed UVI=1.

COT retrieved from the MSG satellite has been used as input for the UVIOS together with typical optical properties of the clouds as discussed in Sect. 2.1. The evaluation of all stations for cloudless and cloudy conditions can be seen in Figure 12

that shows the relative frequency distribution of all stations (colours) and the mean (black line) for cloudless (upper plot) and cloudy conditions (lower plot). Mean bias error of the modeled by UVIOS and measured UVI for all- and clear sky conditions and the percentage of clear sky time steps data is presented in Figure 13. The mean bias for clear sky conditions is found to be less than that for the all sky conditions for the stations AKR, ATH and THE (having most days of the year being cloudless as the clear sky percentage is above 70%). The MBE for DAV, LIN and MAN is less for clear sky relative to all sky conditions even though most days of the year are cloudy (clear sky annual percentage less than 45%) at the particular stations. While, stations BEL, HEL, INN, LAN, SOD, UCC and VIE, that have mostly cloudy skies throughout the year (clear sky annual percentage less than 50%), are having more MBE for clear sky conditions than the all sky condition. This can be due to the erroneous classification of a cloudy sky as clear sky, which is also discussed in the following section. MBE is also larger for AOS and ARE which have mostly clear skies throughout the year. Stations ROM and VAL have comparatively much smaller MBE for clear sky conditions.

As shown in Table 6 there are 45.4% of cases with underestimations and 54.6% cases with overestimations for cloudless conditions (COT=0). For all the other cases, overestimations (62.5%) are more predominant than underestimations (37.5%). The difference in the modelled and the measured values goes beyond  $\pm 1$  UVI for only 5.1% cases for cloudless conditions and 14.7% for all other cases. In general, under cloudy conditions, UVIOS shows an overestimation for UVI in contrast to the ground measurements. One explanation for the overestimations could be the erroneous determination of COT from MSG above the ground-based stations, giving cloud input that can be overestimated or underestimated. The results show that there is a general tendency for a small underestimation of MSG COT that leads to a systematic but small UVIOS UVI overestimation under cloudy conditions. Another possible explanation is the spatial representativeness of MSG COT. The MSG COT determination is available at 5 by 5 km pixels that may differ from the actual situation of the cloud prevailing above the station, especially in broken cloud conditions and in case when it blocks the direct radiation from the sun. Moreover, for lower solar elevations, the direct sun irradiance can be blocked by cloud in neighbouring pixels. The first effect has been explored in the relative frequency distribution of Figure 12 that shows a higher number (~ 63%) of data on the right of the zero UVI difference vertical line for cloudy skies. When comparing data outside the 0.5 and 1 difference limits we also see that 1 – 4 times more data show a UVIOS overestimation as compared to the clear sky case. This shows that in general there is a small (in UVI terms) but significant UVIOS overestimation for non-zero COT conditions. Moreover, for clear skies, as determined from the MSG, we observe a less pronounced UVIOS overestimation that corresponds to the fact that even if MSG defines the situation as completely cloudless, in reality there may be some cases where clouds near the ground-based station affect the measured UVI. This effect is easier to understand when showing these differences as a function of solar zenith angle which is explored through Figure 14. It is observed that the absolute difference between the modelled and the measured values decreases with increasing solar zenith angle and most of the difference lies within  $\pm 4$  UVI. The seasonal variation of the percentage UVI difference as a function of SZA shows that while absolute UVI is small in winter the percentage difference is higher compared to other seasons.



Figure 15 (a) shows the shadow volume at the surface level of a cloud, relative to the SEVIRI angle view, as a function of cloud height and SZA, highlighting the ray tracing in the presence of clouds and the accompanied angular dependence due to the 3D geometry. 15 (b) shows the scatter of the UVI difference under clear sky conditions for all stations as a function of SZA. It is observed that there is an obvious pattern of scattered data for UVI differences higher than 1.5 compared with the ones for differences less than -1.5. These data represent UVIOS overestimation for UVI retrievals due to the underestimation of the cloudiness just above the stations. These data illustrate the well-known spatial representativeness issues whereby a COT value for a satellite grid is not fully representative of a point measurement station. In addition, absolute and percentage relative differences are shown in Fig. 15 (c) and (d) respectively for SZA up to 65 degrees. The differences between the UVIOS and the ground-based UVI decreases in absolute level but increases in percent with an increase in SZA. This is due to the decrease of UVI with increasing SZA. Modelled and the measured UVI difference is close to zero both for mean and median values. For SZA below 30 degrees, differences are 0 to -0.2, while 20 to 80 percentiles range from -0.6 to -0.2. Percentage difference increases with SZA as absolute UVI decreases with the 20 to 80 percentiles showing differences between -10% and 10%

#### 4. Summary and conclusions

In this study, a fast RTM model of UVI, the so-called UVIOS, using inputs of the SZA, aerosol optical depth, total ozone column, cloud optical depth, elevation and surface albedo that implicitly includes temporal effects and the effect of cloud and aerosol physics, allows for the generation of high-resolution maps of UVI. Ground based measurements of UV are the most accurate way to determine this important health related parameter. However, such stations are sparse and hence, satellite observations can be used in order to have a nowcasted UV service. To date polar orbiting satellites like TOMS, OMI and recently TROPOMI provided a global UV dataset with a major disadvantage being the temporal resolution (one measurement per day). This, combined with the large temporal variability of clouds can lead to huge deviations from reality when a single daily measurement is included. Geostationary satellite, MSG, have been used in order to try to improve on such limitations using cloud information every 15 minutes.

Comparison of the forecasted and the ground-based measurements indicated that at least 70% and 80% of comparisons were within 0.5 UVI difference for all sky condition and clear sky, respectively. The mean differences TEMIS TOC and the ground measured TOC from the WOUDC for one year of comparison data showed that TEMIS tends to slightly overestimate the TOC for some stations along with underestimating it for other stations. While, in general, in most of the cases UVI mean differences are less than 0.1, the TOC differences have a larger impact in percent UVI differences at higher SZAs. Such small differences can also be the result of daily TOC variation not captured in TEMIS.

CAMS AOD seems to be slightly overestimated as compared with AERONET data that leads to a UVIOS underestimation. CAMS data are found to overestimate the AOD from AERONET measurements with a mean difference of 0.07 at 500 nm. All the stations have a mean positive bias up to 0.071 except one station that had a mean negative bias of 0.007. The analysis of the impact of the mean bias error of the CAMS – AERONET AOD impact on UVI for all stations showed that the mean

bias decreases with an increase in the SZA as the values of UVI also decreases with SZA. The greatest deviation is for station VIE which is consistent with the poor correlation between the CAMS forecasted input and the measurements for this station. The real time data provision approach of UVIOS requires using a maximum of one-day ozone and aerosol forecast using the TEMIS and CAMS service respectively. Uncertainties in the used SSA increase the overall uncertainty of the simulated UVI, especially for high levels of atmospheric aerosols. However, as systematic SSA measurements in the UV region are not available, quantification of these uncertainties were not possible.

Cloudy conditions show high percentage differences but low UVI differences, and have a general tendency to lead to a UVIOS overestimation. It was found that 45.4% of cases have underestimations while 54.6% cases have overestimations for the cloudless conditions, while overestimations (62.5%) were more predominant than underestimations (37.5%) for all the other cases. In general, UVIOS showed an overestimation for UVI in contrast to the ground measurements under cloudy conditions with the difference in the modeled and the measured values going beyond  $\pm 1$  for 5.1% cases for cloudless conditions and 14.7% for all other cases. At individual stations the results for cloudless sky conditions, which are the most important for health related issues, showed good agreement. In general, ~85% of all and 95% of cloudless cases are within 1 UVI difference. The relative percentage biases can be large for low UVI cases due to clouds or at high SZAs, above  $75^\circ$ , due to the absence of accurate information for clouds. The results show that there is a general tendency of small underestimation of MSG COT that leads to a systematic but small UVIOS overestimation under cloudy conditions. Another possible explanation is the spatial representativeness issues between a satellite and a single point on the ground.

Using climatological surface albedo has little impact at low albedo sites but mainly leads to underestimations in UVIOS simulations for high albedo situations (snow cover). Most of the percentage difference between forecasted and the measured UVI values varied from -30% to 10% for SZA between  $20^\circ$  to  $70^\circ$  (climate albedo), while it was found to vary from -20% to 10% for dynamically changing albedo. Since high surface albedo conditions correspond to winter months (i.e. high SZAs and relatively low UVI) for the stations used in the study, the corresponding absolute differences in the UVI are generally smaller than 2 UVI. However, there was a huge variation in the percentage difference beyond 70 degree SZA with mostly underestimations from the UVIOS simulations. Finally, for uncertainties in elevation inputs, the UVI percentage difference is found to increase almost linearly with the increase in elevation for a particular total ozone column and beyond that, it is seen that the rate of increase in the percentage difference decreases with increase in the total ozone column.

UVIOS system forms a novel tool for widespread estimations of UVI using real-time and forecasted EO inputs. UVIOS utilizes the MSG domain with high spatiotemporal resolution, producing outputs within acceptable limits of accuracy for UV health related applications. It captures basic cloud features and all major atmospheric and geospatial parameters that affect UVI. Under cloudless conditions it performs to within the uncertainty of the ground based measurements to which it has been compared. Further development and improvement of the model can be achieved in the future. Meteosat Third Generation (MTG) satellites are expected to be launched in the following years and give aerosol and cloud products which would improve the performance of nowcast and forecast UV models when used as inputs. A future goal is to compare the UVIOS accuracy under cloudy conditions by using, (i) the current MSG cloud information (5 km, 15 min), (ii) the ECMWF forecast cloud

586 information (4 km, 1 hour) and (iii) the forthcoming MTG cloud information (500m, 5 min), in order to quantify the  
587 uncertainties of the forecasted cloud data as compared to the satellite observations, as well as the overall improvement of the  
588 MTG data compared to the MSG due to the MTG's higher resolution.

#### 589 **Author contribution**

590 PGK was responsible for the design of the study and the whole analysis, with support from SK, AWS, PIR, KP, IF, AM and  
591 J.G. PGK and SK are the developers of UVIOS. All authors contributed to editing the paper.

#### 592 **Code/Data availability**

593 All data used as inputs to the UVIOS system are open access, while all data sets produced by the UVIOS for the purposes of  
594 this paper can be requested from the corresponding author. The ground-based measurements can be requested from the PIs of  
595 the stations. The UVIOS suite of algorithms and LUTs can be used for various applications after consultation with the  
596 corresponding author.

#### 597 **Competing interests**

598 The authors declare that they have no conflict of interest.

#### 599 **Acknowledgements**

600 We acknowledge the Eumetsat SAFNWC, the Copernicus and TEMIS services as well as the Aerocom and GOME teams for  
601 providing all the necessary data used in this study. We would like to thank the 17 site instrument operators and technical staff  
602 that made the ground based measurements feasible.

#### 603 **Financial support**

604 The UVIOS development received no specific grant from any funding agency in the public, commercial, or not-for-profit  
605 sectors. The evaluation part of this study has been partly funded by the European Commission project EuroGEO e-shape (grant  
606 agreement No 820852).

607 **References**

- 608 Andrady, A.L., Aucamp, P.J., Austin, A.T., Bais, A.F., Ballare, C.L., Barnes, P.W., Bernhard, G.H., Bornman, J.F., Caldwell,  
609 M.M., de Gruijl, F.R., and Erickson, D.J.: Environmental effects of ozone depletion and its interactions with climate change:  
610 2014 assessment executive summary. *Photochemical and Photobiological Sciences* 14(1), 14-18, 10.1039/c4pp90042a, 2015.
- 611 Arola, A., Kazadzis, S., Lindfors, A., Krotkov, N., Kujanpää, J., Tamminen, J., Bais, A., di Sarra, A., Villaplana, J. M.,  
612 Brogniez, C., Siani, A. M., Janouch, M., Weihs, P., Webb, A., Koskela, T., Kouremeti, N., Meloni, D., Buchard, V., Auriol,  
613 F., Ialongo, I., Staneck, M., Simic, S., Smedley, A., and Kinne, S.: A new approach to correct for absorbing aerosols in OMI  
614 UV, *Geophysical Research Letters*, 36, 10.1029/2009gl041137, 2009.
- 615 Badosa, J., and Van Weele, M.: Effects of aerosols on UV-index, KNMI Scientific Report WR-2002-07, 2002.
- 616 Badosa, J., Calbó, J., McKenzie, R., Liley, B., González, J.-A., Forgan, B., and Long, C. N.: Two Methods for Retrieving UV  
617 Index for All Cloud Conditions from Sky Imager Products or Total SW Radiation Measurements, *Photochemistry and*  
618 *Photobiology*, 90, 941-951, <https://doi.org/10.1111/php.12272>, 2014.
- 619 Bais, A. F., Zerefos, C. S., Meleti, C., Ziomas, I. C., and Tourpali, K.: Spectral measurements of solar UVB radiation and its  
620 relations to total ozone, SO<sub>2</sub>, and clouds, *Journal of Geophysical Research: Atmospheres*, 98, 5199-5204, 10.1029/92jd02904,  
621 1993.
- 622 Bais, A. F., Lucas, R. M., Bornman, J. F., Williamson, C. E., Sulzberger, B., Austin, A. T., Wilson, S. R., Andrady, A. L.,  
623 Bernhard, G., McKenzie, R. L., Aucamp, P. J., Madronich, S., Neale, R. E., Yazar, S., Young, A. R., de Gruijl, F. R., Norval,  
624 M., Takizawa, Y., Barnes, P. W., Robson, T. M., Robinson, S. A., Ballaré, C. L., Flint, S. D., Neale, P. J., Hylander, S., Rose,  
625 K. C., Wängberg, S. Å., Häder, D. P., Worrest, R. C., Zepp, R. G., Paul, N. D., Cory, R. M., Solomon, K. R., Longstreth, J.,  
626 Pandey, K. K., Redhwi, H. H., Torikai, A., and Heikkilä, A. M.: Environmental effects of ozone depletion, UV radiation and  
627 interactions with climate change: UNEP Environmental Effects Assessment Panel, update 2017, *Photochemical &*  
628 *Photobiological Sciences*, 17, 127-179, 10.1039/c7pp90043k, 2018.
- 629 Bais, A. F., Bernhard, G., McKenzie, R. L., Aucamp, P. J., Young, P. J., Ilyas, M., Jöckel, P., and Deushi, M.: Ozone–climate  
630 interactions and effects on solar ultraviolet radiation, *Photochemical & Photobiological Sciences*, 18, 602-640,  
631 10.1039/c8pp90059k, 2019.
- 632 Bernhard, G.: Trends of solar ultraviolet irradiance at Barrow, Alaska, and the effect of measurement uncertainties on trend  
633 detection, *Atmos. Chem. Phys.*, 11, 13029-13045, 10.5194/acp-11-13029-2011, 2011.
- 634 Bernhard, G., and Stierle, S.: Trends of UV Radiation in Antarctica, *Atmosphere*, 11, 10.3390/atmos11080795, 2020.
- 635 Bieliński, T.: A Parallax Shift Effect Correction Based on Cloud Height for Geostationary Satellites and Radar Observations,  
636 *Remote Sensing*, 12, 10.3390/rs12030365, 2020.
- 637 Blumthaler, M., and Ambach, W.: SOLAR UVB-ALBEDO OF VARIOUS SURFACES, *Photochemistry and Photobiology*,  
638 48, 85-88, <https://doi.org/10.1111/j.1751-1097.1988.tb02790.x>, 1988.
- 639 Blumthaler, M., Ambach, W., and Ellinger, R.: Increase in solar UV radiation with altitude, *Journal of Photochemistry and*  
640 *Photobiology B: Biology*, 39, 130-134, [https://doi.org/10.1016/S1011-1344\(96\)00018-8](https://doi.org/10.1016/S1011-1344(96)00018-8), 1997.
- 641 Boynard, A., Hurtmans, D., Garane, K., Goutail, F., Hadji-Lazaro, J., Koukouli, M. E., Wespes, C., Vigouroux, C., Keppens,  
642 A., Pommereau, J. P., Pazmino, A., Balis, D., Loyola, D., Valks, P., Sussmann, R., Smale, D., Coheur, P. F., and Clerbaux,

643 C.: Validation of the IASI FORLI/EUMETSAT ozone products using satellite (GOME-2), ground-based (Brewer–Dobson,  
644 SAOZ, FTIR) and ozonesonde measurements, *Atmos. Meas. Tech.*, 11, 5125-5152, 10.5194/amt-11-5125-2018, 2018.

645 Carrer, D., Roujean, J.-L., and Meurey, C.: Comparing Operational MSG/SEVIRI Land Surface Albedo Products From Land  
646 SAF With Ground Measurements and MODIS, *IEEE Transactions on Geoscience and Remote Sensing*, 48, 1714-1728,  
647 10.1109/TGRS.2009.2034530, 2010.

648 Cede, A., Herman, J., Richter, A., Krotkov, N., and Burrows, J.: Measurements of nitrogen dioxide total column amounts using  
649 a Brewer double spectrophotometer in direct Sun mode, *Journal of Geophysical Research: Atmospheres*, 111,  
650 <https://doi.org/10.1029/2005JD006585>, 2006.

651 Chubarova, N., Zhdanova, Y., and Nezval, Y.: A new parameterization of the UV irradiance altitude dependence for clear-sky  
652 conditions and its application in the on-line UV tool over Northern Eurasia. *Atmos. Chem. Phys.*, 16, 11867-11881,  
653 10.5194/acp-16-11867-2016, 2016.

654 Chubarova, N.E., Pastukhova, A.S., Zhdanova, E.Y., Volpert, E.V., Smyshlyaev, S.P., and Galin, V.Y.: Effects of ozone and  
655 clouds on temporal variability of surface UV radiation and UV resources over Northern Eurasia derived from measurements  
656 and modeling. *Atmosphere*, 11(1), 59, 10.3390/atmos11010059, 2020.

657 Corr, C. A., Krotkov, N., Madronich, S., Slusser, J. R., Holben, B., Gao, W., Flynn, J., Lefer, B., and Kreidenweis, S. M.:  
658 Retrieval of aerosol single scattering albedo at ultraviolet wavelengths at the T1 site during MILAGRO, *Atmos. Chem. Phys.*,  
659 9, 5813-5827, 10.5194/acp-9-5813-2009, 2009.

660 Czerwińska, A. E., Krzyścin, J. W., Jarosławski, J., and Posyniak, M.: Effects of urban agglomeration on surface-UV doses: a  
661 comparison of Brewer measurements in Warsaw and Belsk, Poland, for the period 2013–2015, *Atmos. Chem. Phys.*, 16,  
662 13641-13651, 10.5194/acp-16-13641-2016, 2016.

663 Dahlback, A.: Dahlback, Measurements of biologically effective UV doses, total ozone abundances, and cloud effects with  
664 multichannel, moderate bandwidth filter instruments, *Appl. Opt.* Vol. 35, No. 33, 1996. Further references, see. Eg. Bernhard  
665 et al, Johnsen et al. *JGR*, 2008, *Applied Optics*, 35, 6514 - 6521, 10.1364/AO.35.006514, 1996.

666 De Bock, V., De Backer, H., Van Malderen, R., Mangold, A., and Delcloo, A.: Relations between erythemal UV dose, global  
667 solar radiation, total ozone column and aerosol optical depth at Uccle, Belgium, *Atmos. Chem. Phys.*, 14, 12251-12270,  
668 10.5194/acp-14-12251-2014, 2014.

669 Derrien, M., and Le Gléau, H.: MSG/SEVIRI cloud mask and type from SAFNWC, *International Journal of Remote Sensing*,  
670 26, 4707-4732, 10.1080/01431160500166128, 2005.

671 Eleftheratos, K., Kazadzis, S., Zerefos, C. S., Tourpali, K., Meleti, C., Balis, D., Zyrichidou, I., Lakkala, K., Feister, U.,  
672 Koskela, T., Heikkilä, A., and Karhu, J. M.: Ozone and Spectroradiometric UV Changes in the Past 20 Years over High  
673 Latitudes, *Atmosphere-Ocean*, 53, 117-125, 10.1080/07055900.2014.919897, 2015.

674 Eskes, H., Huijnen, V., Arola, A., Benedictow, A., Blechschmidt, A. M., Botek, E., Boucher, O., Bouarar, I., Chabrillat, S.,  
675 Cuevas, E., Engelen, R., Flentje, H., Gaudel, A., Griesfeller, J., Jones, L., Kapsomenakis, J., Katragkou, E., Kinne, S.,  
676 Langerock, B., Razinger, M., Richter, A., Schultz, M., Schulz, M., Sudarchikova, N., Thouret, V., Vrekoussis, M., Wagner,  
677 A., and Zerefos, C.: Validation of reactive gases and aerosols in the MACC global analysis and forecast system, *Geosci. Model*  
678 *Dev.*, 8, 3523-3543, 10.5194/gmd-8-3523-2015, 2015.

Eskes, H. J., Velthoven, P. F. J. V., Valks, P. J. M., and Kelder, H. M.: Assimilation of GOME total-ozone satellite observations in a three-dimensional tracer-transport model, *Quarterly Journal of the Royal Meteorological Society*, 129, 1663-1681, <https://doi.org/10.1256/qj.02.14, 2003>.

Eskes, H. J., Wagner, A., Schulz, M., Christophe, Y., Ramonet, M., Basart, S., Benedictow, A., Bennouna, Y., Blechschmidt, A.-M., Chabrilat, S., Clark, H., Cuevas, E., Flentje, H., Hansen, K. M., IM, U., Kapsomenakis, J., Langerock, B., Petersen, K., Richter, A., Sudarchikova, N., Thouret, V., Warneke, T., and Zerefos, C.: Validation report of the cams near-real-time global atmospheric composition service: period September-November 2017., *Copernicus Atmosphere Monitoring Service (CAMS) Report*, CAMS84\_2015SC3\_D84.1.1.10\_2017SON\_V1.pdf, February 2018., 2018.

Feister, U., and Grewe, R.: SPECTRAL ALBEDO MEASUREMENTS IN THE UV and VISIBLE REGION OVER DIFFERENT TYPES OF SURFACES, *Photochemistry and Photobiology*, 62, 736-744, <https://doi.org/10.1111/j.1751-1097.1995.tb08723.x, 1995>.

Fioletov, V., Kerr, J. B., and Fergusson, A.: The UV Index: Definition, Distribution and Factors Affecting It, *Canadian Journal of Public Health*, 101, I5-I9, 10.1007/bf03405303, 2010.

Fioletov, V. E., Kerr, J. B., McArthur, L. J. B., Wardle, D. I., and Mathews, T. W.: Estimating UV Index Climatology over Canada, *Journal of Applied Meteorology and Climatology*, 42, 417-433, 10.1175/1520-0450(2003)042<0417:EUICOC>2.0.CO;2, 2003.

Fioletov, V. E., McArthur, L. J. B., Mathews, T. W., and Marrett, L.: On the relationship between erythema and vitamin D action spectrum weighted ultraviolet radiation, *Journal of Photochemistry and Photobiology B: Biology*, 95, 9-16, <https://doi.org/10.1016/j.jphotobiol.2008.11.014, 2009>.

Fioletov, V.E., Griffioen, E., Kerr, J.B., Wardle, D.I., and Uchino, O.: Influence of volcanic sulfur dioxide on spectral UV irradiance as measured by Brewer spectrophotometers. *Geophysical Research Letters*, 25(10), 1665-1668, 1998.

Fountoulakis, I., Bais, A. F., Fragkos, K., Meleti, C., Tourpali, K., and Zempila, M. M.: Short- and long-term variability of spectral solar UV irradiance at Thessaloniki, Greece: effects of changes in aerosols, total ozone and clouds, *Atmos. Chem. Phys.*, 16, 2493-2505, 10.5194/acp-16-2493-2016, 2016.

Fountoulakis, I., Zerefos, C. S., Bais, A. F., Kapsomenakis, J., Koukouli, M.-E., Ohkawara, N., Fioletov, V., De Backer, H., Lakkala, K., Karppinen, T., and Webb, A. R.: Twenty-five years of spectral UV-B measurements over Canada, Europe and Japan: Trends and effects from changes in ozone, aerosols, clouds, and surface reflectivity, *Comptes Rendus Geoscience*, 350, 393-402, <https://doi.org/10.1016/j.crte.2018.07.011, 2018>.

Fountoulakis, I., Natsis, A., Siomos, N., Drosoglou, T., and Bais, F. A.: Deriving Aerosol Absorption Properties from Solar Ultraviolet Radiation Spectral Measurements at Thessaloniki, Greece, *Remote Sensing*, 11, 10.3390/rs11182179, 2019.

Fountoulakis, I., Diémoz, H., Siani, A.-M., Laschewski, G., Filippa, G., Arola, A., Bais, A. F., De Backer, H., Lakkala, K., Webb, A. R., De Bock, V., Karppinen, T., Garane, K., Kapsomenakis, J., Koukouli, M.-E., and Zerefos, C. S.: Solar UV Irradiance in a Changing Climate: Trends in Europe and the Significance of Spectral Monitoring in Italy, *Environments*, 7, 10.3390/environments7010001, 2020a.

Fountoulakis, I., Diémoz, H., Siani, A. M., Hülsen, G., and Gröbner, J.: Monitoring of solar spectral ultraviolet irradiance in Aosta, Italy, *Earth Syst. Sci. Data*, 12, 2787-2810, 10.5194/essd-12-2787-2020, 2020b.

Gal, S.: Computing elementary functions: A new approach for achieving high accuracy and good performance, *Accurate Scientific Computations*, Berlin, Heidelberg, 1986, 1-16,

717 Garane, K., Bais, A. F., Kazadzis, S., Kazantzidis, A., and Meleti, C.: Monitoring of UV spectral irradiance at Thessaloniki  
718 (1990&ndash;2005): data re-evaluation and quality control, *Ann. Geophys.*, 24, 3215-3228, 10.5194/angeo-24-3215-2006,  
719 2006.

720 Garane, K., Lerot, C., Coldewey-Egbers, M., Verhoelst, T., Koukouli, M. E., Zyrichidou, I., Balis, D. S., Danckaert, T.,  
721 Goutail, F., Granville, J., Hubert, D., Keppens, A., Lambert, J. C., Loyola, D., Pommereau, J. P., Van Roozendaal, M., and  
722 Zehner, C.: Quality assessment of the Ozone\_cci Climate Research Data Package (release 2017) – Part 1: Ground-based  
723 validation of total ozone column data products, *Atmos. Meas. Tech.*, 11, 1385-1402, 10.5194/amt-11-1385-2018, 2018.

724 Garane, K., Koukouli, M. E., Verhoelst, T., Lerot, C., Heue, K. P., Fioletov, V., Balis, D., Bais, A., Bazureau, A., Dehn, A.,  
725 Goutail, F., Granville, J., Griffin, D., Hubert, D., Keppens, A., Lambert, J. C., Loyola, D., McLinden, C., Pazmino, A.,  
726 Pommereau, J. P., Redondas, A., Romahn, F., Valks, P., Van Roozendaal, M., Xu, J., Zehner, C., Zerefos, C., and Zimmer,  
727 W.: TROPOMI/S5P total ozone column data: global ground-based validation and consistency with other satellite missions,  
728 *Atmos. Meas. Tech.*, 12, 5263-5287, 10.5194/amt-12-5263-2019, 2019.

729 Giles, D. M., Sinyuk, A., Sorokin, M. G., Schafer, J. S., Smirnov, A., Slutsker, I., Eck, T. F., Holben, B. N., Lewis, J. R.,  
730 Campbell, J. R., Welton, E. J., Korkin, S. V., and Lyapustin, A. I.: Advancements in the Aerosol Robotic  
731 Network (AERONET) Version 3 database – automated near-real-time quality control algorithm with improved cloud  
732 screening for Sun photometer aerosol optical depth (AOD) measurements, *Atmos. Meas. Tech.*, 12, 169-209, 10.5194/amt-12-  
733 169-2019, 2019.

734 Gratien, A., Nilsson, E., Doussin, J.F., Johnson, M.S., Nielsen, C.J., Stenström, Y., and Picquet-Varrault, B.: UV and IR  
735 absorption cross-sections of HCHO, HCDO, and DCDO. *The journal of Physical Chemistry, A*, 111(45), 11506-11513, 2007.

736 Gröbner, J., Schreder, J., Kazadzis, S., Bais, A. F., Blumthaler, M., Görts, P., Tax, R., Koskela, T., Seckmeyer, G., Webb, A.  
737 R., and Rembges, D.: Traveling reference spectroradiometer for routine quality assurance of spectral solar ultraviolet irradiance  
738 measurements, *Applied Optics*, 44, 5321-5331, 10.1364/ao.44.005321, 2005.

739 Gröbner, J., and Sperfeld, P.: Direct traceability of the portable QASUME irradiance scale to the primary irradiance standard  
740 of the PTB, *Metrologia*, 42, 134-139, 10.1088/0026-1394/42/2/008, 2005.

741 Gröbner, J., Kröger, I., Egli, L., Hülsen, G., Riechelmann, S., and Sperfeld, P.: The high-resolution extraterrestrial solar  
742 spectrum (QASUMEFTS) determined from ground-based solar irradiance measurements, *Atmos. Meas. Tech.*, 10, 3375-3383,  
743 10.5194/amt-10-3375-2017, 2017.

744 Gröbner, J.: Example datasets from PMOD/WRC Davos, Switzerland with the double Brewer B163 and QASUME II  
745 compared with the UVIOS model. *Atmos. Meas. Tech. (supplement comment)*, 10.5194/amt-2020506-CC1, 2021.

746 Heikkilä, A., Kaurola, J., Lakkala, K., Karhu, J. M., Kyrö, E., Koskela, T., Engelsen, O., Slaper, H., and Seckmeyer, G.:  
747 European UV DataBase (EUVDB) as a repository and quality analyser for solar spectral UV irradiance monitored in  
748 Sodankylä, *Geosci. Instrum. Method. Data Syst.*, 5, 333-345, 10.5194/gi-5-333-2016, 2016.

749 Henderson-Sellers, A., and Wilson, M. F.: Surface albedo data for climatic modeling, *Reviews of Geophysics*, 21, 1743-1778,  
750 <https://doi.org/10.1029/RG021i008p01743>, 1983.

751 Henken, C. C., Schmeits, M. J., Deneke, H., and Roebeling, R. A.: Using MSG-SEVIRI Cloud Physical Properties and Weather  
752 Radar Observations for the Detection of Cb/TCu Clouds, *Journal of Applied Meteorology and Climatology*, 50, 1587-1600,  
753 2011.

754 Herman, J. R.: Global increase in UV irradiance during the past 30 years (1979–2008) estimated from satellite data, *Journal*  
755 *of Geophysical Research: Atmospheres*, 115, 10.1029/2009jd012219, 2010.

756 Holick, M. F.: Vitamin D: the underappreciated D-lightful hormone that is important for skeletal and cellular health, *Current*  
757 *Opinion in Endocrinology, Diabetes and Obesity*, 9, 2002.

758 Hülsen, G., Gröbner, J., Bais, A., Blumthaler, M., Disterhoft, P., Johnsen, B., Lantz, K. O., Meleti, C., Schreder, J., Vilaplana  
759 Guerrero, J. M., and Ylianttila, L.: Intercomparison of erythral broadband radiometers calibrated by seven UV calibration  
760 facilities in Europe and the USA, *Atmos. Chem. Phys.*, 8, 4865-4875, 10.5194/acp-8-4865-2008, 2008.

761 Hülsen, G., Gröbner, J., Nevas, S., Sperfeld, P., Egli, L., Porrovecchio, G., and Smid, M.: Traceability of solar UV  
762 measurements using the Qasume reference spectroradiometer, *Applied Optics*, 55, 7265 - 7275, 10.1364/AO.55.007265, 2016.

763 Hülsen, G., Gröbner, J., Bais, A., Blumthaler, M., Diemoz, H., Bolsee, D., Rodríguez, A. D., Fountoulakis, I., Naranen, E.,  
764 Schreder, J., Stefania, F., and Vilaplana Guerrero, J. M.: Second solar ultraviolet radiometer comparison campaign UVC-II,  
765 *Metrologia*, 2020.

766 Juzeniene, A., Brekke, P., Dahlback, A., Andersson-Engels, S., Reichrath, J., Moan, K., Holick, M. F., Grant, W. B., and  
767 Moan, J.: Solar radiation and human health, *Reports on Progress in Physics*, 74, 066701, 10.1088/0034-4885/74/6/066701,  
768 2011.

769 Kato, S., and Marshak, A.: Solar zenith and viewing geometry-dependent errors in satellite retrieved cloud optical thickness:  
770 *Marine stratocumulus case. Journal of Geophysical Research*, 114, D01202, 10.1029/2008JD010579, 2009.

771 Kazadzis, S., Bais, A., Balis, D., Kouremeti, N., Zempila, M., Arola, A., Giannakaki, E., Amiridis, V., and Kazantzidis, A.:  
772 Spatial and temporal UV irradiance and aerosol variability within the area of an OMI satellite pixel, *Atmos. Chem. Phys.*, 9,  
773 4593-4601, 10.5194/acp-9-4593-2009, 2009a.

774 Kazadzis, S., Kouremeti, N., Bais, A., Kazantzidis, A., and Meleti, C.: Aerosol forcing efficiency in the UVA region from  
775 spectral solar irradiance measurements at an urban environment, *Ann. Geophys.*, 27, 2515-2522, 10.5194/angeo-27-2515-  
776 2009, 2009b.

777 Kazadzis, S., Raptis, P., Kouremeti, N., Amiridis, V., Arola, A., Gerasopoulos, E., and Schuster, G. L.: Aerosol absorption  
778 retrieval at ultraviolet wavelengths in a complex environment, *Atmos. Meas. Tech.*, 9, 5997-6011, 10.5194/amt-9-5997-2016,  
779 2016.

780 Kerr, J. B., Evans, W. F. J., and Asbridge, I. A.: Recalibration of Dobson Field Spectrophotometers with a Travelling Brewer  
781 Spectrophotometer Standard, *Atmospheric Ozone*, Dordrecht, 1985, 381-386,

782 Kerr, J. B., and Fioletov, V. E.: Surface ultraviolet radiation, *Atmosphere-Ocean*, 46, 159-184, 10.3137/ao.460108, 2008.

783 Kinne, S.: The MACv2 aerosol climatology, *Tellus B: Chemical and Physical Meteorology*, 71, 1-21,  
784 10.1080/16000889.2019.1623639, 2019.

785 Koren, I., Remer, L. A., Kaufman, Y. J., Rudich, Y., and Martins, J. V.: On the twilight zone between clouds and aerosols,  
786 *Geophysical Research Letters*, 34, <https://doi.org/10.1029/2007GL029253>, 2007.

787 Kosmopoulos, P. G., Kazadzis, S., Taylor, M., Raptis, P. I., Keramitsoglou, I., Kiranoudis, C., and Bais, A. F.: Assessment of  
788 surface solar irradiance derived from real-time modelling techniques and verification with ground-based measurements,  
789 *Atmos. Meas. Tech.*, 11, 907-924, 10.5194/amt-11-907-2018, 2018.



790 Kreuter, A., Buras, R., Mayer, B., Webb, A., Kift, R., Bais, A., Kouremeti, N., and Blumthaler, M.: Solar irradiance in the  
791 heterogeneous albedo environment of the Arctic coast: measurements and a 3-D model study, *Atmos. Chem. Phys.*, 14, 5989-  
792 6002, 10.5194/acp-14-5989-2014, 2014.

793 Krotkov, N. A., Bhartia, P. K., Herman, J. R., Fioletov, V., and Kerr, J.: Satellite estimation of spectral surface UV irradiance  
794 in the presence of tropospheric aerosols: 1. Cloud-free case, *Journal of Geophysical Research: Atmospheres*, 103, 8779-8793,  
795 <https://doi.org/10.1029/98JD00233>, 1998.

796 Lacaze, R., Smets, B., Trigo, I., Calvet, J.C., Jann, A., Camacho, F., Baret, F., Kidd, R., Defourny, P., Tansey, K., et al.: The  
797 Copernicus Global Land Service: Present and future. In *Proceedings of the EGU General Assembly*, Vienna, Austria, 7-12  
798 April, 2013.

799 Lakkala, K., Arola, A., Heikkilä, A., Kaurola, J., Koskela, T., Kyrö, E., Lindfors, A., Meinander, O., Tanskanen, A., Gröbner,  
800 J., and Hülsen, G.: Quality assurance of the Brewer spectral UV measurements in Finland, *Atmos. Chem. Phys.*, 8, 3369-3383,  
801 10.5194/acp-8-3369-2008, 2008.

802 Lakkala, K., Redondas, A., Meinander, O., Thölix, L., Hamari, B., Almansa, A. F., Carreno, V., García, R. D., Torres, C.,  
803 Deferrari, G., Ochoa, H., Bernhard, G., Sanchez, R., and de Leeuw, G.: UV measurements at Marambio and Ushuaia during  
804 2000–2010, *Atmos. Chem. Phys.*, 18, 16019-16031, 10.5194/acp-18-16019-2018, 2018.

805 Lakkala, K., Kujanpää, J., Brogniez, C., Henriot, N., Arola, A., Aun, M., Auriol, F., Bais, A. F., Bernhard, G., De Bock, V.,  
806 Catalfamo, M., Deroo, C., Diémoz, H., Egli, L., Forestier, J. B., Fountoulakis, I., Garcia, R. D., Gröbner, J., Hassinen, S.,  
807 Heikkilä, A., Henderson, S., Hülsen, G., Johnsen, B., Kalakoski, N., Karanikolas, A., Karppinen, T., Lamy, K., León-Luis, S.  
808 F., Lindfors, A. V., Metzger, J. M., Minvielle, F., Muskatel, H. B., Portafaix, T., Redondas, A., Sanchez, R., Siani, A. M.,  
809 Svendby, T., and Tamminen, J.: Validation of TROPOMI Surface UV Radiation Product, *Atmos. Meas. Tech. Discuss.*, 2020,  
810 1-37, 10.5194/amt-2020-121, 2020.

811 Larkin, A., Haigh, J. D., and Djavidnia, S.: The Effect of Solar UV Irradiance Variations on the Earth's Atmosphere, *Space*  
812 *Science Reviews*, 94, 199-214, 10.1023/a:1026771307057, 2000.

813 Levelt, P. F., Oord, G. H. J. v. d., Dobber, M. R., Malkki, A., Huib, V., Johan de, V., Stammes, P., Lundell, J. O. V., and Saari,  
814 H.: The ozone monitoring instrument, *IEEE Transactions on Geoscience and Remote Sensing*, 44, 1093-1101,  
815 10.1109/tgrs.2006.872333, 2006.

816 Levelt, P. F., Joiner, J., Tamminen, J., Veefkind, J. P., Bhartia, P. K., Stein Zweers, D. C., Duncan, B. N., Streets, D. G., Eskes,  
817 H., van der A, R., McLinden, C., Fioletov, V., Carn, S., de Laat, J., DeLand, M., Marchenko, S., McPeters, R., Ziemke, J., Fu,  
818 D., Liu, X., Pickering, K., Apituley, A., González Abad, G., Arola, A., Boersma, F., Chan Miller, C., Chance, K., de Graaf,  
819 M., Hakkarainen, J., Hassinen, S., Ialongo, I., Kleipool, Q., Krotkov, N., Li, C., Lamsal, L., Newman, P., Nowlan, C.,  
820 Suleiman, R., Tilstra, L. G., Torres, O., Wang, H., and Wargan, K.: The Ozone Monitoring Instrument: overview of 14 years  
821 in space, *Atmos. Chem. Phys.*, 18, 5699-5745, 10.5194/acp-18-5699-2018, 2018.

822 López-Solano, J., Redondas, A., Carlund, T., Rodríguez-Franco, J. J., Diémoz, H., León-Luis, S. F., Hernández-Cruz, B.,  
823 Guirado-Fuentes, C., Kouremeti, N., Gröbner, J., Kazadzis, S., Carreño, V., Berjón, A., Santana-Díaz, D., Rodríguez-Valido,  
824 M., De Bock, V., Moreta, J. R., Rimmer, J., Smedley, A. R. D., Boulkelia, L., Jepsen, N., Eriksen, P., Bais, A. F., Shirovov,  
825 V., Vilaplana, J. M., Wilson, K. M., and Karppinen, T.: Aerosol optical depth in the European Brewer Network, *Atmos. Chem.*  
826 *Phys.*, 18, 3885-3902, 10.5194/acp-18-3885-2018, 2018.

827 Lucas, R., McMichael, T., Smith, W., Armstrong, B. K., Prüss-Üstün, A., and World Health, O.: Solar ultraviolet radiation :  
828 global burden of disease from solar ultraviolet radiation / Robyn Lucas ... [et al.] ; editors, Annette Prüss-Üstün ... [et al.].  
829 Environmental burden of disease series ; no. 13, World Health Organization, Geneva, 2006.

830 Lucas, R. M., Byrne, S. N., Correale, J., Ilschner, S., and Hart, P. H.: Ultraviolet radiation, vitamin D and multiple sclerosis,  
831 *Neurodegenerative Disease Management*, 5, 413-424, 10.2217/nmt.15.33, 2015.

832 Madronich, S.: Environmental UV Photobiology, *Environ. UV Photobiol.*, 10.1007/978-1-4899-2406-3, 1993.

833 Mayer, B., Kylling, A., Madronich, S., and Seckmeyer, G.: Enhanced absorption of UV radiation due to multiple scattering in  
834 clouds: Experimental evidence and theoretical explanation, *Journal of Geophysical Research: Atmospheres*, 103, 31241-  
835 31254, <https://doi.org/10.1029/98JD02676>, 1998.

836 Mayer, B., and Kylling, A.: Technical note: The libRadtran software package for radiative transfer calculations - description  
837 and examples of use, *Atmos. Chem. Phys.*, 5, 1855-1877, 10.5194/acp-5-1855-2005, 2005.

838 McKenzie, R., Bernhard, G., Liley, B., Disterhoft, P., Rhodes, S., Bais, A., Morgenstern, O., Newman, P., Oman, L., Brogniez,  
839 C., and Simic, S.: Success of Montreal Protocol Demonstrated by Comparing High-Quality UV Measurements with “World  
840 Avoided” Calculations from Two Chemistry-Climate Models, *Scientific Reports*, 9, 12332, 10.1038/s41598-019-48625-z,  
841 2019.

842 McKenzie, R. L., Aucamp, P. J., Bais, A. F., Björn, L. O., Ilyas, M., and Madronich, S.: Ozone depletion and climate change:  
843 impacts on UV radiation, *Photochemical & Photobiological Sciences*, 10, 182-198, 10.1039/c0pp90034f, 2011.

844 Meinander, O., Kazadzis, S., Arola, A., Riihelä, A., Räisänen, P., Kivi, R., Kontu, A., Kouznetsov, R., Sofiev, M., Svensson,  
845 J., Suokanerva, H., Aaltonen, V., Manninen, T., Roujean, J. L., and Hauteceur, O.: Spectral albedo of seasonal snow during  
846 intensive melt period at Sodankylä, beyond the Arctic Circle, *Atmos. Chem. Phys.*, 13, 3793-3810, 10.5194/acp-13-3793-  
847 2013, 2013.

848 MétéoFrance: Algorithm theoretical basis document for cloud products (CMa-PGE01 v3.2, CT-PGE02 v2.2 & CTTH-PGE03  
849 v2.2), Technical Report SAF/NWC/CDOP/MFL/SCI/ATBD/01, Paris: MétéoFrance, 2013.

850 Mok, J., Krotkov, N. A., Torres, O., Jethva, H., Li, Z., Kim, J., Koo, J. H., Go, S., Irie, H., Labow, G., Eck, T. F., Holben, B.  
851 N., Herman, J., Loughman, R. P., Spinei, E., Lee, S. S., Khatri, P., and Campanelli, M.: Comparisons of spectral aerosol single  
852 scattering albedo in Seoul, South Korea, *Atmos. Meas. Tech.*, 11, 2295-2311, 10.5194/amt-11-2295-2018, 2018.

853 Myhre, G., and Myhre, A.: Uncertainties in Radiative Forcing due to Surface Albedo Changes Caused by Land-Use Changes,  
854 *Journal of Climate*, 16, 1511-1524, 10.1175/1520-0442(2003)016<1511:uirfdt>2.0.co;2, 2003.

855 NOAA: Data Announcement 88-MGG-02, Digital relief of the surface of the Earth. NOAA, National Geophysical Data Center,  
856 Boulder, Colorado, 1988.

857 Noël, S., Mieruch, S., Bovensmann, H., and Burrows, J. P.: Preliminary results of GOME-2 water vapour retrievals and first  
858 applications in polar regions, *Atmos. Chem. Phys.*, 8, 1519-1529, 10.5194/acp-8-1519-2008, 2008.

859 Peeters, P., Simon, P. C., Hansen, G., Meerkoetter, R., Verdebout, J., Seckmeyer, G., Taalas, P., and Slaper, H.: MAUVE: A  
860 European Initiative for Developing and Improving Satellite Derived Ultraviolet Maps, *Radiation Protection Dosimetry*, 91,  
861 201-202, 10.1093/oxfordjournals.rpd.a033200, 2000.

862 Pfeifroth, U., Kothe, S., and Trentmann, J.: Validation report: Meteosat solar surface radiation and effective cloud albedo  
863 climate data record (Sarah 2), EUMETSAT SAF CM Validation report with reference number SAF/CM/DWD/VAL/  
864 METEOSAT/HEL, 2.1, [https://doi.org/10.5676/EUM\\_SAF\\_CM/SARAH/V002](https://doi.org/10.5676/EUM_SAF_CM/SARAH/V002), 2016.

865 Probst, P., Rizzi, R., Tosi, E., Lucarini, V., and Maestri, T.: Total cloud cover from satellite observations and climate models,  
866 *Atmospheric Research*, 107, 161-170, <https://doi.org/10.1016/j.atmosres.2012.01.005>, 2012.

867 Raptis, I.-P., Kazadzis, S., Eleftheratos, K., Amiridis, V., and Fountoulakis, I.: Single Scattering Albedo's Spectral Dependence  
868 Effect on UV Irradiance., *Atmosphere*, 9, 10.3390/atmos9090364, 2018.

869 Reda, I., and Andreas, A.: Solar position algorithm for solar radiation applications. NREL Technical Report, NREL/TP-560-  
870 34302, Prepared under Task No. WU1D5600, 2008.

871 Renaud, A., Staehelin, J., Fröhlich, C., Philipona, R., and Heimo, A.: Influence of snow and clouds on erythral UV radiation:  
872 Analysis of Swiss measurements and comparison with models, *Journal of Geophysical Research: Atmospheres*, 105, 4961-  
873 4969, <https://doi.org/10.1029/1999JD900160>, 2000.

874 Rimmer, J. S., Redondas, A., and Karppinen, T.: EuBrewNet – A European Brewer network (COST Action ES1207), an  
875 overview, *Atmos. Chem. Phys.*, 18, 10347-10353, 10.5194/acp-18-10347-2018, 2018.

876 Schmalwieser, A., and Siani, A.: Review on Non-Occupational Personal Solar UV Exposure Measurements, *Photochemistry*  
877 *and Photobiology*, 94, 10.1111/php.12946, 2018.

878 Schmalwieser, A. W., Gröbner, J., Blumthaler, M., Klotz, B., De Backer, H., Bolsée, D., Werner, R., Tomsic, D., Metelka, L.,  
879 Eriksen, P., Jepsen, N., Aun, M., Heikkilä, A., Duprat, T., Sandmann, H., Weiss, T., Bais, A., Toth, Z., Siani, A.-M., Vaccaro,  
880 L., Diémoz, H., Grifoni, D., Zipoli, G., Lorenzetto, G., Petkov, B. H., di Sarra, A. G., Massen, F., Yousif, C., Aculinin, A. A.,  
881 den Outer, P., Svendby, T., Dahlback, A., Johnsen, B., Bieszczuk-Jakubowska, J., Krzyscin, J., Henriques, D., Chubarova, N.,  
882 Kolarž, P., Mijatovic, Z., Groselj, D., Pribulova, A., Gonzales, J. R. M., Bilbao, J., Guerrero, J. M. V., Serrano, A., Andersson,  
883 S., Vuilleumier, L., Webb, A., and O'Hagan, J.: UV Index monitoring in Europe, *Photochemical & Photobiological Sciences*,  
884 16, 1349-1370, 10.1039/c7pp00178a, 2017.

885 Schmalwieser, A. W.: Possibilities to estimate the personal UV radiation exposure from ambient UV radiation measurements,  
886 *Photochemical & Photobiological Sciences*, 19, 1249-1261, 10.1039/d0pp00182a, 2020.

887 Seckmeyer, G., Erb, R., and Albold, A.: Transmittance of a cloud is wavelength-dependent in the UV-range, *Geophysical*  
888 *Research Letters*, 23, 2753-2755, <https://doi.org/10.1029/96GL02614>, 1996.

889 Seckmeyer, G., Pissulla, D., Glandorf, M., Henriques, D., Johnsen, B., Webb, A., Siani, A.-M., Bais, A., Kjeldstad, B.,  
890 Brogniez, C., Lenoble, J., Gardiner, B., Kirsch, P., Koskela, T., Kaurola, J., Uhlmann, B., Slaper, H., Den Outer, P., Janouch,  
891 M., Werle, P., Gröbner, J., Mayer, B., De La Casiniere, A., Simic, S., and Carvalho, F.: Variability of UV Irradiance in Europe,  
892 *Photochemistry and Photobiology*, 84, 172-179, 10.1111/j.1751-1097.2007.00216.x, 2008.

893 Siani, A. M., Casale, G. R., Diémoz, H., Agnesod, G., Kimlin, M. G., Lang, C. A., and Colosimo, A.: Personal UV exposure  
894 in high albedo alpine sites, *Atmos. Chem. Phys.*, 8, 3749-3760, 10.5194/acp-8-3749-2008, 2008.

895 Slaper, H., Reinen, H. A. J. M., Blumthaler, M., Huber, M., and Kuik, F.: Comparing ground-level spectrally resolved solar  
896 UV measurements using various instruments: A technique resolving effects of wavelength shift and slit width, *Geophysical*  
897 *Research Letters*, 22, 2721-2724, 10.1029/95gl02824, 1995.

898 Smedley, A. R. D., Rimmer, J. S., Moore, D., Toumi, R., and Webb, A. R.: Total ozone and surface UV trends in the United  
899 Kingdom: 1979–2008, *International Journal of Climatology*, 32, 338-346, 10.1002/joc.2275, 2012.

900 Svendby, T., Hansen, G. H., Bäcklund, A., and Dahlback, A.: Monitoring of the atmospheric ozone layer and natural ultraviolet  
901 radiation: Annual report 2018, NILU M-1462 | 2019, 39, 2018.

902 Taylor, M., Kosmopoulos, P. G., Kazadzis, S., Keramitsoglou, I., and Kiranoudis, C. T.: Neural network radiative transfer  
903 solvers for the generation of high resolution solar irradiance spectra parameterized by cloud and aerosol parameters, *Journal*  
904 *of Quantitative Spectroscopy and Radiative Transfer*, 168, 176-192, <https://doi.org/10.1016/j.jqsrt.2015.08.018>, 2016.

905 Vanicek, K., Frei, T., Litynska, Z., and Schmalwieser, A.: UV-Index for the Public, European Union, 2000.

906 Verdebout, J.: A method to generate surface UV radiation maps over Europe using GOME, Meteosat and ancillary geophysical  
907 data. *Journal of Geophysical Research: Atmospheres*, 105(D4), 5049-5058, 2000.

908 Vitt, R., Laschewski, G., Bais, A. F., Diémoz, H., Fountoulakis, I., Siani, A.-M., and Matzarakis, A.: UV-Index Climatology  
909 for Europe Based on Satellite Data, *Atmosphere*, 11, 10.3390/atmos11070727, 2020.

910 Webb, A. R., and Engelsen, O.: Ultraviolet Exposure Scenarios: Risks of Erythema from Recommendations on Cutaneous  
911 Vitamin D Synthesis, in: *Sunlight, Vitamin D and Skin Cancer*, edited by: Reichrath, J., Springer New York, New York, NY,  
912 72-85, 2008.

913 Webb, A. R., Slaper, H., Koepke, P., and Schmalwieser, A. W.: Know Your Standard: Clarifying the CIE Erythema Action  
914 Spectrum, *Photochemistry and Photobiology*, 87, 483-486, 10.1111/j.1751-1097.2010.00871.x, 2011.

915 WHO: Global Solar UV Index: A Practical Guide, No. WHO/SD., Geneva, Switzerland, 2002.

916 WMO: Report of the WMO Meeting of Experts on UVB Measurements, Data Quality and Standardization of UV Indices,  
917 1994, 1995.

918 Zempila, M.-M., Koukouli, M.-E., Bais, A., Fountoulakis, I., Arola, A., Kouremeti, N., and Balis, D.: OMI/Aura UV product  
919 validation using NILU-UV ground-based measurements in Thessaloniki, Greece, *Atmospheric Environment*, 140, 283-297,  
920 <https://doi.org/10.1016/j.atmosenv.2016.06.009>, 2016.

921 Zerefos, C. S., Tourpali, K., Eleftheratos, K., Kazadzis, S., Meleti, C., Feister, U., Koskela, T., and Heikkilä, A.: Evidence of  
922 a possible turning point in solar UV-B over Canada, Europe and Japan, *Atmos. Chem. Phys.*, 12, 2469-2477, 10.5194/acp-12-  
923 2469-2012, 2012.

924

925

926

927

928

929

930

931

932

933

934  
935  
936  
937  
938  
939  
940  
941  
942  
943  
  
944  
945  
946  
947  
948  
949  
950  
951  
952  
953

**Table 1:** UVIOS model input parameters

Parameter	Description (spatial – temporal resolution)	Source	Reference
Cloud microphysics	Nowcast cloud optical thickness (COT), cloud phase (CPH) (5 km – 15 minutes)	Meteosat Second Generation (MSG4) NOA Antenna	(MétéoFrance, 2013)
Aerosol optical depth	1-day forecast aerosol optical depth (AOD) (40 km – 3 hours)	Copernicus Atmosphere Monitoring Service (CAMS) – FTP access	(Eskes et al., 2015)
Aerosol optical properties	Single scattering albedo (SSA), Angstrom exponent (AE) (1 x 1 degrees – 1 month)	Aerosol Comparisons between Observations and Models (Aerocom)	(Kinne, 2019)
Solar elevation	Solar zenith angle (SZA) (5 km – 15 minutes)	Astronomical model In-house software (NOA)	(Reda and Andreas, 2008)
Surface albedo	Surface albedo (ALB) (1 km – 12 days)	Copernicus Global Land Service (CGLS)	(Carrer et al., 2010)
Water vapor	H <sub>2</sub> O observation (40 x 80 km – 1day)	Global Ozone Monitoring Experiment 2 Level 2 data (GOME-2 L2)	(Noël et al., 2008)
Surface elevation	Elevation observation (ELE) (1 m – fixed)	Digital Elevation Model (DEM) In-house database (NOAA)	(NOAA, 1988)
Ozone	1-day forecast total ozone column (TOC) (1 x 1 degrees – 1 day)	Tropospheric Emission Monitoring Internet Service (TEMIS) with Assimilated Ozone Fields from GOME-2 (METOP-B)	(Eskes et al., 2003)

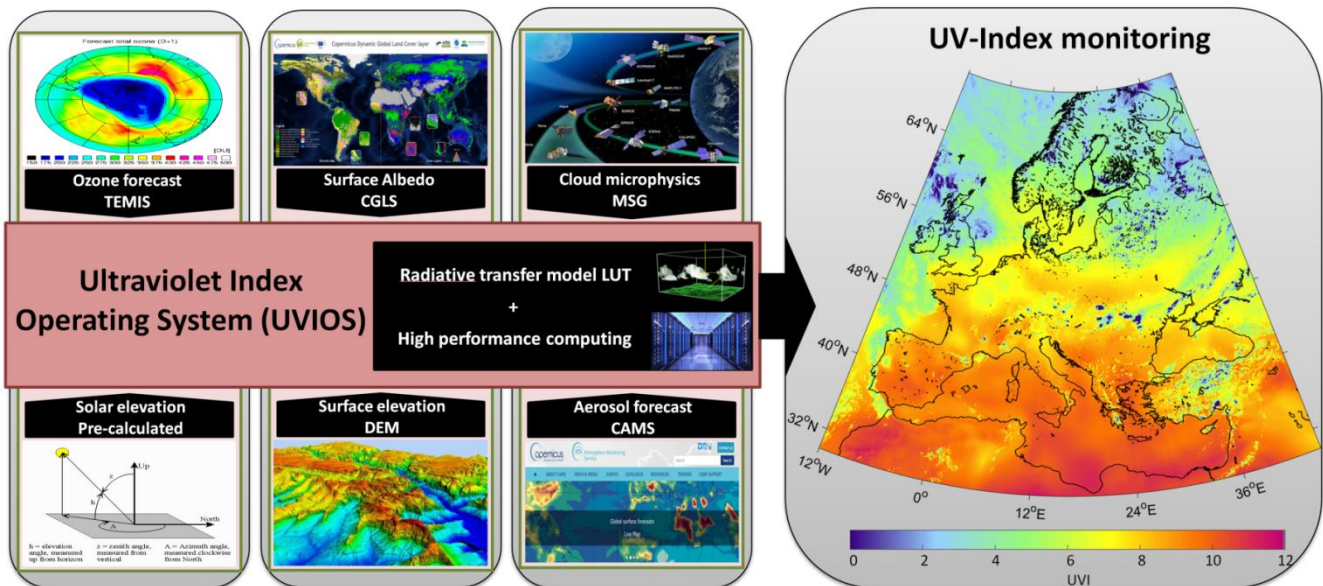


**Figure 1:** Flowchart illustration of the UVIOS modelling technique scheme. The pre-calculated effects of solar and surface elevation and albedo followed by the aerosol and ozone forecasts and the real-time cloud observations to the UVIOS solver result in the spectrally weighted output of UVI for the European region.

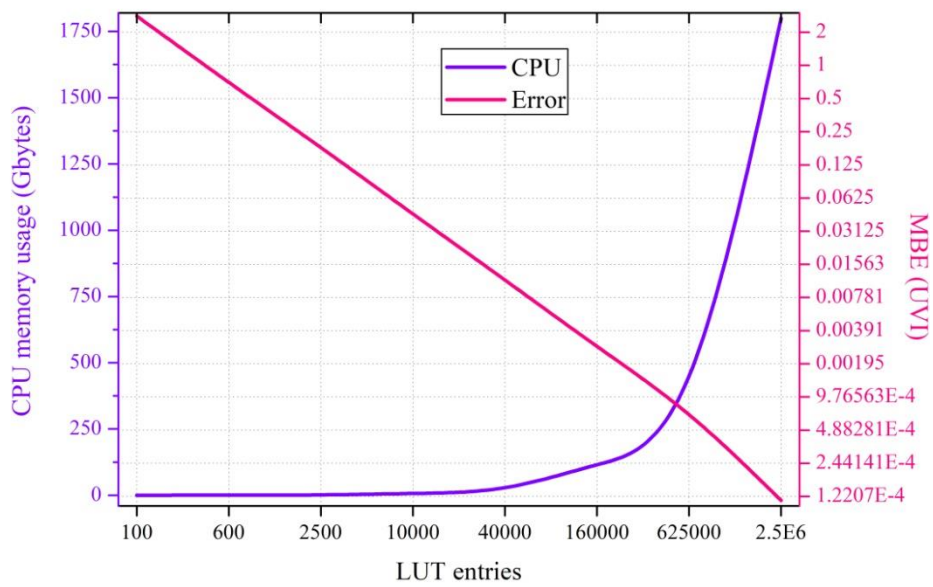


**Figure 2:** UVIOS memory usage and error statistics in terms of mean bias error (MBE) for a range of different LUT sizes.



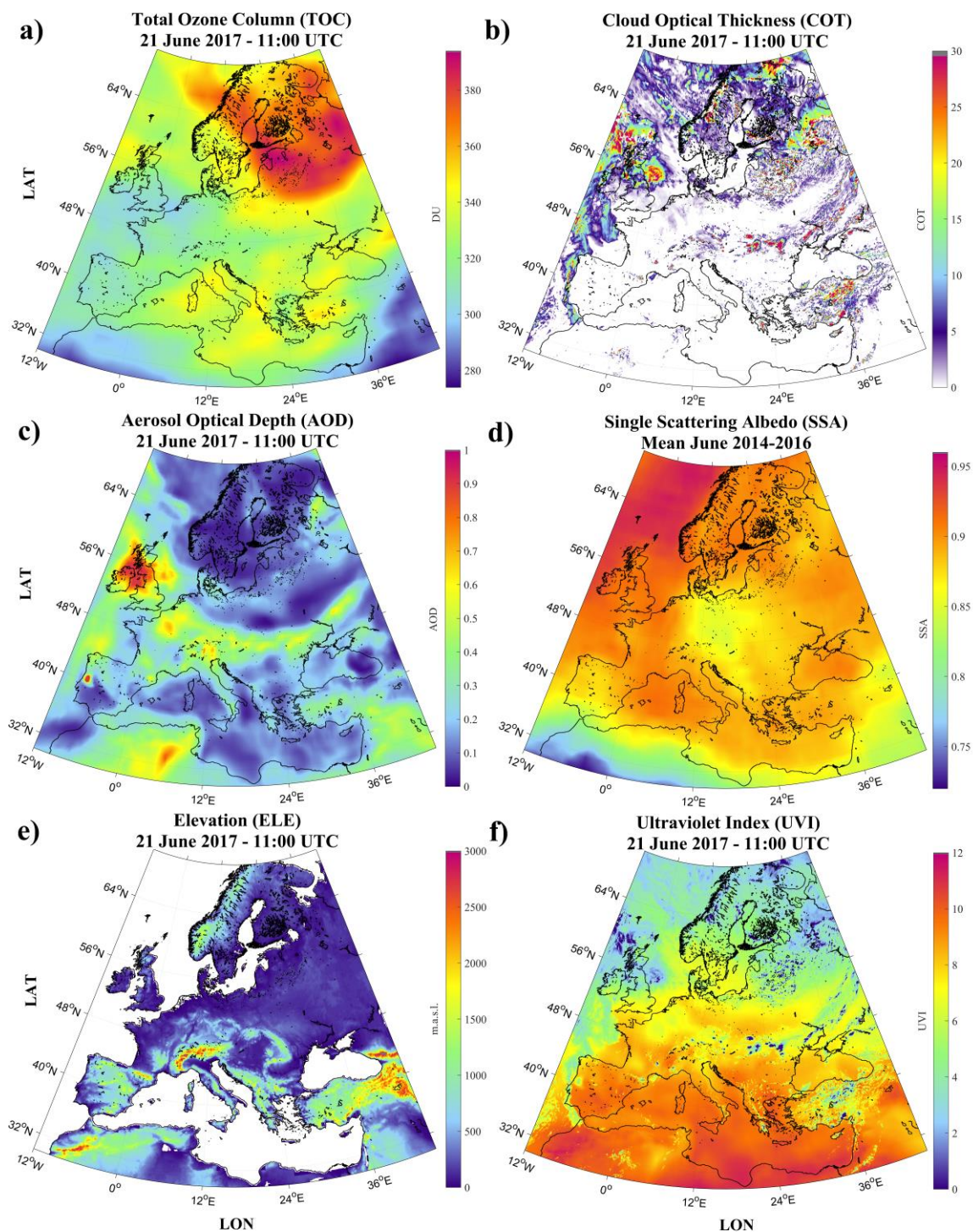


**Figure 3:** An example of the input TOC (a), COT (b), AOD (c), SSA (d), ELE (e) and output UVI (f) maps based on the UVIOS modelling technique applied for the 21<sup>st</sup> of June 2017 at 11:00 UTC.



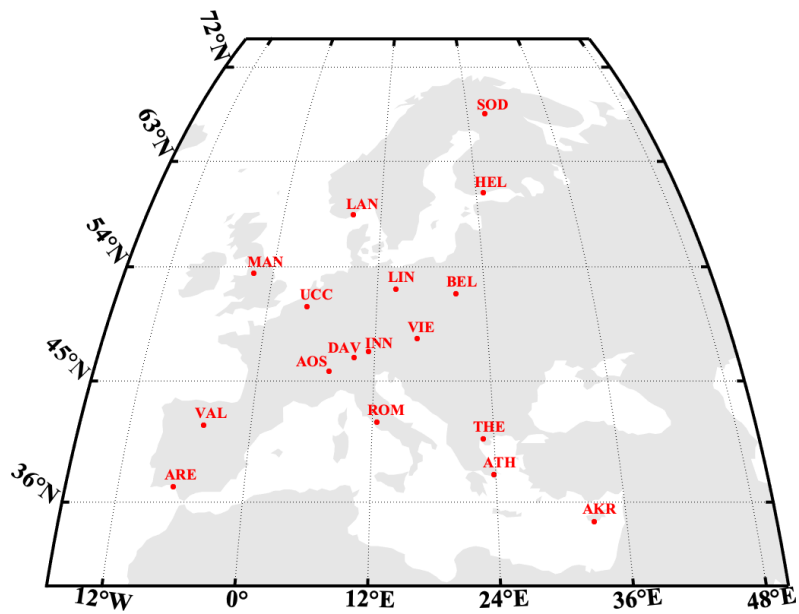


**Figure 4:** Study region and UVI ground measurement locations.

1019  
1020  
1021  
1022  
1023  
1024  
1025  
1026

1027  
1028  
1029  
1030  
1031

**Table 2:** Coordinates (degrees), instrument type, height (metres above sea level) and maximum UVI measured levels of the European stations used for the comparison.

Station	Country	Code	Latitude (°N)	Longitude (°E)	Instrument	Height (m.a.s.l.)	UVImax	Reference
Akrotiri	Cyprus	<b>AKR</b>	34.59	32.99	SL501	23	9.14	(Fountoulakis et al., 2020b)
Aosta	Italy	<b>AOS</b>	45.74	7.36	Bentham DTMc300	570	9.60	
El Arenosillo	Spain	<b>ARE</b>	37.10	-6.73	Brewer MKIII	52	9.78	
Athens	Greece	<b>ATH</b>	37.99	23.78	Brewer MKIV	180	10.20	(Czerwińska et al., 2016)
Belsk	Poland	<b>BEL</b>	51.84	20.79	Brewer MKIII	176	7.54	
Davos	Switzerland	<b>DAV</b>	46.81	9.84	Brewer MKIII	1590	10.57	
Helsinki	Finland	<b>HEL</b>	60.20	24.96	Brewer MKIII	48	5.68	(Lakkala et al., 2008)
Innsbruck	Austria	<b>INN</b>	47.26	11.38	SL501	577	8.35	(Hülßen et al., 2020)
Landvik	Norway	<b>LAN</b>	58.33	8.52	GUV-541	10	6.65	(Svendby et al., 2018)
Lindenberg	Germany	<b>LIN</b>	52.21	14.11	Bentham DTMc300	127	8.86	(Smedley et al., 2012)
Manchester	United Kingdom	<b>MAN</b>	53.47	-2.23	Brewer MKII	76	7.30	
Rome	Italy	<b>ROM</b>	41.90	12.50	Brewer MKIV	75	8.38	
Sodankylä	Finland	<b>SOD</b>	67.37	26.63	Brewer MKIII	179	4.51	(Heikkilä et al., 2016; Lakkala et al., 2008)
Thessaloniki	Greece	<b>THE</b>	40.63	22.96	Brewer MKIII	60	10.40	(Fountoulakis et al., 2016; Garane et al., 2006)
Uccle	Belgium	<b>UCC</b>	50.80	4.35	Brewer MKIII	100	8.99	(De Bock et al., 2014)
Valladolid	Spain	<b>VAL</b>	41.66	-4.71	YES	705	10.32	(Hülßen et al., 2020)
Vienna	Austria	<b>VIE</b>	48.26	16.43	SL501	153	8.09	(Hülßen et al., 2020)

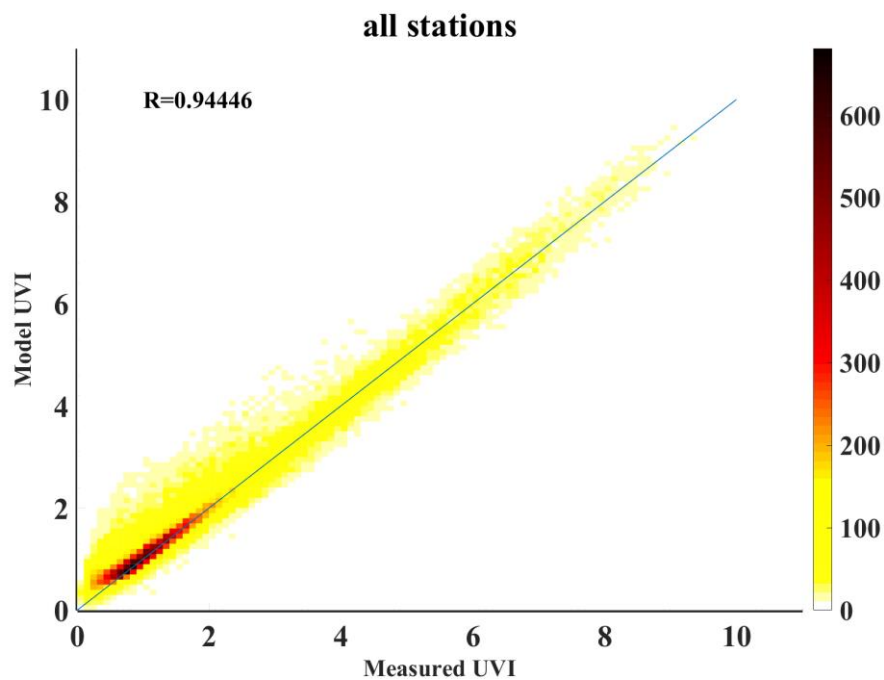
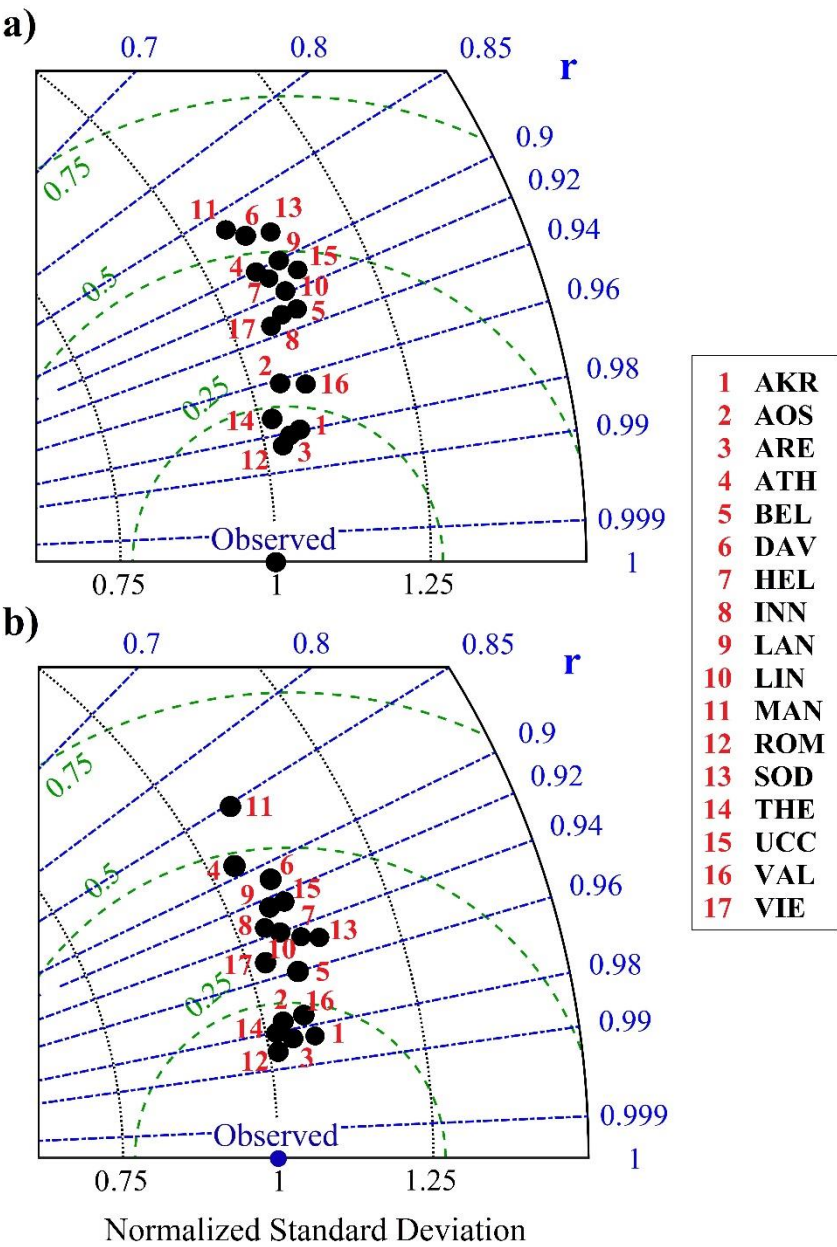


**Figure 5:** Scatter plot of the overall UVIOS performance for all stations. The analytical statistics for each station can be found in the Appendix A.

1052  
1053  
1054



1055  
1056  
1057  
1058

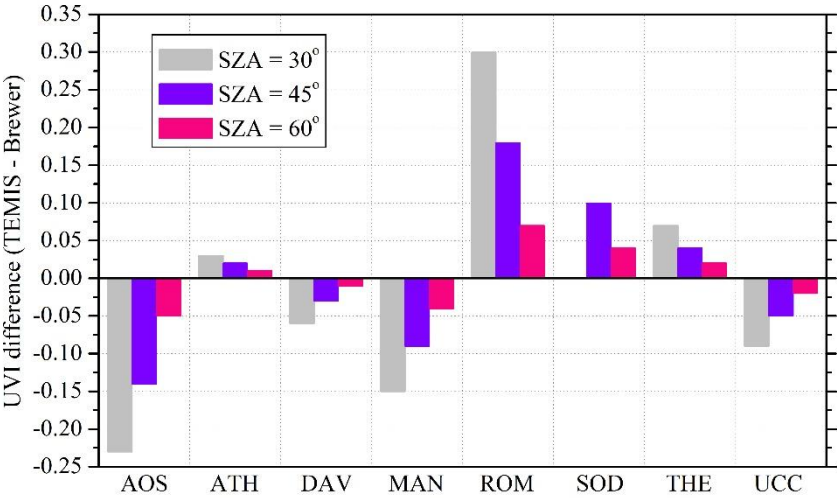
**Figure 6:** Taylor diagram for the overall UVIOS accuracy for all ground-stations under all sky (a) and clear sky (b) conditions.



**Table 4:** Mean bias error of the TEMIS TOC as compared to the WOUDC ground-based measurements.

Station	AOS	ATH	DAV	MAN	ROM	SOD	THE	UCC
MBE TOC (DU)	7.6	-0.9	1.9	5.0	-9.9	-5.4	-2.2	2.9
RMSE TOC (DU)	15.8	10.0	9.1	11.3	12.5	13.1	6.2	7.8
r	0.92	0.95	0.97	0.97	0.94	0.97	0.99	0.98

1111  
1112  
1113  
1114  
1115  
1116  
1117  
1118  
1119  
1120  
1121  
1122



1123  
1124  
1125  
1126  
1127  
1128  
1129  
1130  
1131  
1132  
1133

**Figure 7:** Differences of UVI derived by the UVIOS using as input the TEMIS and the Brewer TOC respectively at all stations with available data. (lower possible SOD SZA is 44 degrees).

1134  
1135  
1136  
1137  
1138  
1139  
1140  
1141  
1142  
1143  
1144  
1145  
1146  
1147  
1148  
1149  
1150  
  
1151  
1152  
1153  
1154  
1155  
1156  
1157  
1158  
1159  
1160  
1161  
1162  
1163

**Table 5:** Comparison results between CAMS forecasted AOD values used as UVIOS input and AERONET ground-based AOD measurements. The AOD MBE and RMSE statistical scores are shown in absolute units, along with correlation coefficient.

Station	AKR	ARE	ATH	DAV	HEL	LIN	ROM	SOD	THE	UCC	VAL	VIE
MBE	0.037	0.042	0.030	0.029	0.062	0.026	0.017	0.047	0.008	-0.007	0.024	0.071
RMSE	0.074	0.070	0.074	0.053	0.078	0.074	0.056	0.065	0.066	0.150	0.073	0.157
r	0.77	0.91	0.80	0.73	0.70	0.69	0.80	0.63	0.76	0.50	0.78	0.10



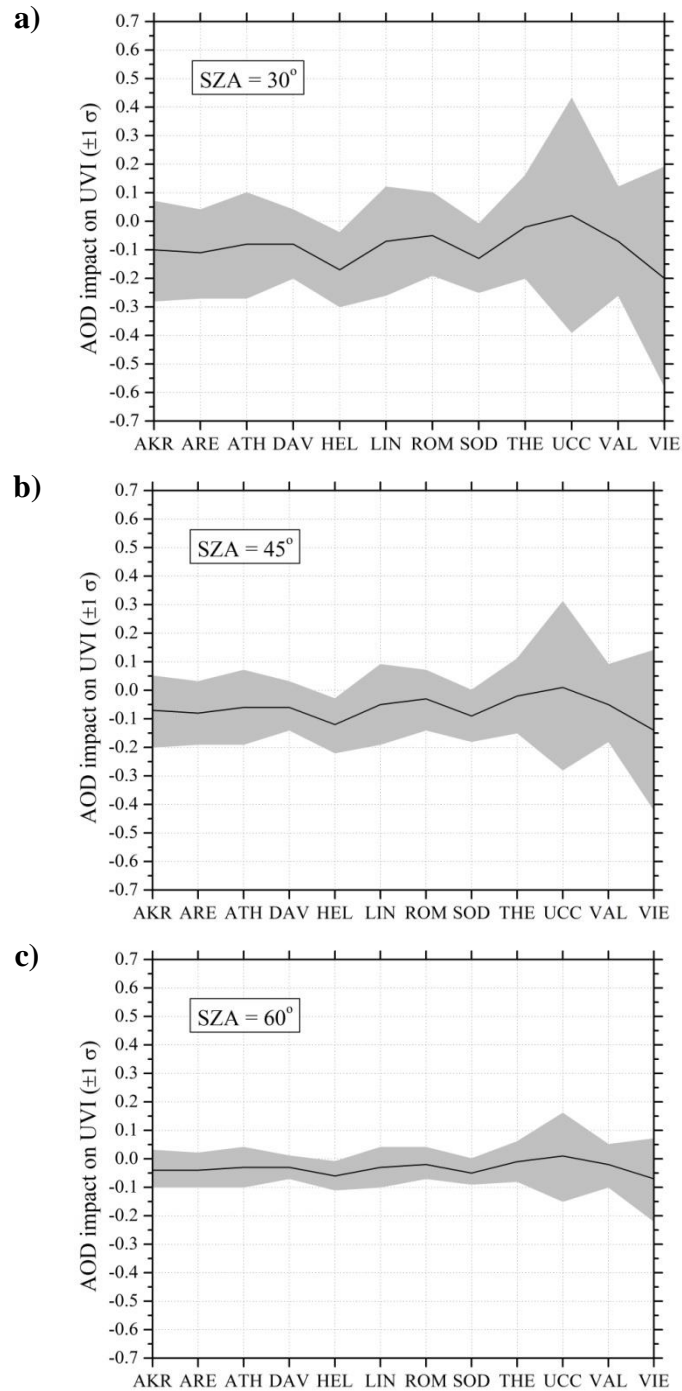
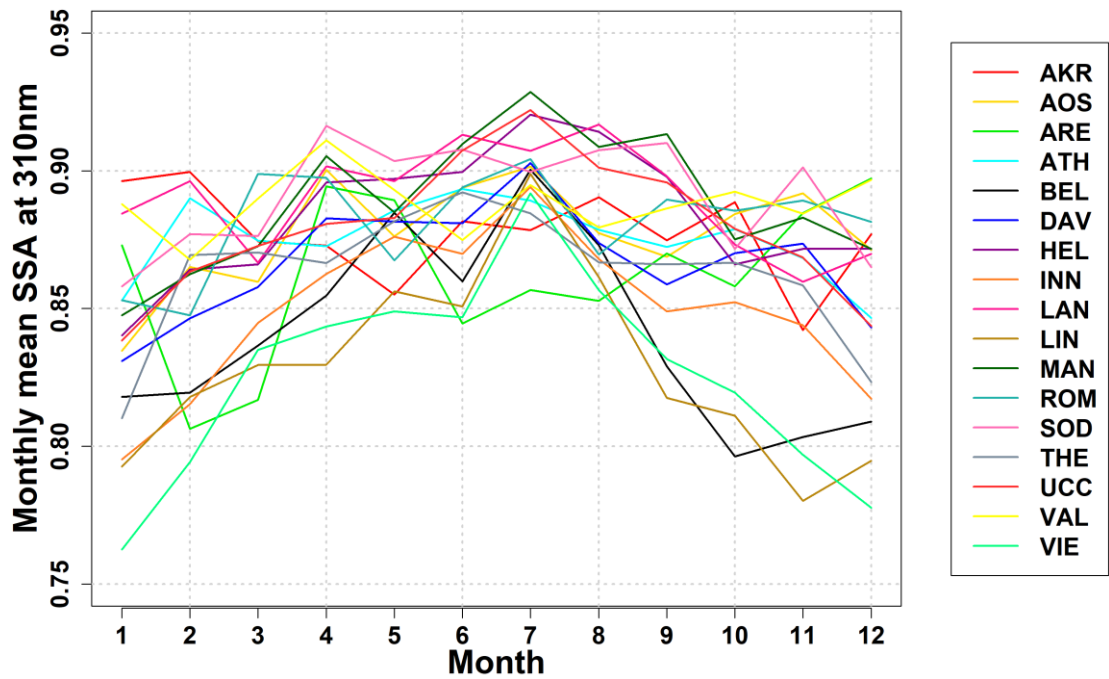


**Figure 8:** The mean bias error of the CAMS – AERONET AOD impact on UVI for all stations with available data as a function of SZA at 30 (a), 45 (b) and 60 (c) degrees together with the uncertainty range ( $\pm 1 \sigma$ ).

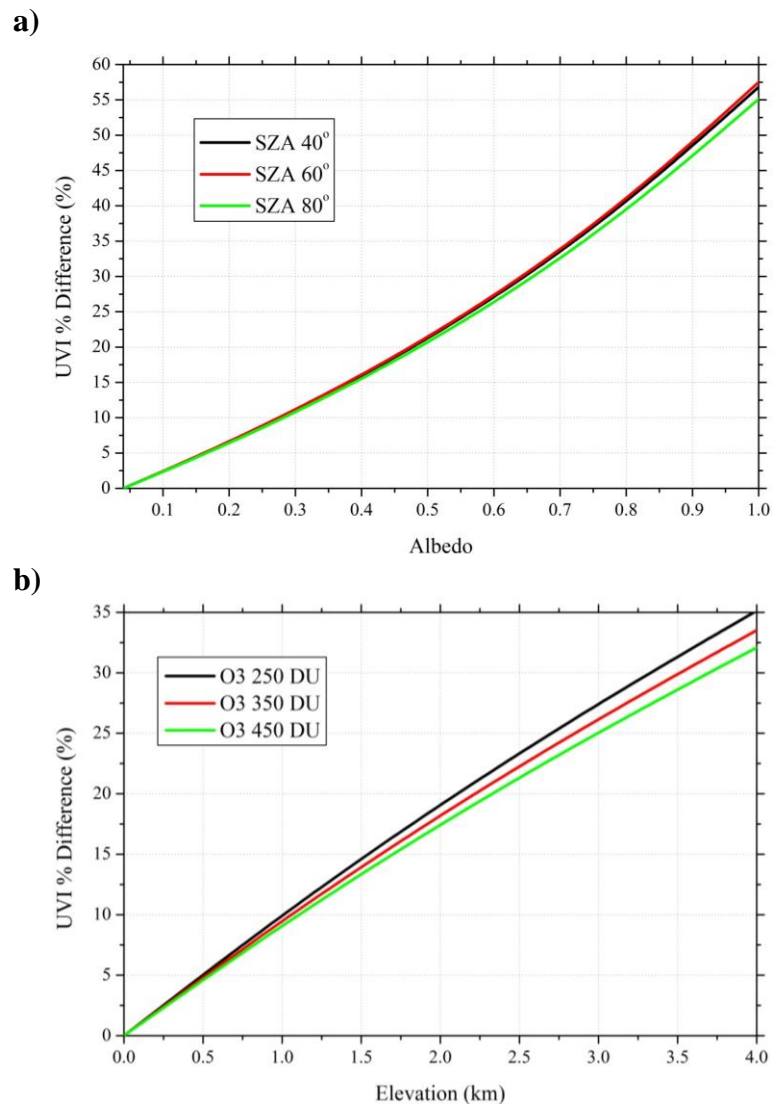
1167  
1168  
1169  
1170  
1171  
1172  
1173  
1174



1175  
1176  
1177  
1178  
1179  
1180  
1181  
1182  
1183

**Figure 9:** The monthly mean (i.e. 1-12 = Jan-Dec) SSA levels for all ground stations as derived by the MACv2 database.

1184  
1185  
1186  
1187  
1188



1189  
1190  
1191  
1192  
1193

**Figure 10:** The surface albedo effect on UVI as a function of percentage difference for various SZAs (a). The surface elevation effect on UVI as a function of percentage difference for various total ozone columns (b).

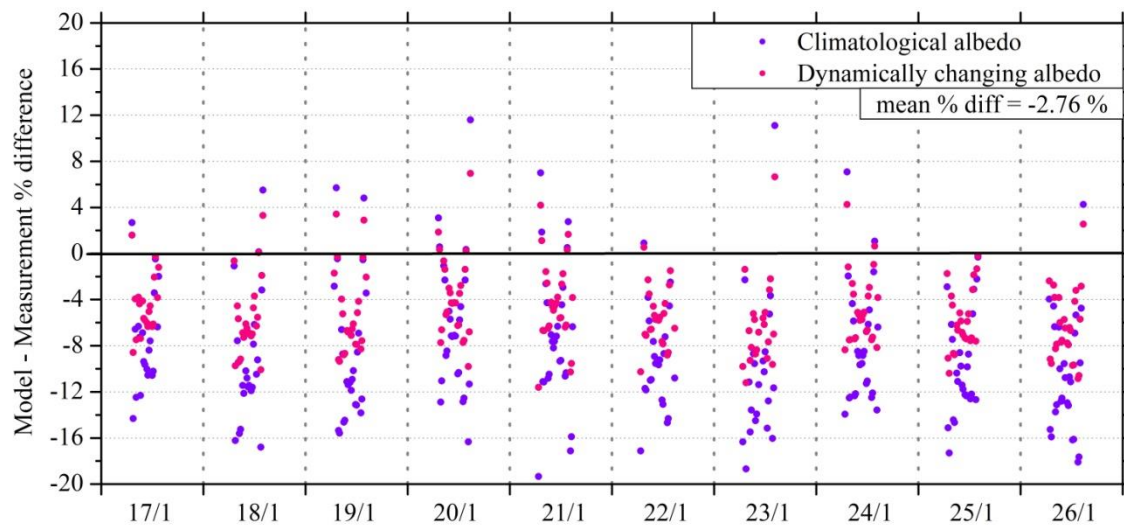
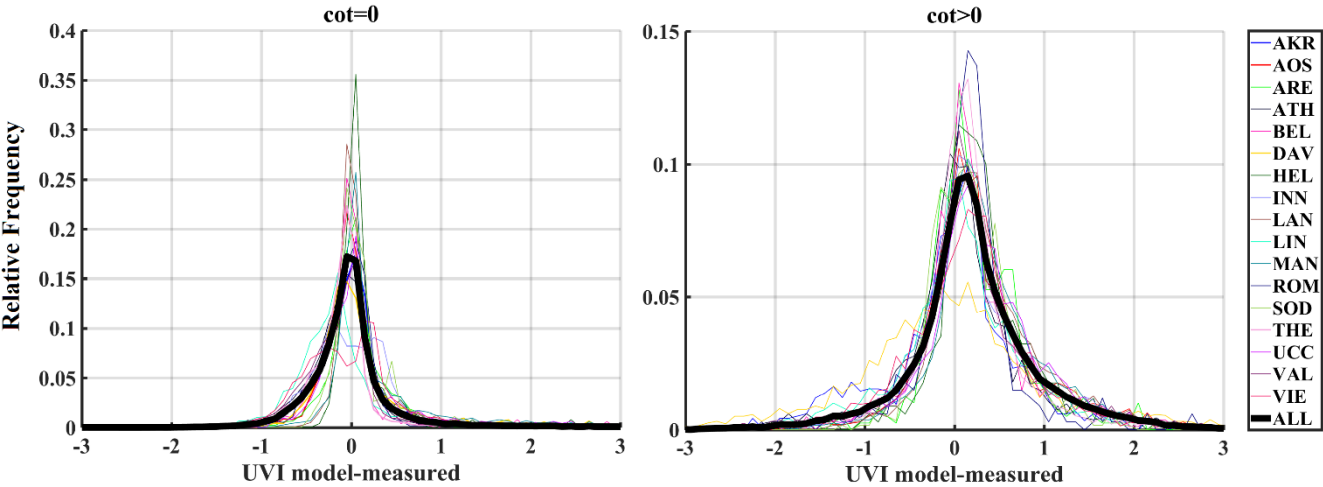


**Figure 11:** The effect of surface albedo correction on UVI for the Davos station. The climatological and the dynamically changing albedo in terms of percentage differences of modelled and ground measurements during a snow covered period (17/1 - 26/1) under clear sky conditions.

1218  
1219  
1220  
1221  
1222  
1223  
1224  
1225  
1226  
1227  
1228  
1229



1230  
1231  
1232  
1233  
1234  
1235  
1236  
1237  
1238  
1239  
1240

**Figure 12:** Relative frequency distribution of UVI residuals for all stations (coloured lines) and the mean (bold black line) for cloudless (left plot) and cloudy (right plot) conditions.

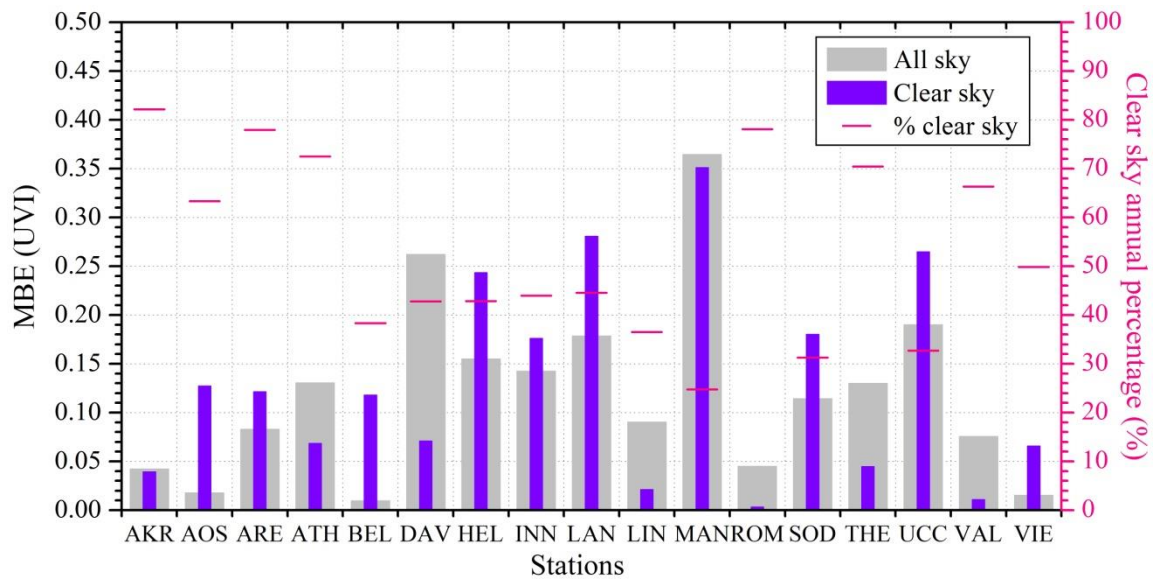


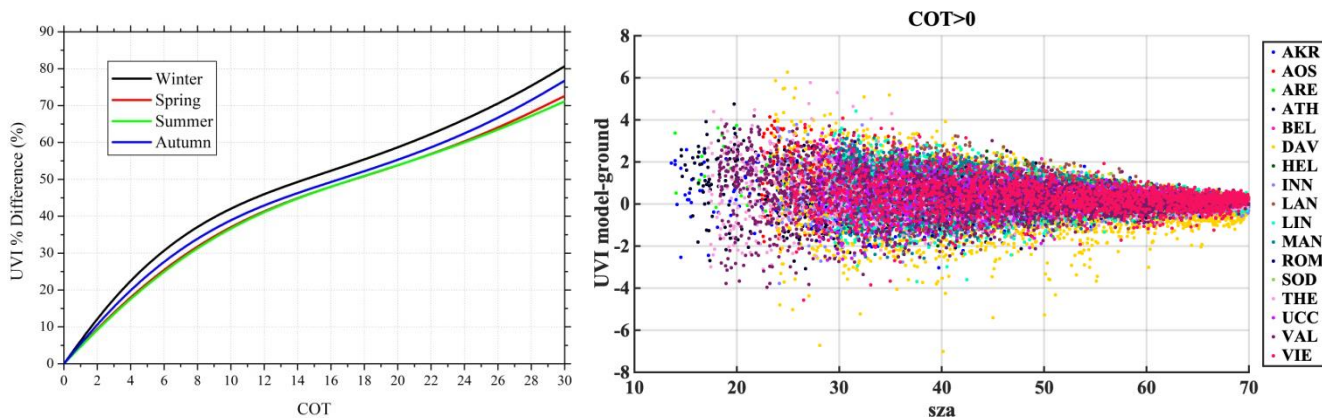
**Figure 13:** Mean bias error of the modelled UVI as compared to the ground-based measurements for all and clear sky conditions. The percentage of clear sky data time steps was also plotted with red lines.

1263  
1264  
1265  
1266  
1267  
1268  
1269  
1270  
1271  
1272  
1273  
1274  
1275  
1276  
1277  
1278  
1279  
  
1280  
1281  
1282  
1283  
1284  
1285  
1286  
1287  
1288  
1289  
1290  
1291  
1292  
1293

**Table 6:** Percentage of data for UVIOS underestimation (A1-A3) and overestimation (B1-B3) under clear and cloudy sky conditions for various UVI difference (modelled-ground) classes.

Difference of UVI	< -1.0 (A1)	< -0.5 (A2)	< 0.0 (A3)	> 0.0 (B3)	> 0.5 (B2)	> 1.0 (B1)
% of data COT > 0	3.6	11.5	37.5	62.5	24.8	11.1
% of data COT = 0	0.9	10.2	45.4	54.6	11.4	4.2

1294  
1295  
1296  
1297  
1298  
1299  
1300  
1301  
1302  
1303  
1304  
1305  
1306

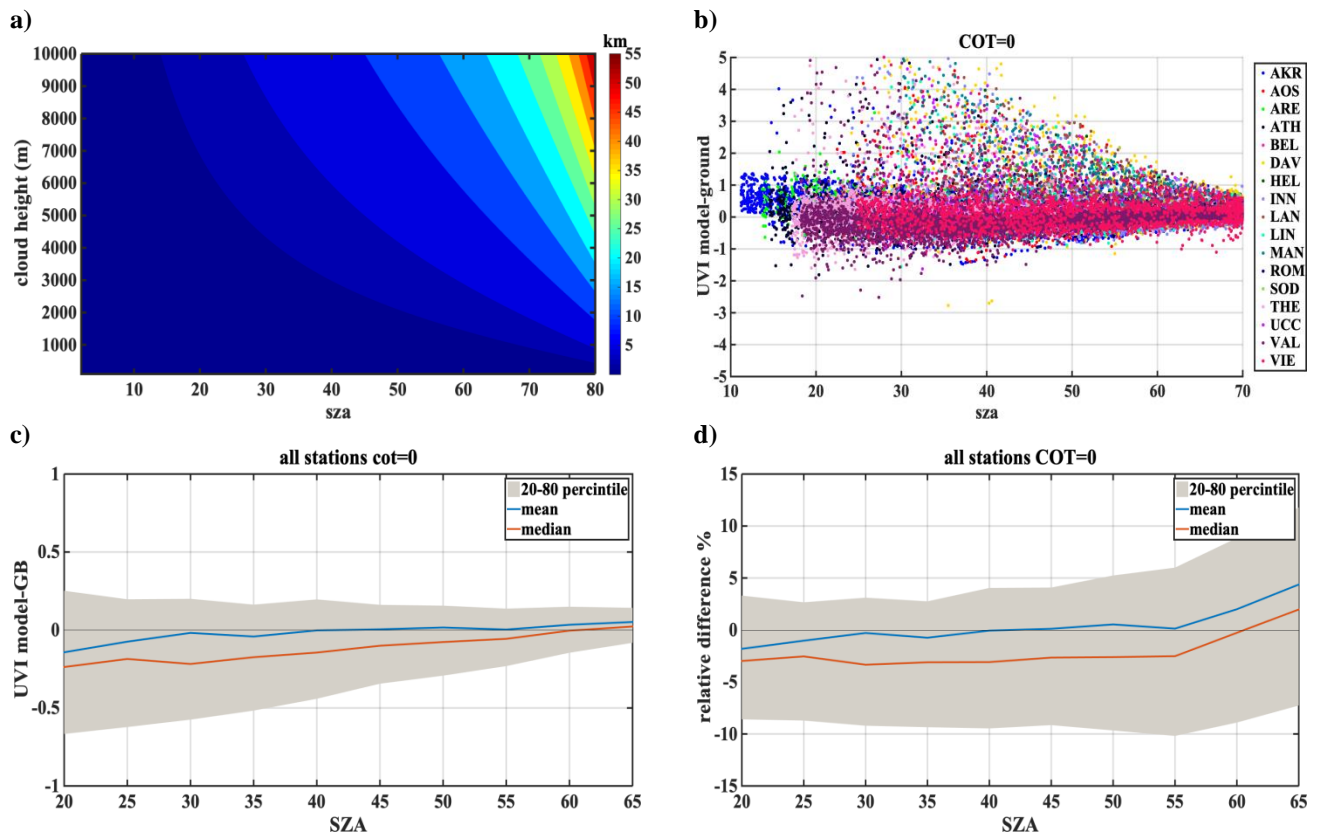


1307 **Figure 14:** The average COT effect on UVI as a function of percentage difference for all seasons (left) and scatterplot of the UVI difference  
1308 under cloudy sky conditions for all stations (right).

1309  
1310  
1311  
1312  
1313  
1314  
1315  
1316  
1317  
1318



1319  
1320  
1321  
1322  
1323  
1324  
1325



1326  
1327  
1328  
1329  
1330  
1331  
1332  
1333

**Figure 15:** The shadow volume at the surface level of a cloud relative to the SEVIRI angle view, as a function of cloud height and SZA (a). Scatterplot of the UVI difference under clear sky conditions for all stations (b). UVI mean, median and 20-80 percentile differences (c) and percentage differences (d) derived by the UVIOS as compared to the ground-based measurements for clear sky conditions as a function of SZA.

**Appendix A**

The following set of Figures (A.1 – A.17) show for all stations, density scatterplots of measured and modeled UVI for all sky and clear sky conditions (upper row), normalized probability histogram of differences (middle row), and boxplot of differences (lower row) as a function of SZA, representing median (red lines), mean (blue dotted lines) 25-75 percentiles (blue boxes) and 5-95 whiskers (dotted lines). Table A.1 shows additionally the amount of data points that represent both all sky and clear sky conditions for the studied stations.

We have categorized the stations mostly based on cloud cover as Mediterranean, Central Europe, High altitude and High latitude. Each of the station has its own characteristics in terms of atmospheric conditions and parameters affecting the UVI reaching the ground. A summary of the results with possible explanation of the differences observed are shown here. The Mediterranean region includes the stations THE, ATH, AKR, ROM, VAL and ARE. Analysis of TOC showed that in most of the cases UVI mean differences are less than 0.1 in general while a negative bias between TOC and the ground measurements was seen to be highest for ROM (-9.9) that corresponds to the UVI difference of 0.3. Impact of AOD uncertainty showed the correlation coefficient between the modelled and the measured UVI values above 0.7 for most of the stations while it was as high as 0.91 for ARE. The mean bias between the modelled and measured UVI for clear sky condition was found to be less than that for the all sky condition for the stations AKR, ATH and THE that had most days of the year as cloud-free (the clear sky percentage is above 70%). The mean bias between the modelled and measured UVI for clear sky condition was more than the all sky condition for ARE even though it had mostly clear skies throughout the year. The analysis of the combined effect of the aerosol and ozone at Thessaloniki revealed that the model showed a slight underestimation with real inputs (AERONET and Brewer) while overestimations for forecasted inputs (CAMS and TEMIS). However, the coefficient of correlation was found to be as 0.989 and 0.992 for the model with forecasted and real inputs, respectively. Stations of this classification have the single scattering albedo ranging from 0.76 to 0.93, with most of them having SSA values between 0.83 to 0.93 except stations ARE and THE that had relatively smaller SSA values (0.76-0.9) and greater variability, and large MBE. AKR station comparison showed some UVIOS calculated UVI at higher levels than the ground-based measurements especially in low SZA's. However, ground-based UVI measurements seem more unrealistic than the UVIOS calculated UVI for summer local noon conditions as modeled UVIs with real AOD and TOC measurements at the area tend to agree with UVIOS outputs.

The second classification is the Central European regions including AOS, UCC, BEL, MAN, LIN, VIE and INN. The median of the absolute UVI differences between the model and the measurement for all sky condition were higher for MAN and UCC while for others it was close to zero. Larger UVI difference of -0.22 due to TOC uncertainty impact was observed for AOS which might be due to large values of UVI at higher altitude as the positive bias is highest for AOS station (7.6). The UVIOS MBE and RMSE statistical scores for analyzing AOD uncertainty impact showed a mean positive bias up to 0.071 for all the stations except UCC which is showed a mean negative bias of 0.007. The mean bias between the modelled and measured UVI for clear sky condition was more than the all sky condition for AOS even though it had mostly clear skies throughout the year. BEL, UCC and VIE showed more MBE for clear sky condition than the all sky condition as they have mostly cloudy skies

1367 throughout the year (clear sky annual percentage less than 50%). However, stations LIN and MAN also have more MBE for  
1368 clear sky condition even though they have most days of the year as cloudy (clear sky annual percentage less than 45%).  
1369 Analysis of AOD uncertainty showed that UVI difference was highest for VIE than the other stations. The monthly values of  
1370 the single scattering albedo used in UVIOS ranged from 0.76 to 0.93 for stations AOS, UCC and MAN, with most of them  
1371 having SSA values between 0.83 to 0.93, and relatively small variability. While, the stations BEL, INN, LIN and VIE had  
1372 relatively smaller SSA values (0.76-0.9) and greater variability than the other stations and most of these stations have shown  
1373 large MBE.

1374 The high altitude station is DAV and high latitude stations include LAN, HEL and SOD. DAV have less MBE for clear sky  
1375 condition even though they have most days of the year as cloudy (clear sky annual percentage less than 45%). DAV and MAN  
1376 show worse statistical behavior for clear sky, which is probably caused by misclassification of cloudy pixels. For DAV this  
1377 could be explained by the complex mountainous topography of the area. Large UVI differences in SOD and HEL indicate  
1378 higher introduced uncertainties over higher latitudes. Higher aerosol levels in the atmosphere tend to lower the UVI. Highest  
1379 difference in UVI is observed for the stations HEL, SOD and VIE. Since, the aerosol level at the stations HEL and SOD is  
1380 very low this leads to higher UVI which can be the reason for the small UVI differences observed for these stations. The  
1381 stations of this classification have mostly cloudy skies throughout the year (clear sky annual percentage less than 50%) and  
1382 have more MBE for clear sky condition than the all sky condition. This might be due the fact that the clouds are not captured  
1383 well at a point station and a cloudy sky might have been considered as a clear sky. Higher UVI difference was observed for  
1384 HEL and SOD as a result of AOD uncertainty analysis which might be due to the low aerosol content of these stations due to  
1385 higher latitude that leads to higher UVI values.

1386  
1387

Table A.1 Number of data points and clear sky data points, used in the analysis for each station.

Station	All data	Data COT=0
AKR	6547	5379
AOS	5607	3551
ARE	1814	1414
ATH	4892	3548
BEL	1317	505
DAV	5635	2410
HEL	595	255
INN	4365	1919
LAN	7409	3302
LIN	3795	1387
MAN	7854	1946
ROM	1532	1196
SOD	860	269
THE	9750	6867
UCC	3007	983
VAL	9795	6497
VIE	4199	2094

1388

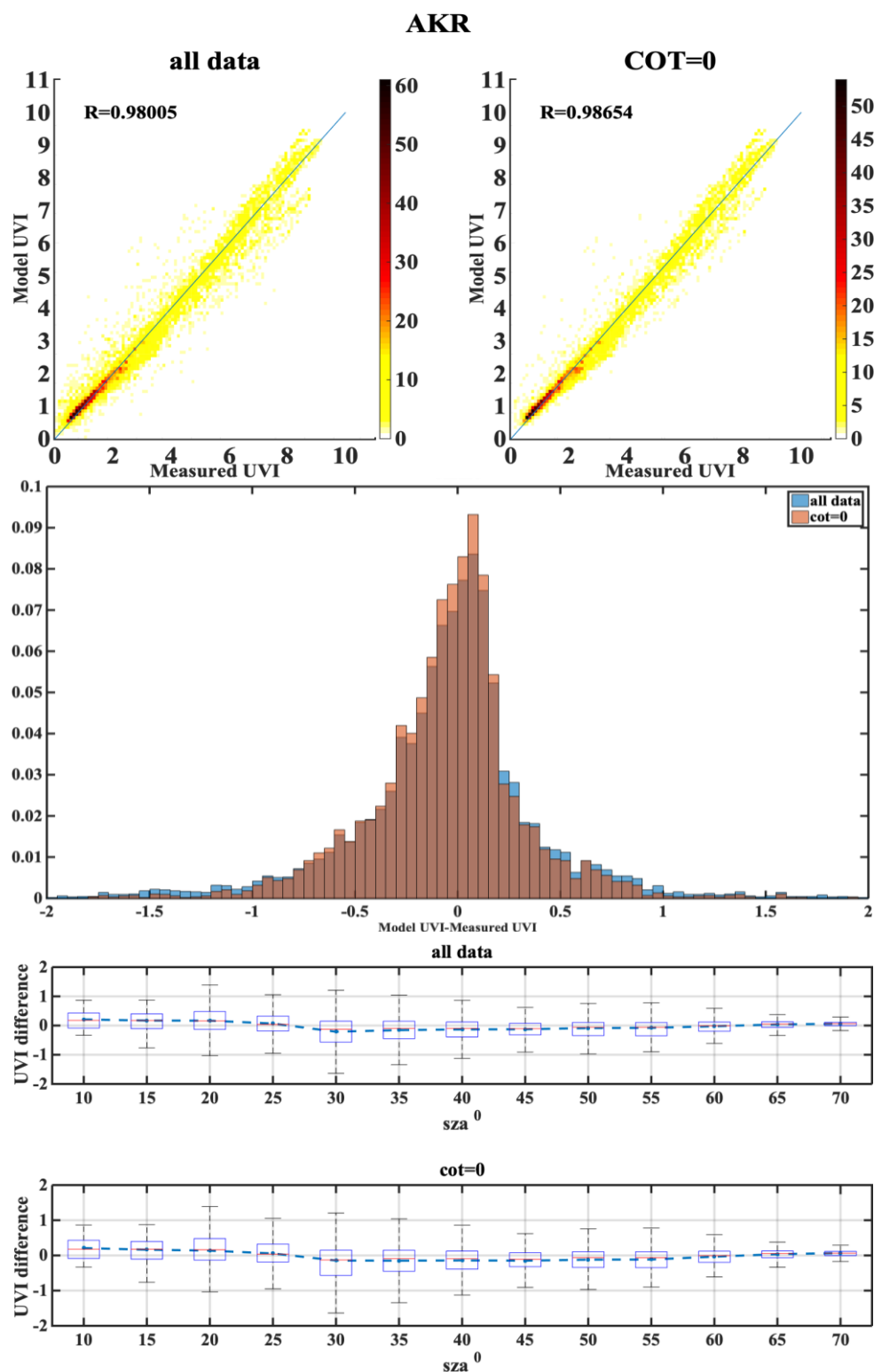


Figure A.1

# AOS

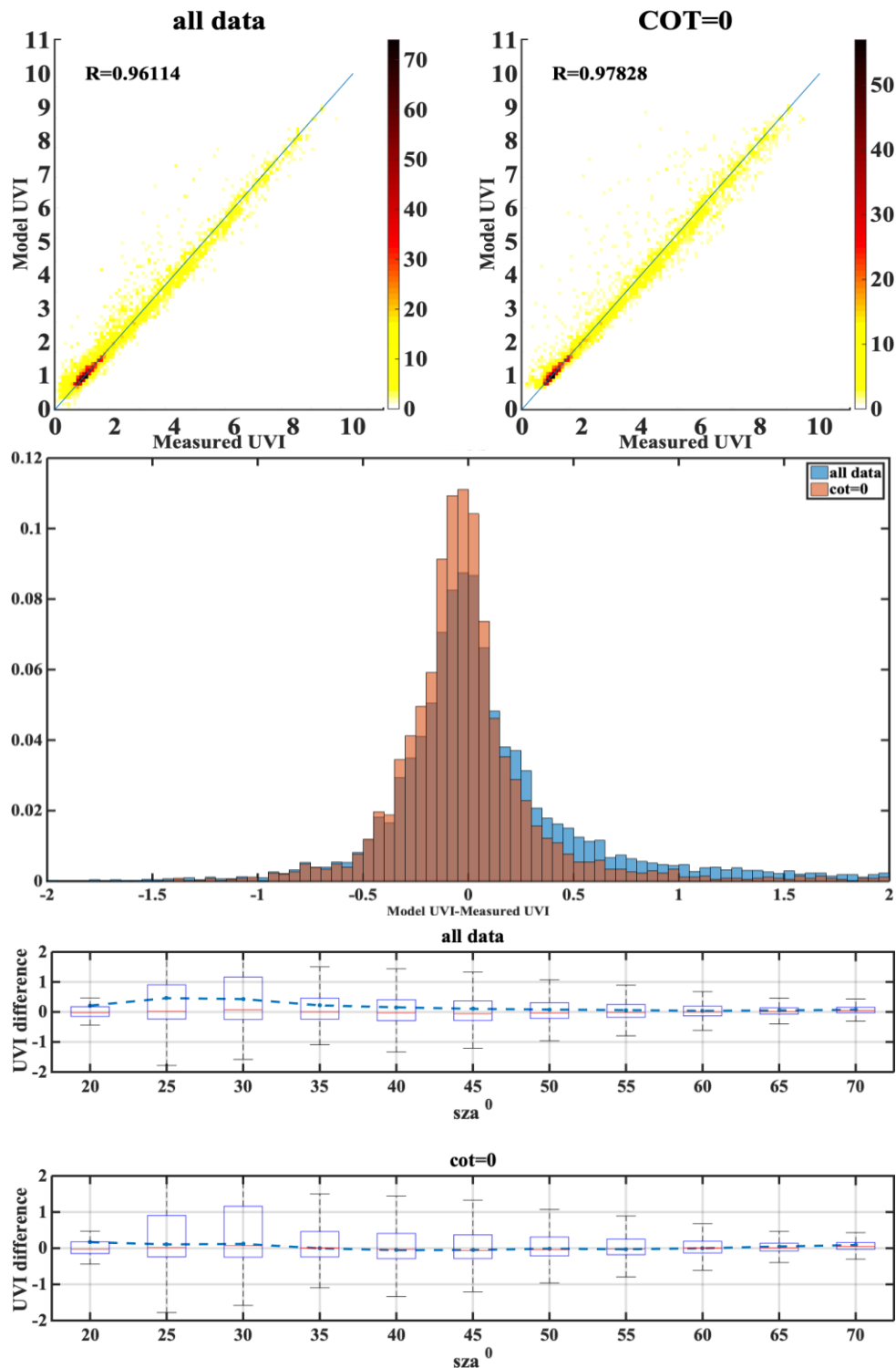


Figure A.2

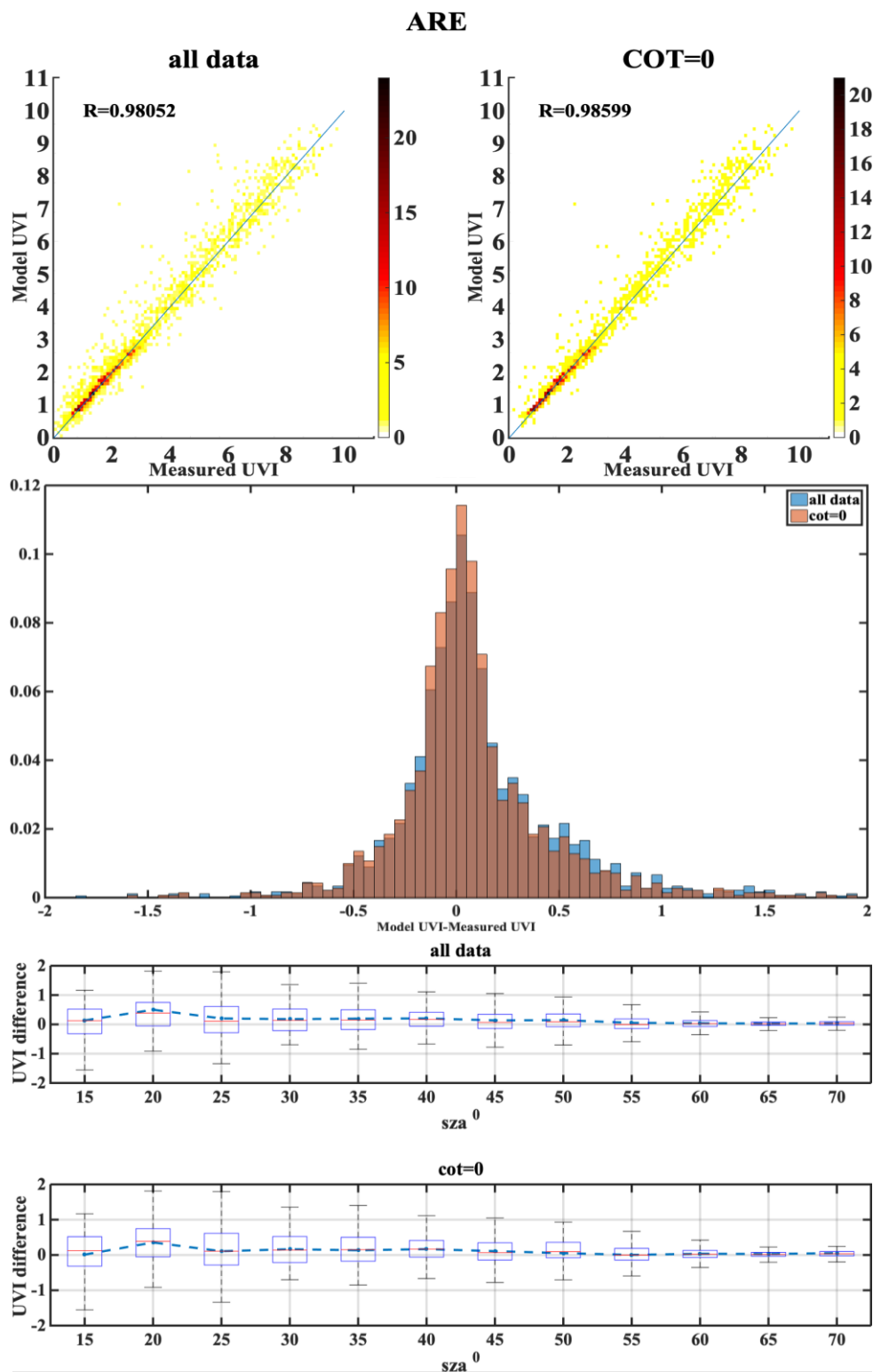


Figure A.3

# ATH

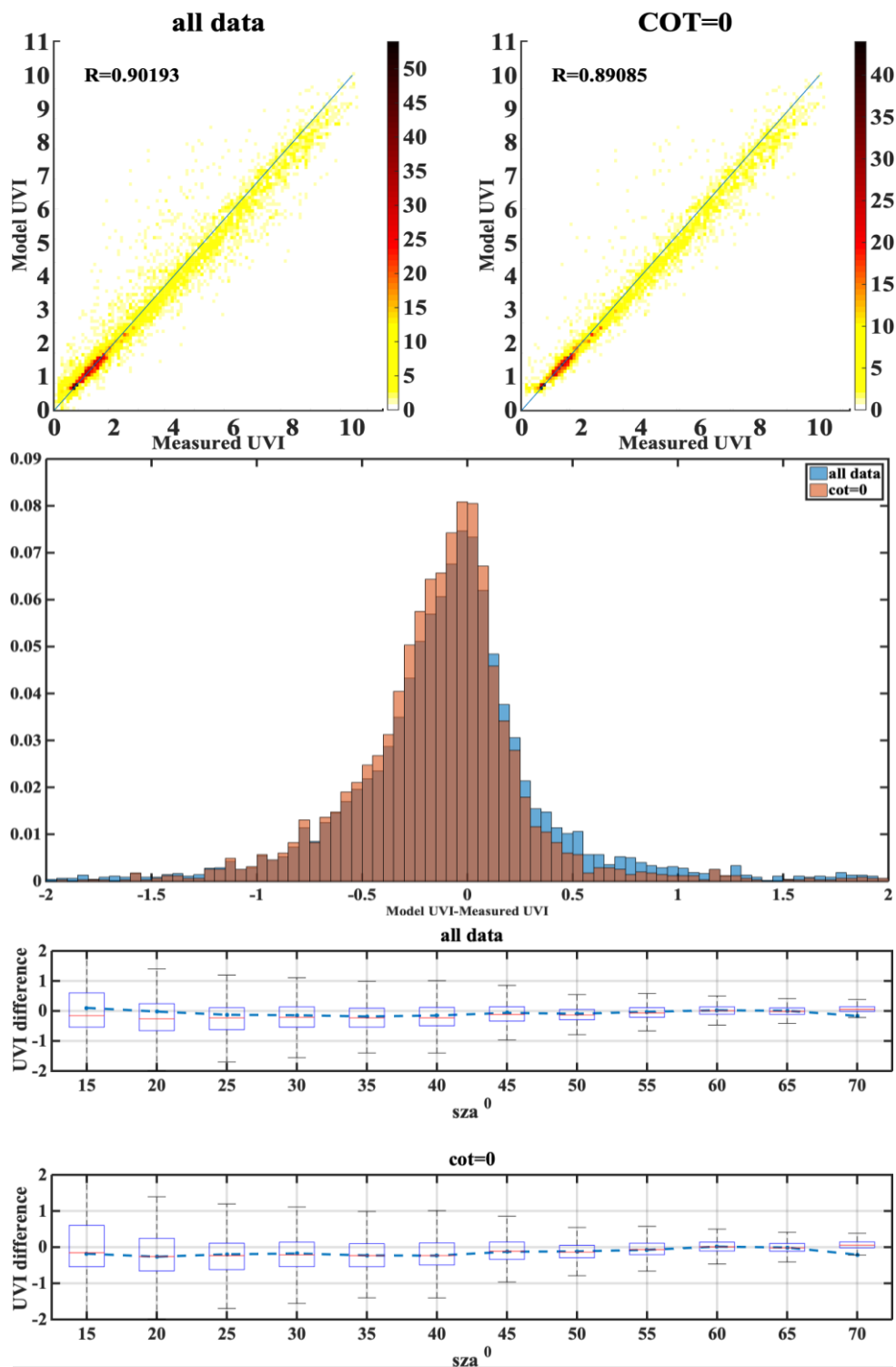


Figure A.4

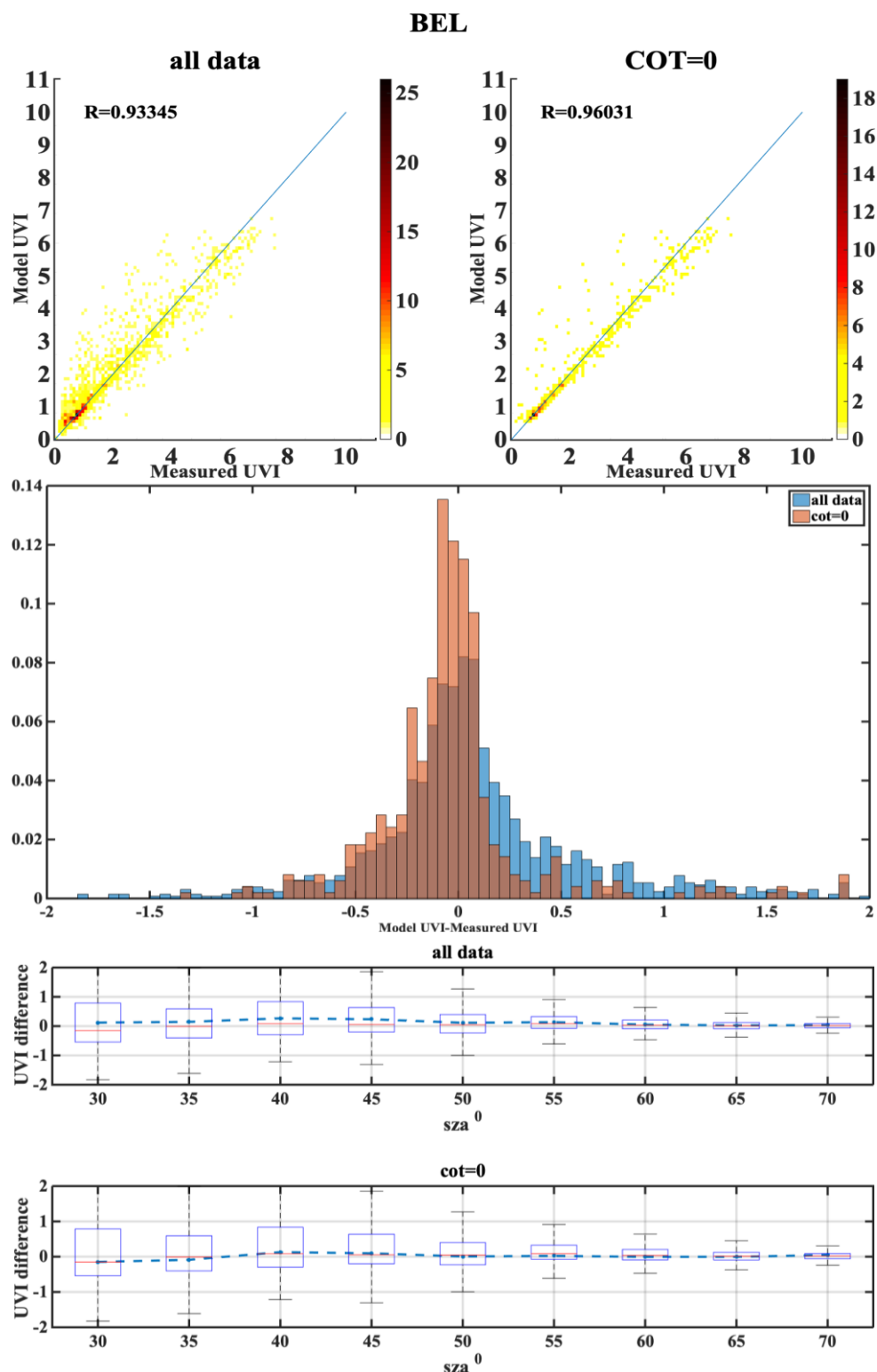


Figure A.5



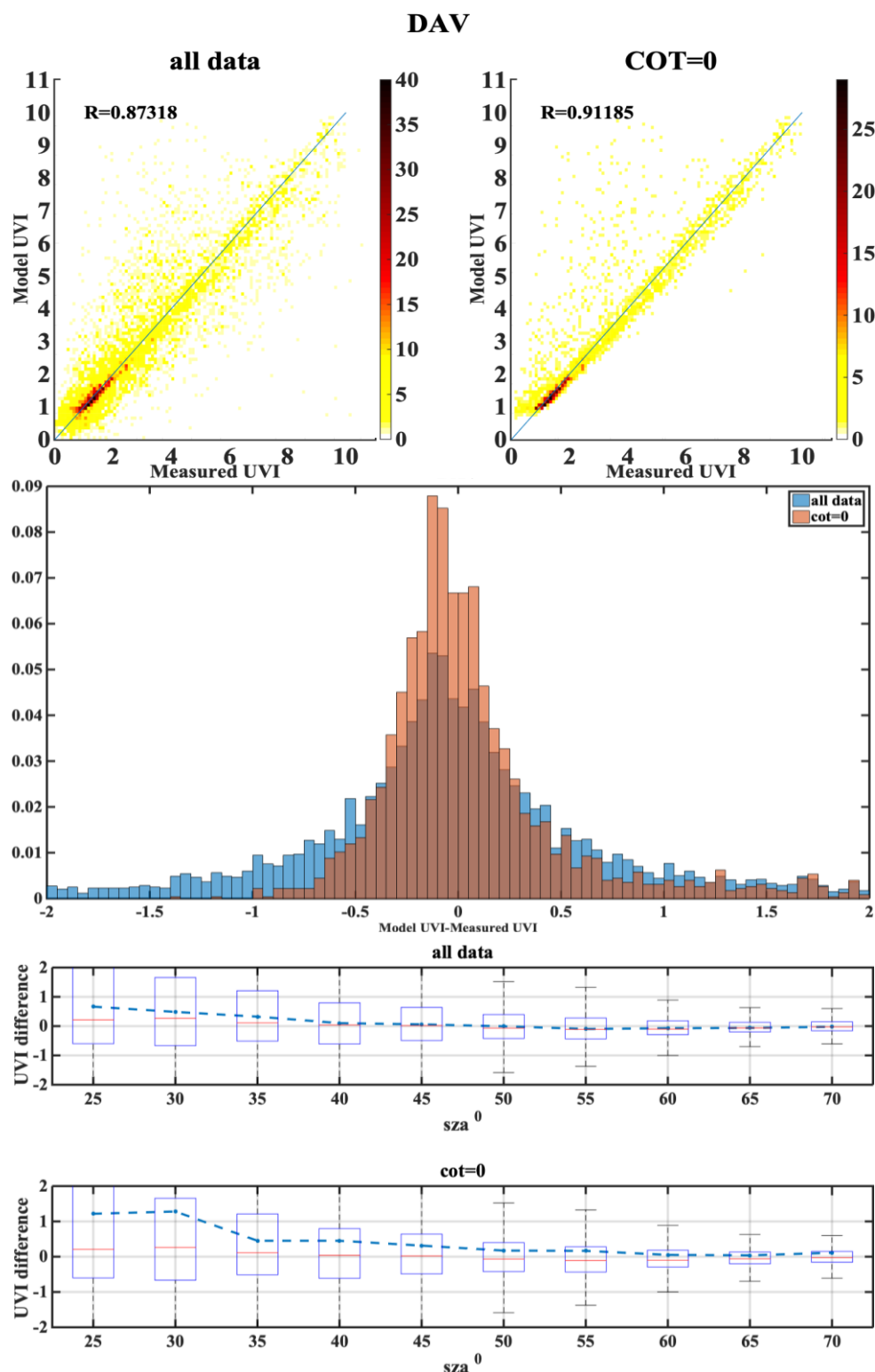


Figure A.6

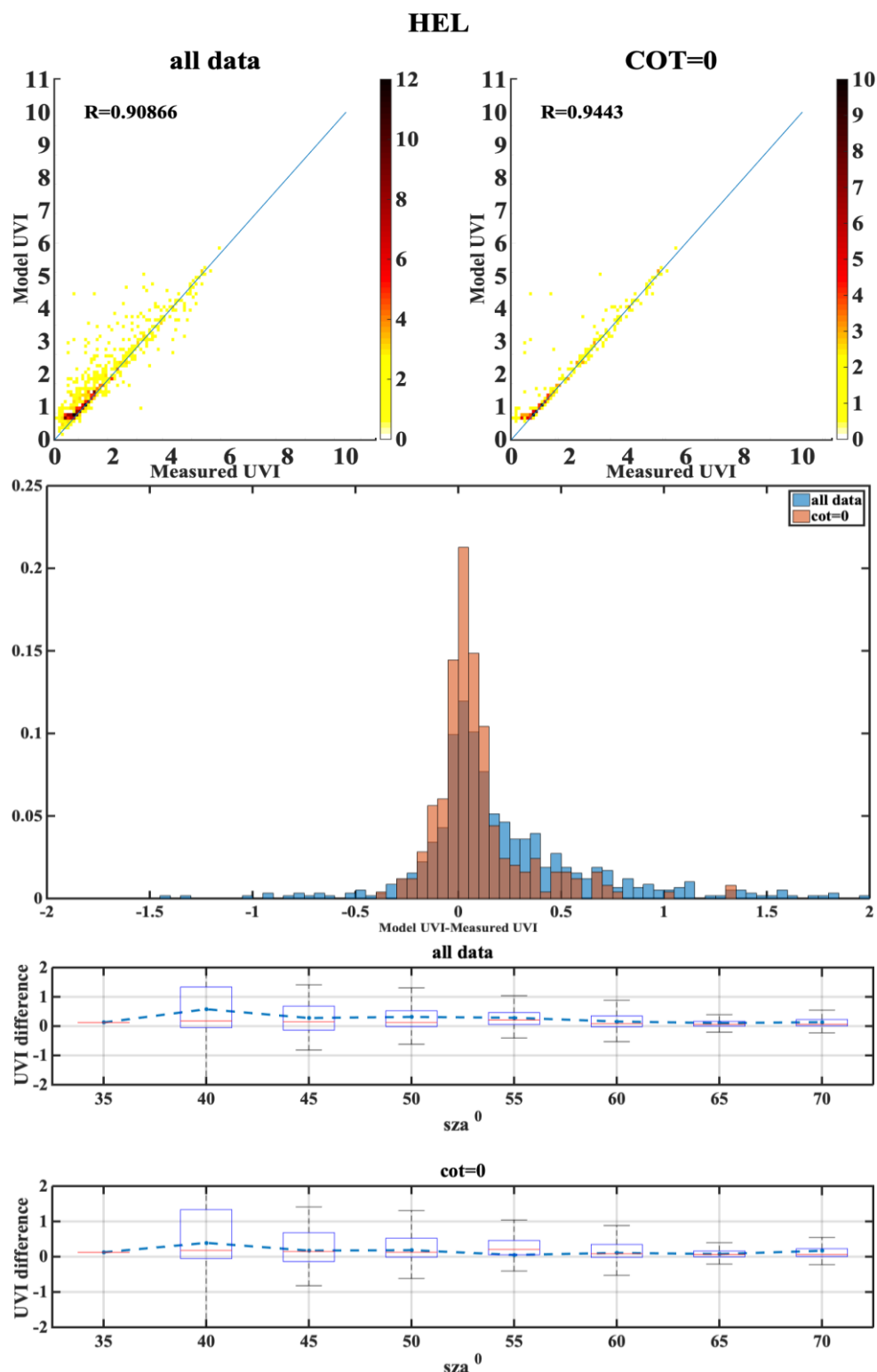


Figure A.7

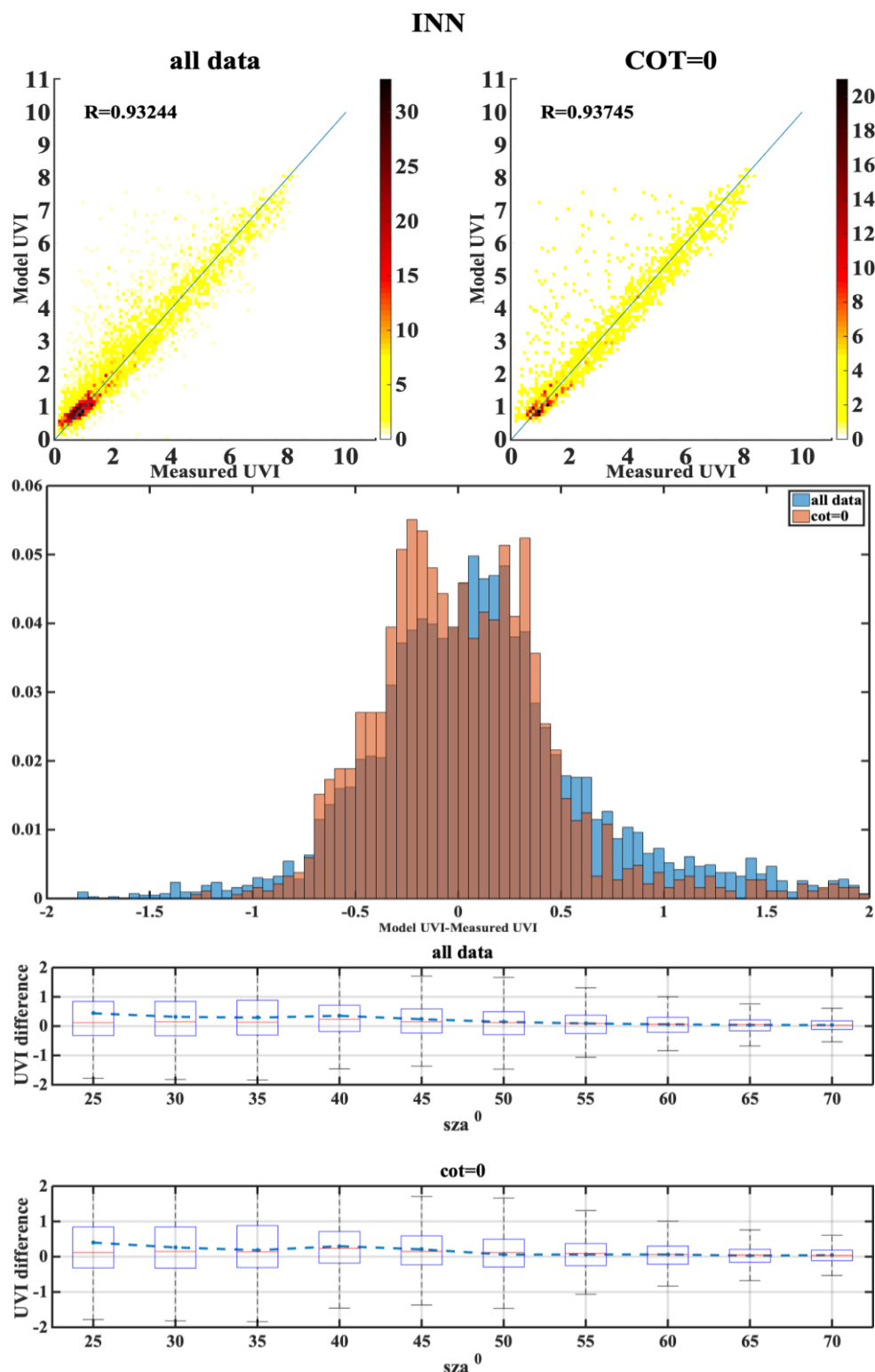


Figure A.8

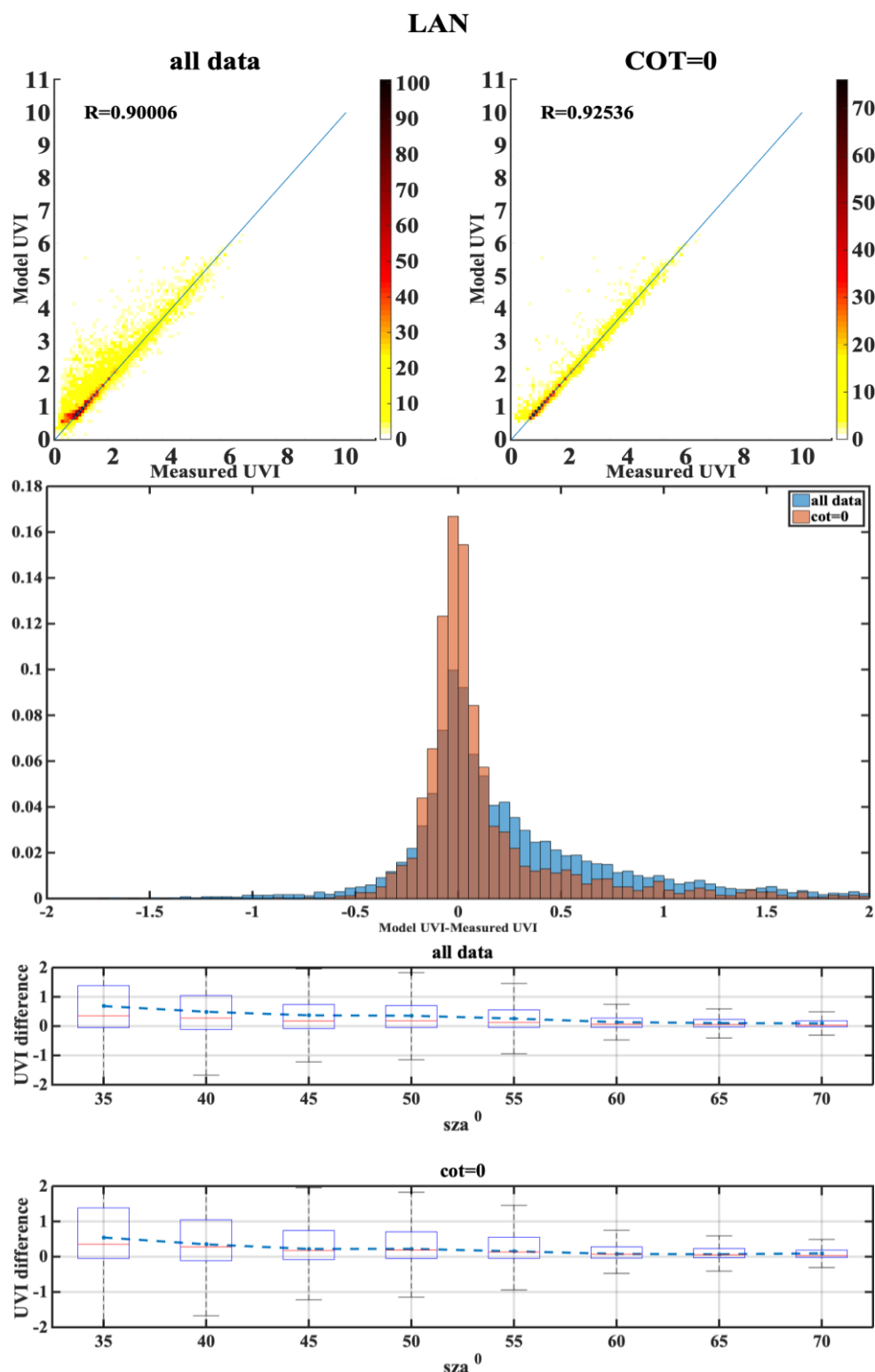


Figure A.9

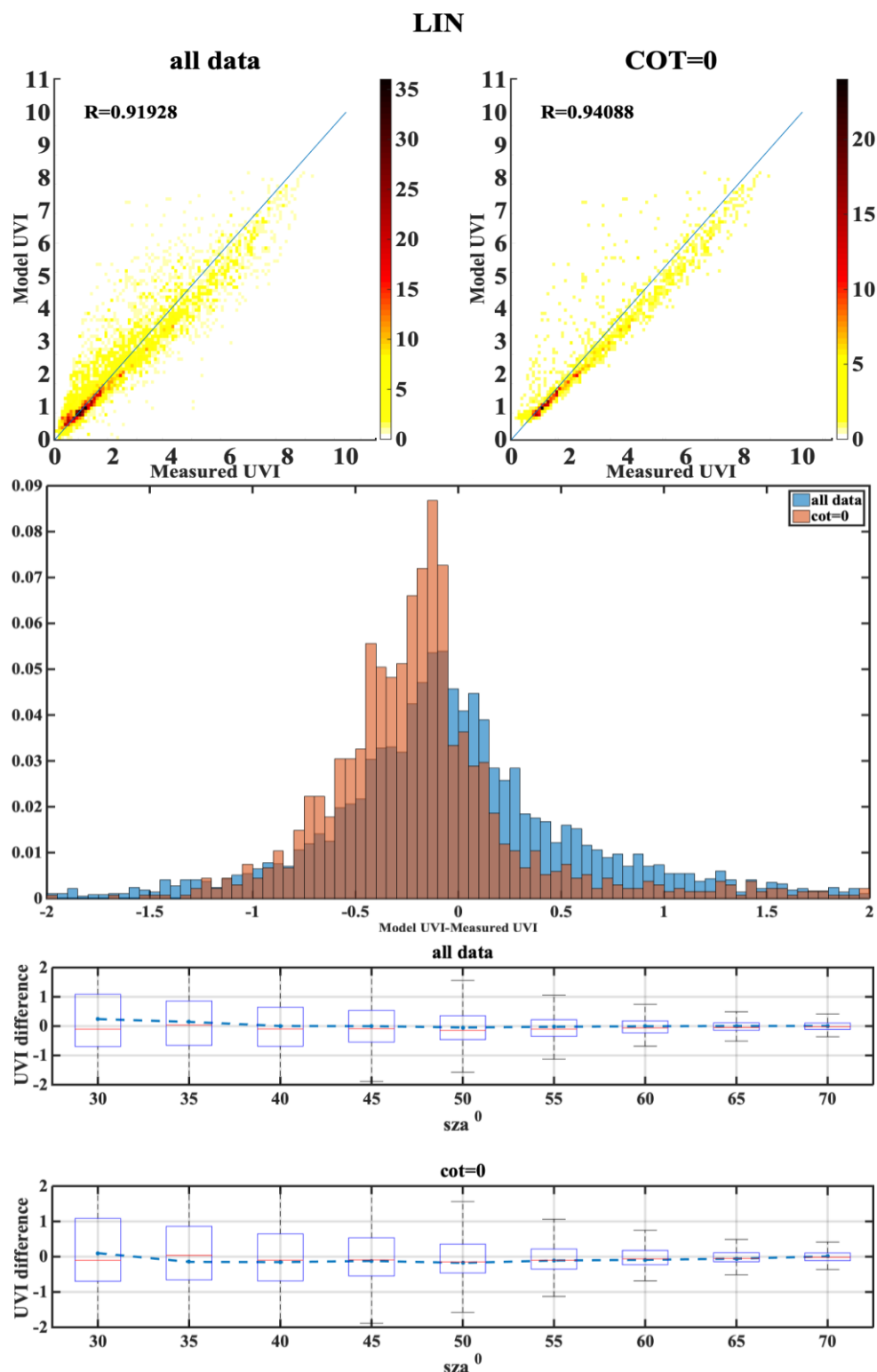


Figure A.10

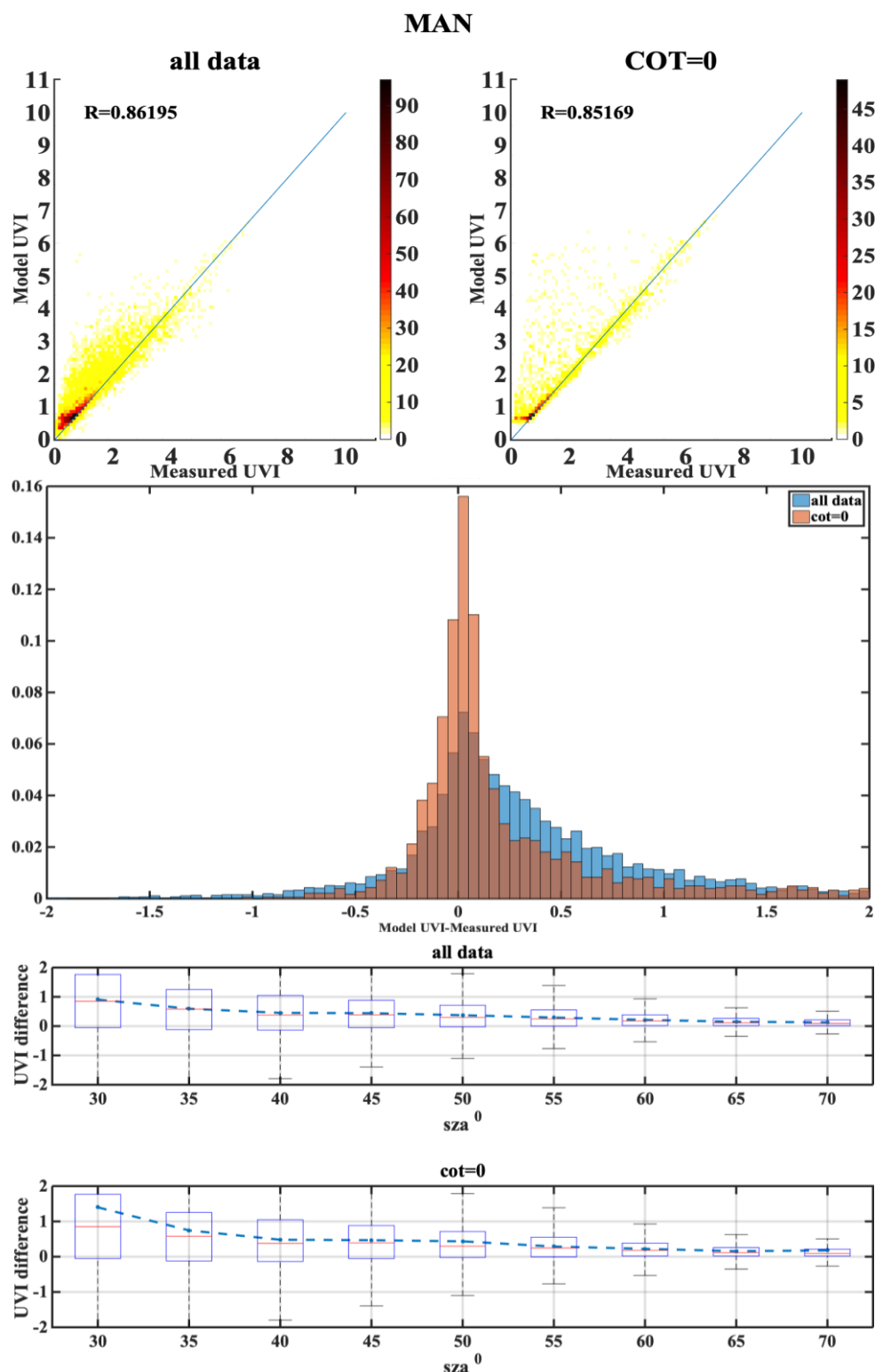


Figure A.11

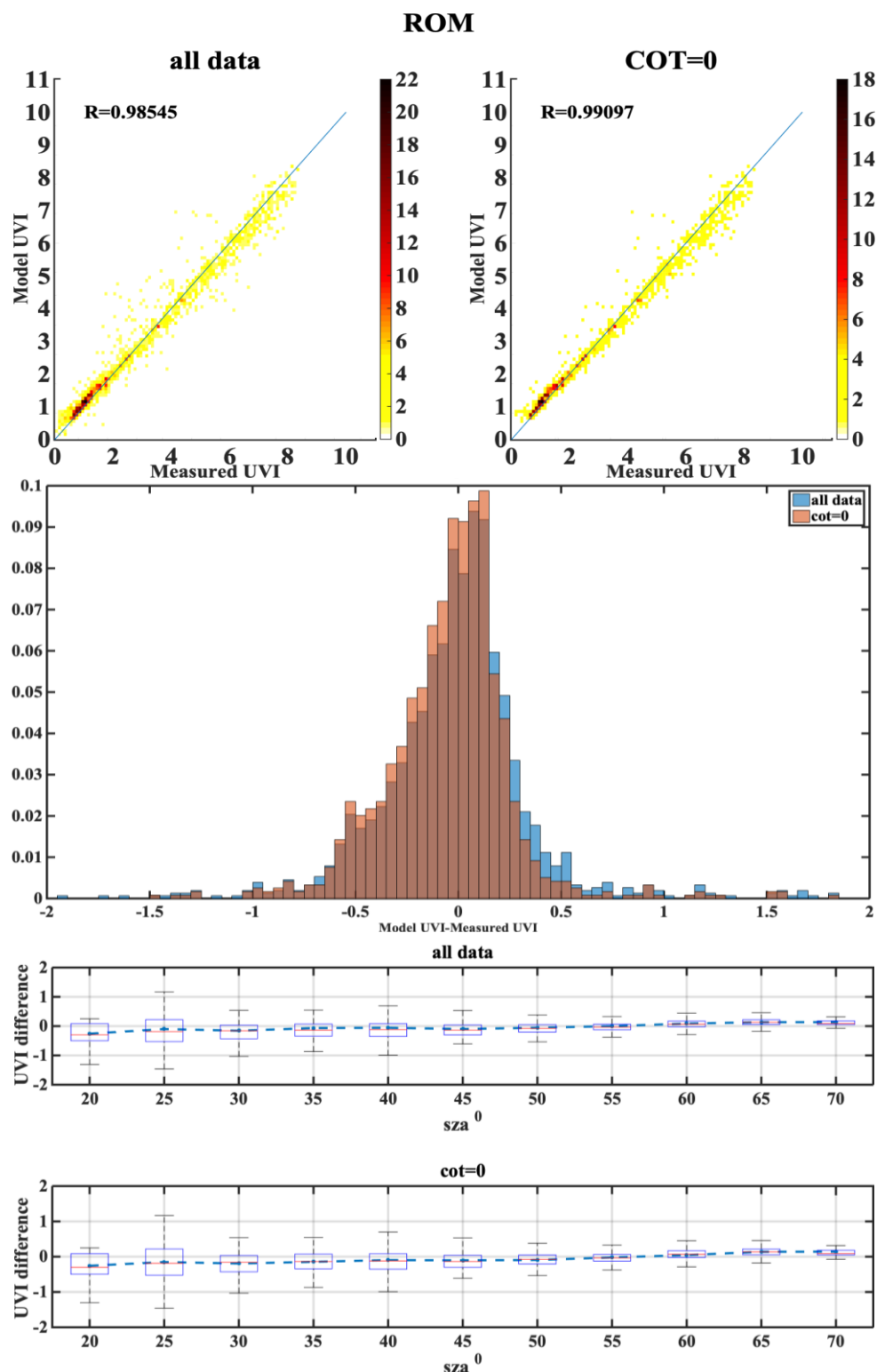


Figure A.12

# SOD

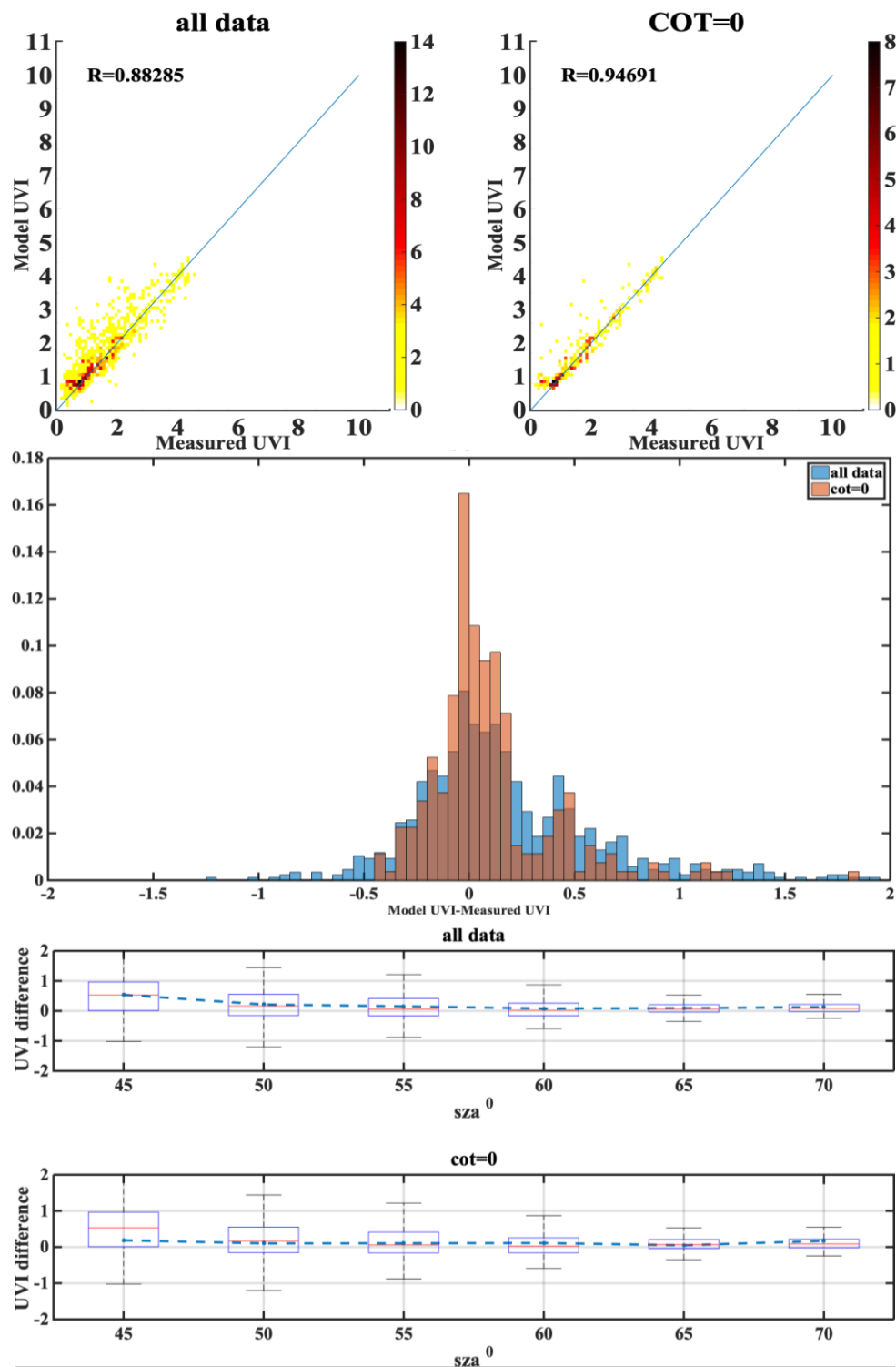


Figure A.13



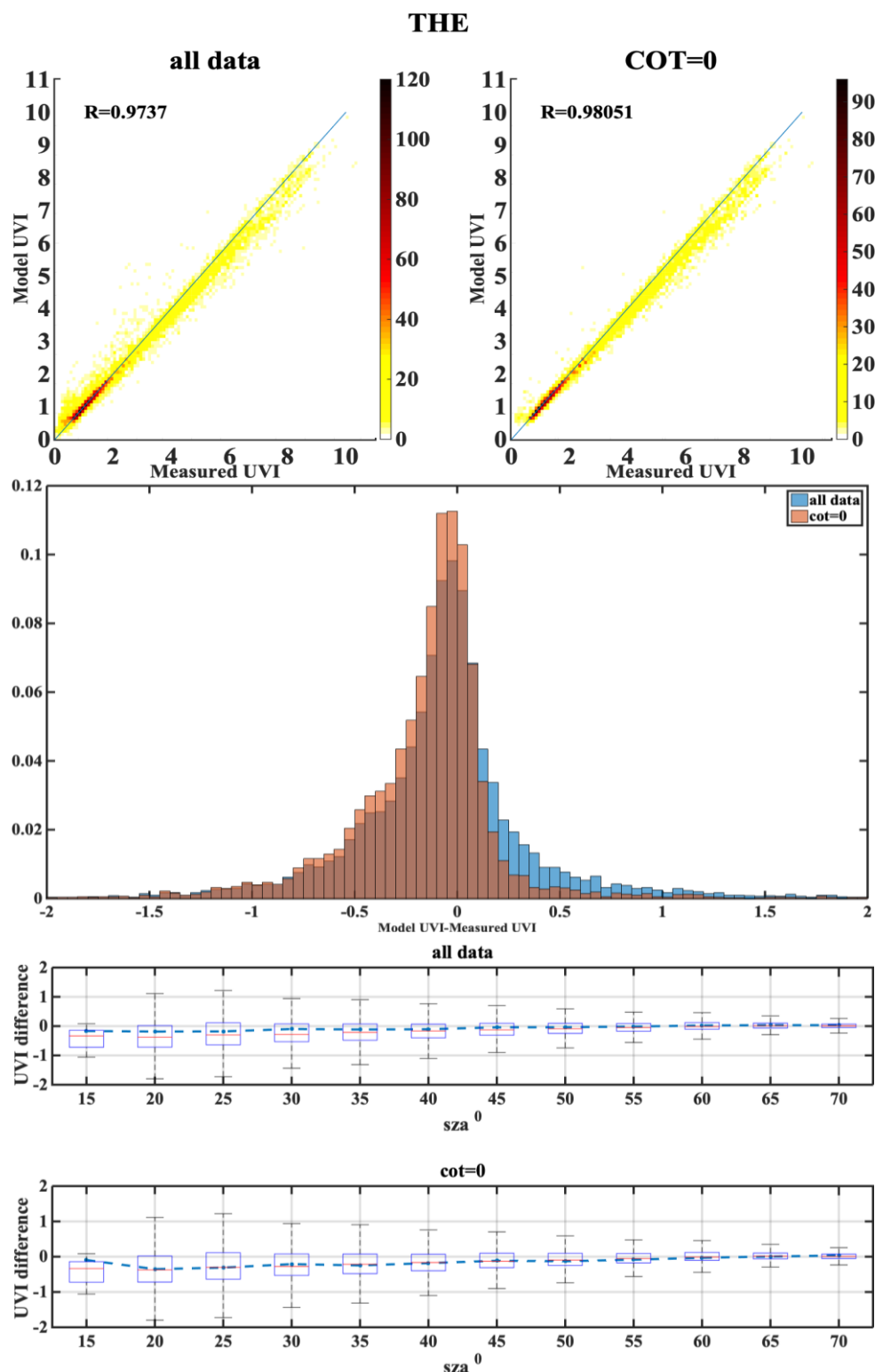


Figure A.14

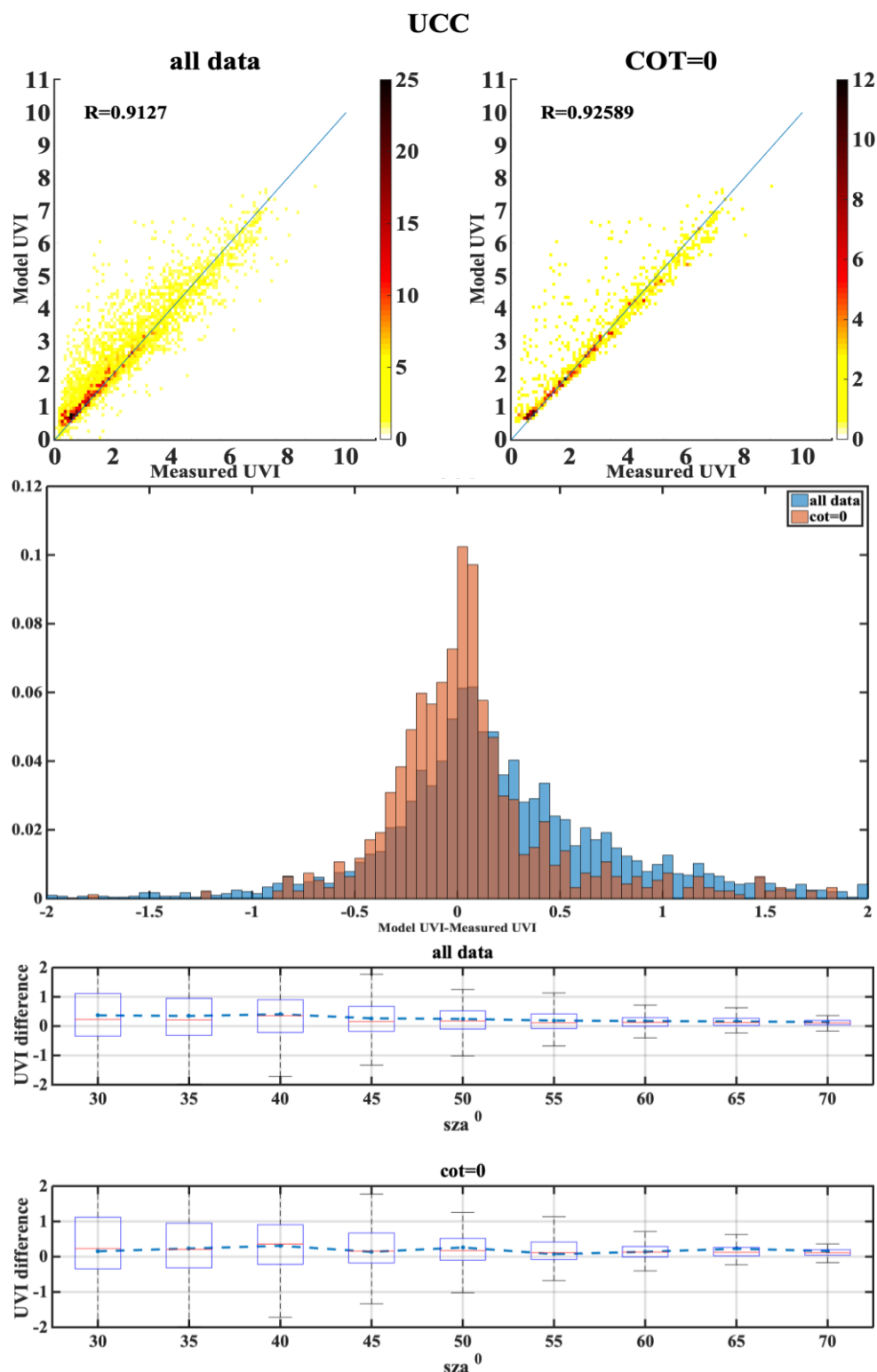


Figure A.15

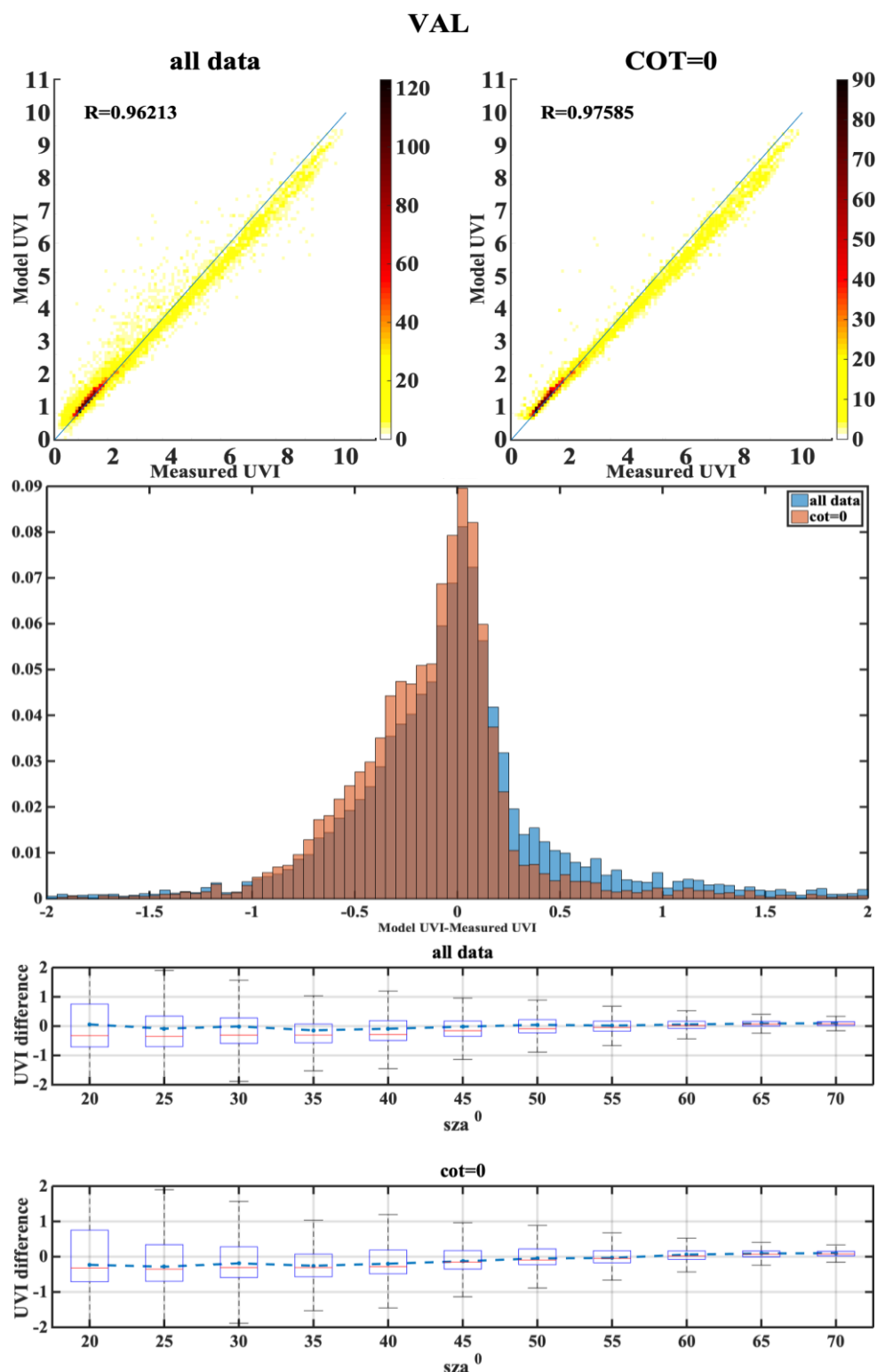


Figure A.16

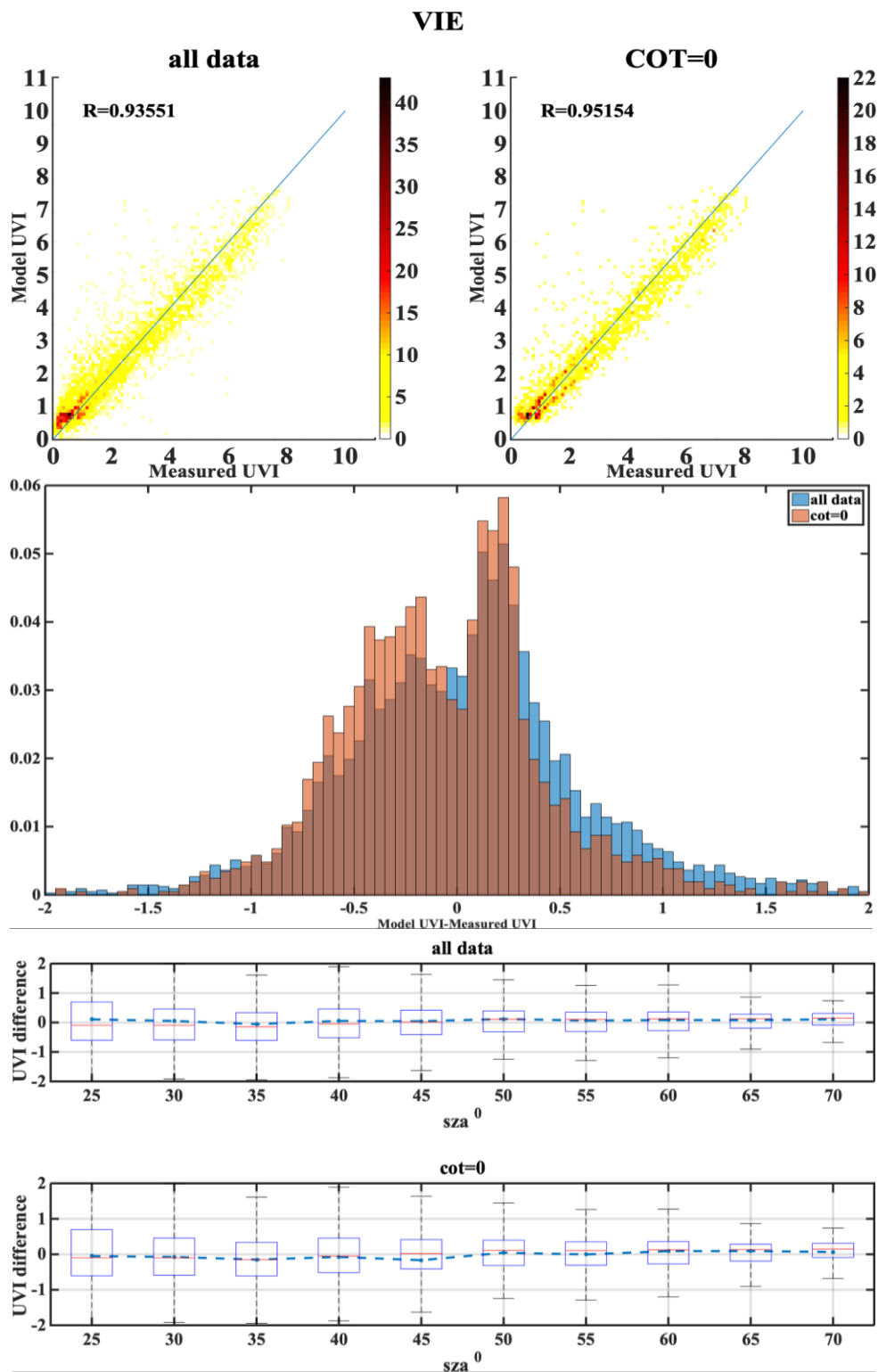


Figure A.17